Tsunamis and sea levels of the past millennium in Puget Sound, Washington

Carolyn E. Garrison-Laney

A dissertation

submitted in partial fulfillment of the

requirements for the degree of

Doctor of Philosophy

University of Washington

2017

Reading Committee:

Dr. Brian Atwater, Chair

Dr. Juliet Crider

Dr. Brian Sherrod

Program Authorized to Offer Degree:

Earth and Space Sciences

University of Washington

Abstract

Tsunamis and sea levels of the past millennium in Puget Sound, Washington

Carolyn E. Garrison-Laney

Chair of the Supervisory Committee:
Dr. Brian Atwater
Department of Earth and Space Sciences

Tidal marsh deposits in the Puget Sound area contain evidence for multiple earthquakes and tsunamis over the past 1,000 years. This dissertation focuses on evidence beneath a salt marsh at Lynch Cove, at the head of the Hood Canal about 40 kilometers southwest of Seattle. Previous work at this marsh described stratigraphic evidence for coseismic uplift and liquefaction from a crustal earthquake or earthquakes about 1,000 years ago. New findings from Lynch Cove include two anomalous silt layers interpreted as tsunami deposits that postdate the earthquake uplift and liquefaction. These layers are better explained by tsunamis than by storms or river floods, based on the layer morphology, extent, sedimentology, and microfossils.

Radiocarbon ages of the two silt layers at Lynch Cove are 1690–1830 A.D. (120–260 cal yr BP, layer A), and 1170–1230 A.D. (720–780 cal yr BP, layer B). These ages more closely

align with the ages of two Cascadia earthquakes than with any other known earthquake in the Puget Sound region within the last 1,000 years. These the silt layers may have been deposited by tsunamis generated by Cascadia subduction thrust earthquakes, as were likely correlative deposits at another tidal marsh at Discovery Bay, along the tsunami path between the Pacific Ocean and Hood Canal.

This study improves the age ranges of the youngest six tsunami deposits at Discovery Bay, and compares them to layers A and B at Lynch Cove, and to the ages of known earthquakes and their secondary effects, including tsunamis and slope failures, of the last 1,200 years in the Pacific Northwest. Beds 1 and 3 at Discovery Bay are attributed to Cascadia subduction thrust tsunamis, and have radiocarbon ages that overlap with the ages of layers A and B at Lynch Cove. Discovery Bay Bed 2 has now been dated to 560-630 cal yr BP (1320-1390 A.D.). It is unclear why no corresponding deposit is present between layers A and B at Lynch Cove, and why no known 14th-century coseismic subsidence or tsunami is preserved at any of the Pacific coast estuaries of southern Washington. The source of the tsunami that deposited Discovery Bay Bed 2 remains to be determined. If the source was a rupture along the Cascadia subduction thrust, it may have been limited to an area offshore southern British Columbia and northern Washington, on the northern end of the subduction zone.

To test whether Cascadia tsunamis could have deposited the silt layers at Lynch Cove and Discovery Bay, numerical tsunami simulations were run for three different rupture styles of great Cascadia earthquakes, a local Seattle fault tsunami, and a transoceanic tsunami from Alaska. The Cascadia earthquake tsunami simulations produced flow depths and current speeds sufficient to deposit the silt layers at both Lynch Cove and Discovery Bay, while the Seattle fault

simulation did not. The Alaska tsunami simulation also produced flooding at Lynch Cove and Discovery Bay, in agreement with historical observations from 1964.

Using the inferred tsunami deposits at Lynch Cove as time markers for great Cascadia earthquakes, the paleoecology of the last ~1,000 years is reconstructed using fossil diatoms to test whether Lynch Cove, 240 km inland of the deformation front, records any Cascadia earthquake cycle deformation. A diatom transfer function was developed by statistically comparing the fossil diatoms at Lynch Cove to a training set of modern intertidal diatoms from Puget Sound. Using this method, 31 paleomarsh surface elevations were reconstructed, and with radiocarbon ages, a relative sea level curve was constructed. An overall rise in relative sea level of about 2.5 m is estimated at Lynch Cove over the last 1,000 years, a rate that is faster than rates estimated by other Puget Sound studies. Superimposed on this overall relative sea level rise, paleomarsh surface elevations are observed to rise by about 25 cm prior to the deposition of both layers A and B. While these may record Cascadia preseismic deformation, these rises are within the error range of adjacent data points, so are inconclusive. Because of this, Lynch Cove marsh is interpreted as a location that probably does not record Cascadia earthquake cycle vertical deformation. Lynch Cove is the only forearc data point of vertical interseismic deformation for the Cascadia subduction zone, and these negative results provide an inland limit of earthquake cycle deformation.

The findings of this research help to better understand hazards from Cascadia earthquakes and tsunamis in the Puget Sound region. The identification of paleotsunami deposits in Hood Canal identifies a tsunami hazard that was previously unknown. The tsunami simulations corroborate the geological evidence, and identify some areas in Puget Sound with greater tsunami hazard. This study also places constraints on the inland limit of Cascadia earthquake

deformation. This is important for accurate estimates of areas of strong shaking, which influence earthquake hazard maps, and for geophysical models. This research also influences estimates of earthquake recurrence. If Bed 2 at Discovery Bay is from a northern Cascadia earthquake, recurrence rates at the northern end of the subduction zone may be shorter than current estimates.

TABLE OF CONTENTS

LIST OF FIGURES

LIST OF TABLES

ACKNOWLEDGEMENTS

There are so many people who supported me over the years, and helped me complete this research. I thank Brian Atwater for discussions, advice, reviews, and for setting a high bar for figure drawing. Brian was also a huge help in the field. Brian Sherrod provided access to his lab, microscope, and references; and shared advice about diatoms and transfer function statistics. Estella Leopold provided access to her microscope and photography equipment. Ian Hutchinson contributed ideas and encouragement and helped dig large pits at Discovery Bay. I thank Liz Nesbitt and Juliet Crider for their support and encouragement, and for understanding the demands of balancing parenthood and grad school. Jody Bourgeois shared ideas, and her classes were as source of inspiration, both as a student and a TA. Thanks to David Schmidt for discussions about Cascadia deformation. Eileen Hemphill-Haley has been an inspiration to me for many years. Her example of scientific excellence and attention to detail has influenced my research. Eileen taught me how to process diatom samples and make slides, and answered countless diatom-related questions over the years. Others who helped with field work include Elizabeth Barnett, Devin Bedard, Topher French, Nick Novoa, Kate Allstadt, and Kendra Pivaroff-Ward.

Loyce Adams and Randy LeVeque provided many hours of assistance and answered countless questions about GeoClaw and Python code, and helped me obtain topography files and earthquake source files for tsunami simulations. Special thanks to Kelin Wang and Dawei Gao for the Cascadia earthquake source files; and to Frank González and Pacific Marine Environmental Laboratory for the Seattle fault earthquake source file.

I would not have been able to run the transfer function statistics without the complimentary C2 software license from Steve Juggins. Thanks to Yong Wei of PMEL for sending me his tsunami

simulation animation that showed Cascadia tsunami waves propagating into Puget Sound. His animation gave me the idea that the silt layers at Lynch Cove might be Cascadia tsunami deposits.

I would like to thank my husband of twenty years, Jim Laney, for support over my many years of education. I thank my funny, smart, and occasionally exasperating daughters Eva and Julia. May you grow up to be awesome and powerful women. I also owe a lot to my mother, Martha Garrison, for raising me as a single parent, and for instilling in me that idea that I was capable of great achievements.

This work was supported by the University of Washington, Department of Earth and Space Sciences; the University of Washington Department of Applied Mathematics; the Quaternary Research Center; the U.S. Geological Survey; and the Geological Society of America. The Theler Wetlands in Belfair, Washington granted easy access to the tidal marsh at Lynch Cove. Washington Sea Grant supported the completion of this dissertation.

Chapter 1. **Introduction**

1.1 Motivation and Findings

This dissertation examines the hazard posed by Cascadia subduction zone tsunamis to inland areas of the southern Salish Sea, including Puget Sound and Discovery Bay (Figure 1.1). This study also asks whether the western part of Puget Sound experiences subduction zone deformation either during or between great earthquakes on the Cascadia subduction zone (Figure 1.1B). An understanding of these hazards influences community and emergency planning, and is critical to preparedness, sustainability, and resilience. The Puget Sound region, within the forearc of the Cascadia subduction zone (CSZ), is populated by over 4 million people, contains two major ports, the Ports of Seattle and Tacoma, the Puget Sound Naval complex, and has commercial and residential shoreline infrastructure vulnerable to tsunamis. Puget Sound seismic hazards include not only Cascadia earthquakes, but also earthquakes on shallow faults in Puget Sound, and deep earthquakes within the subducting Juan de Fuca plate (Figure 1.2A-C).

The three types of earthquakes in the Puget Lowland occur at different recurrence rates, and have different characteristic sizes and associated hazards. Very large (M 8-9) but infrequent Cascadia earthquakes may affect Puget Sound, despite its distance from the Cascadia deformation front (Figure 1.2A). Numerical simulations suggest that areas in Puget Sound will experience strong shaking because its sedimentary basins act as amplifiers of seismic energy. Tsunamis are commonly generated offshore by sea floor deformation during subduction zone earthquakes, and these tsunamis can cross ocean basins, travel to inland waterways, and flow up river channels. The most recent large earthquake on the Cascadia subduction zone was in 1700 A.D. Puget Sound is also crossed by several major crustal faults that can produce large (M ~7)

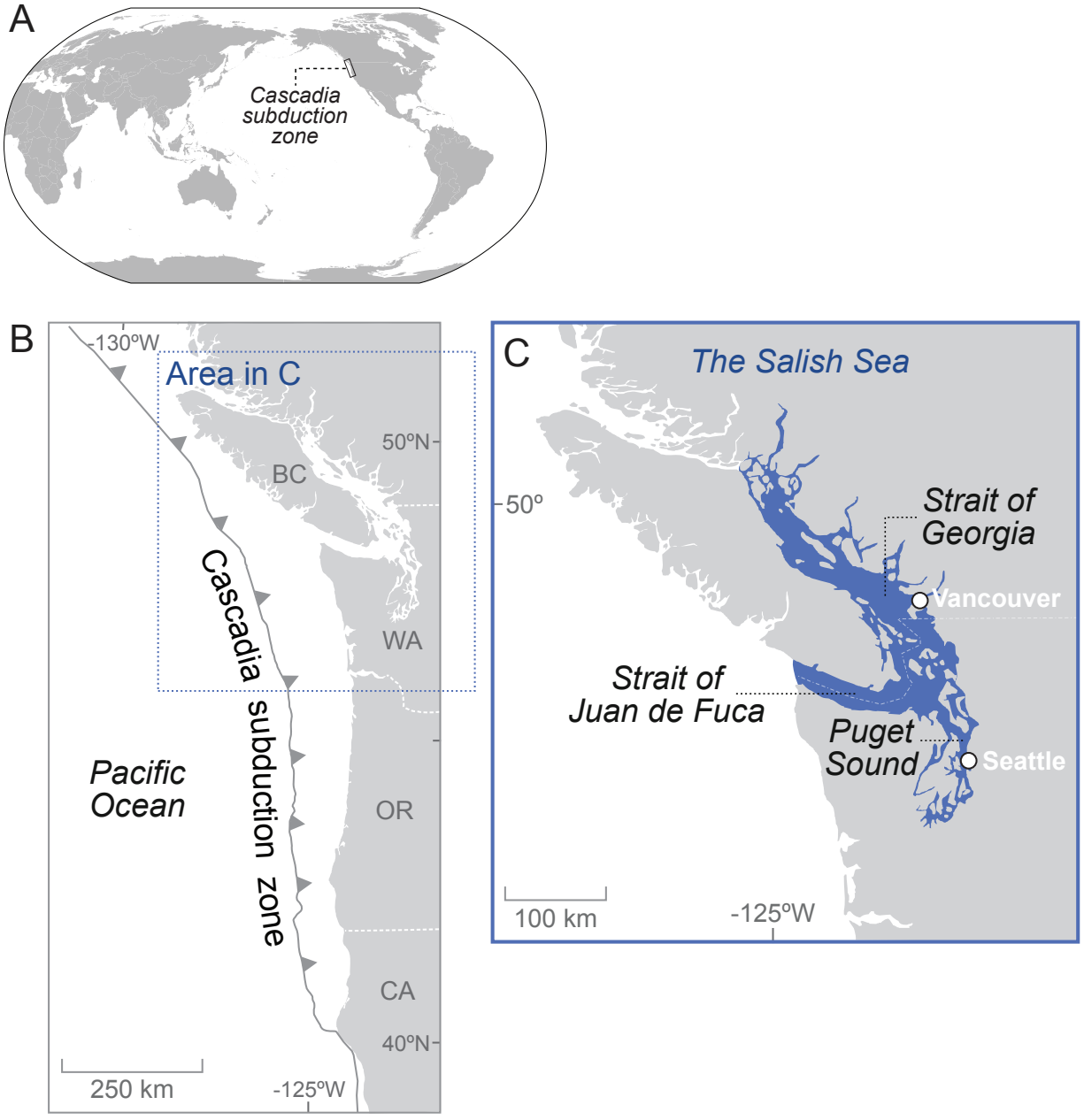

Figure 1.1. Location of study areas. (A) Location of Cascadia subduction zone, (B) Tectonic setting of the Cascadia subduction zone, (C) Area of the Salish Sea.

earthquakes and tsunamis if the fault offsets the sea floor (Figure 1.2C). The recurrence of these earthquakes varies by individual fault, and is still not known for every fault in the Puget Lowland. The most recent large tsunami-generating earthquake of this type in Puget Sound was

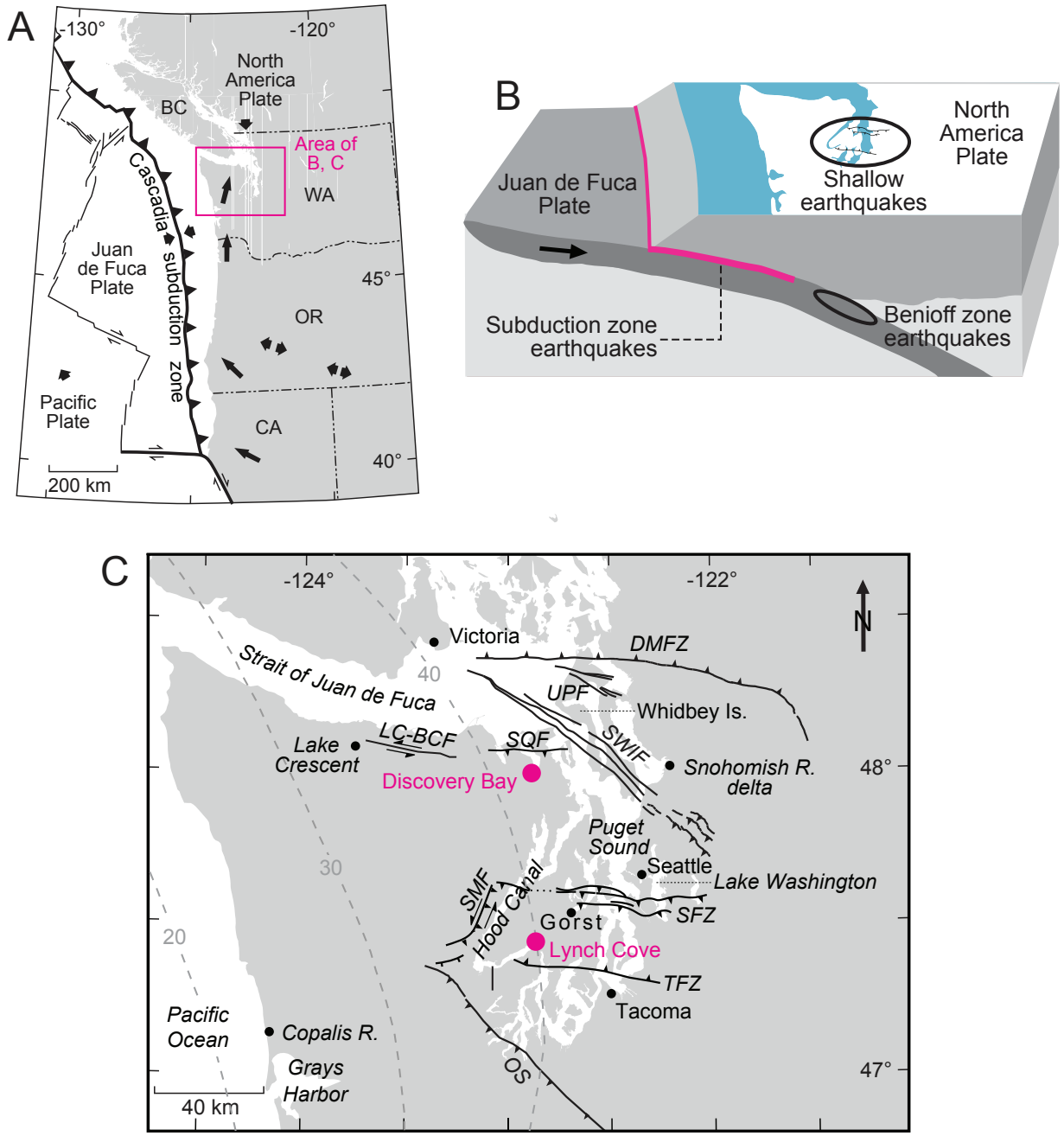

Figure 1.2. Tectonic setting of the Cascadia subduction zone, the Puget Sound area, and Lynch Cove and Discovery Bay locations. (A) Tectonic map of the Cascadia subduction zone with relative motions of tectonic plates shown by arrows (simplified from (Wells and Simpson, 2001). (B) Cross section of the Cascadia subduction zone showing the location of three earthquake sources in study areas. (C) Tectonic setting of the Puget Sound region. Select Holocene faults in black (adapted from Blakely et al., 2009; Nelson et al., 2014). Gray dashed lines are depth (km) of Juan de Fuca slab (McCrory et al., 2012).

about 1,100 years ago on the Seattle fault (Figure 1.2C). The most frequent source of earthquakes in Puget Sound are deep earthquakes that occur within the deforming Juan de Fuca plate as it is subducted deep beneath Puget Sound (Figure 1.2B). There have been six deep earthquakes over magnitude 6.0 in the last 100 years. To understand the earthquake hazards from less frequent types of earthquakes, we must rely on geologic evidence of past events, and use it to predict the impact of future events.

Any of the three earthquake sources can generate a tsunami, either directly by deforming the seafloor, or as a secondary effect of shaking, when slope failures under or into water generate a tsunami. While the hazards from locally-generated tsunamis on crustal faults, and from tsunamigenic landslides are recognized and anticipated in Puget Sound, the hazard from Cascadia tsunamis has only begun to be studied in the last decade. Previously not considered a major threat to remote inland areas such as Puget Sound, Cascadia tsunamis have been recently modeled for areas along and near the Strait of Juan de Fuca. This study examines geologic evidence for tsunamis near the entrance to Puget Sound and within Puget Sound at the head of Hood Canal, and uses numerical tsunami simulations to study Cascadia tsunami behavior in these areas.

Across the Pacific, the Seto Inland Sea in Japan has been historically flooded by Nankai subduction zone tsunamis (Figure 1.3). There, channel morphology and bathymetry have controlled tsunami behavior, and some shorelines experienced higher flow depths and current speeds than others. Cascadia tsunamis entering Puget Sound, with its complex waterways and varying bathymetry, will likely behave similarly, with some areas experiencing more hazardous conditions than others. Understanding the most hazardous areas in Puget Sound will help community planners and emergency managers and ensure community preparedness.

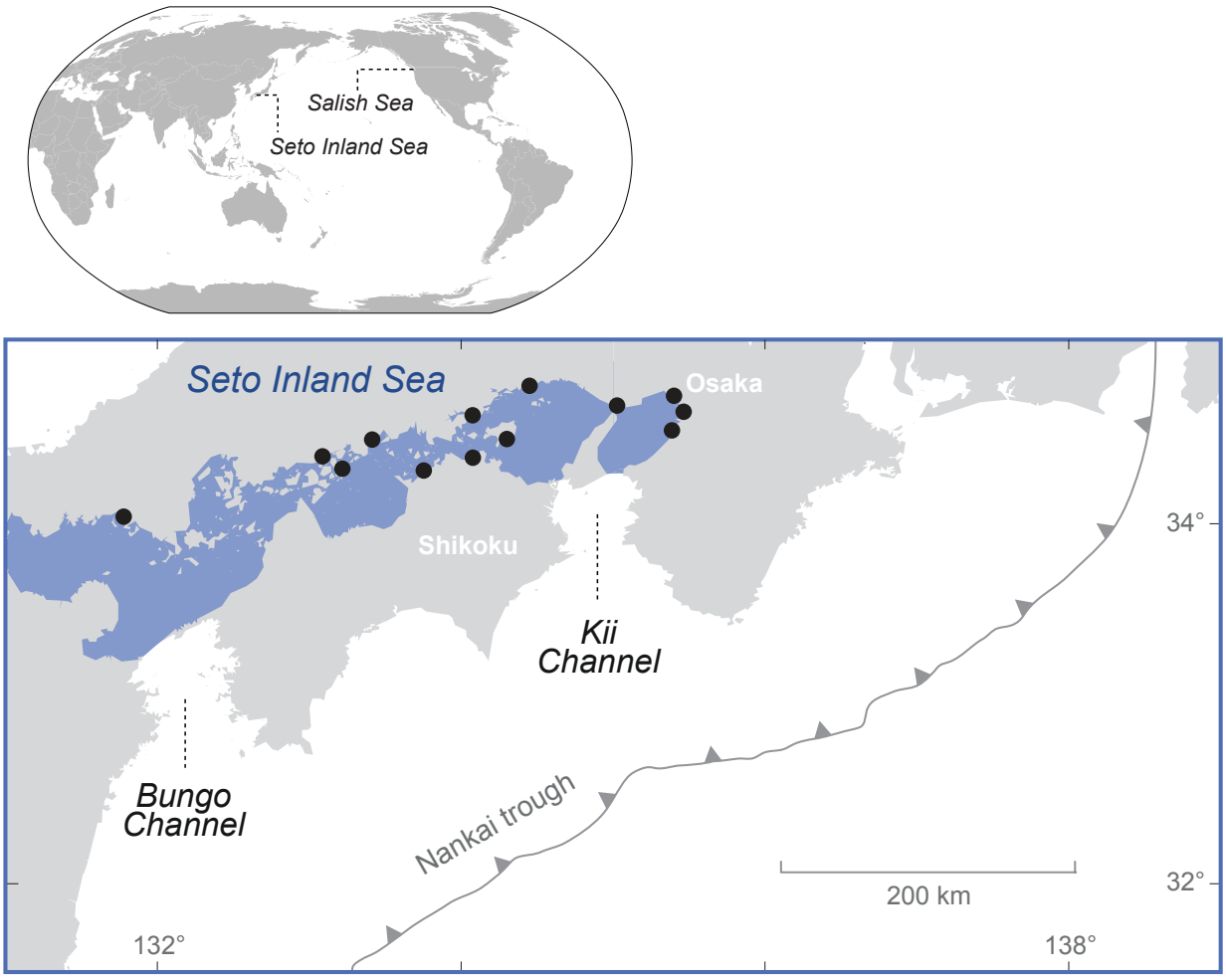

Figure 1.3. Seto Inland Sea north of Shikoku Island in southwest Japan. Map adapted from Lee et al., 2015. Black dots show locations of damage from 1707 Hoei tsunami (Hatori, 1988).

In this study, I examine two tsunami deposits from a tidal marsh at Lynch Cove, at the terminus of Hood Canal in Puget Sound (Figure 1.2C). I describe the physical characteristics of these deposits that supports the interpretation that they were deposited by tsunamis. I discuss the radiocarbon ages of the tsunami deposits, and an age model that constrains the timing of these two tsunamis to within the time of the last two subduction zone earthquakes on the outer coast of Washington: the A.D. 1700 earthquake, and the penultimate earthquake dated ~700-900 cal yr BP. I compare the tsunami deposit ages with other evidence for earthquakes and tsunamis in the

Puget Lowland, including Discovery Bay (Figure 1.2C), a site with a 2,500-year record that includes nine tsunami deposits, and with evidence from other sites on the outer coastlines of Washington, southwestern British Columbia, and Oregon.

To test the source of the tsunami deposits at Lynch Cove, I use numerical tsunami simulations to evaluate different tsunami sources and their ability to leave behind tsunami deposits at Lynch Cove. I test three different types of Cascadia subduction zone earthquake; the Seattle fault earthquake of A.D. 900-930, which generated a tsunami that left deposits in Puget Sound; and an earthquake from the Alaska-Aleutian subduction zone, which generated a tsunami in 1964 that caused local flooding at sites in Puget Sound. From the simulation results, I conclude that Cascadia is the most likely source of the tsunami deposits at Lynch Cove.

Using the tsunami deposits at Lynch Cove as time markers of great Cascadia earthquakes provided an opportunity to determine whether Lynch Cove, located 240 km inland of the Cascadia deformation front, experiences any vertical interseismic deformation. To test this, I analyzed the record of fossil diatoms in the sediment sequence at Lynch Cove. Modern diatoms from a variety of intertidal settings in Puget Sound were used to develop a diatom-based transfer function that estimated marsh elevation over time. From this, a sea level history was created for Lynch Cove. I find that the sea level reconstruction shows that the marsh aggraded as sea level rose by about 2.5 meters over the last ~1,000 years. There is no apparent coseismic or interseismic deformation apparent over the last ~1,000 years, so either there was none, or it was within the error of the reconstruction. These findings, suggest that Lynch Cove has probably not experienced significant vertical deformation associated with the Cascadia subduction zone. This is an important data point because areas that experience deformation are at greatest seismic risk.

The goals of this research were:

- Describe in detail the characteristics of the silt layers at Lynch Cove, including stratigraphic relationships, deposit distribution, grain size, and diatom content to test whether they have the characteristics typical of tsunami deposits,
- Radiocarbon date the tsunami deposits from Lynch Cove,
- Improve the dating of tsunami deposits at Discovery Bay, WA, a previously studied site with multiple tsunami deposits, to enable comparisons to the deposits at Lynch Cove, and other regional earthquake and tsunami evidence,
- Create numerical tsunami simulations using different earthquake sources to determine tsunami behavior, flow depths, and current speeds at both Lynch Cove and Discovery Bay, to identify candidate tsunami sources,
- Quantify the relative sea level change over the last 1,000 years at Lynch Cove, and
- Interpret relative sea level change at Lynch Cove with respect to the Cascadia earthquake cycle.

The primary findings of this research include:

- The deposits at Lynch Cove have characteristics that support deposition by tsunami.
- The ages of the tsunami deposits at Lynch Cove best match the ages of two Cascadia earthquakes documented on the outer coast of Washington.
- No known local or regional earthquake or tsunami besides the Cascadia earthquakes matches the ages of the tsunami deposits at Lynch Cove, with the potential exception of tsunamis that may have been generated by yet-unidentified slope failures.
- Simulated Cascadia tsunamis enter Puget Sound and have flow depths and current speeds that vary considerably based on location, bathymetry, and waterway morphology.

- Simulations predict that some Puget Sound shorelines will be more vulnerable to high tsunami flow depths than others, especially those located at the terminuses of narrow waterways.
- Simulated Cascadia tsunamis have flow depths and current speeds both at Lynch Cove and Discovery Bay sufficient to form tsunami deposits.
- The Discovery Bay Bed 2 tsunami deposit from about 600 cal yr BP, and tsunami deposits of similar age from Vancouver Island to northern Oregon, may be from a Cascadia earthquake or earthquakes that was smaller than the 1700 A.D. earthquake, and may represent a northern subduction zone rupture.
- Lynch Cove has experienced a sea level rise rate of about 2.6 mm/yr over the last ~1,000 years, more than twice the rate of long term records from northern Puget Sound, but in closer agreement with the rates determined by tidal gauge records of the last ~100 years.
- Paleomarsh surface elevation reconstructions for Lynch Cove do not show deformation over the last two subduction zone earthquake cycles, and if it has deformed, the amount has been less than ~0.5 m, the error of the reconstruction.
- Lynch Cove is probably east of the easternmost edge of the downdip rupture area of the Cascadia subduction zone.

1.2 Field Areas

This study focuses on two tidal marsh sites, Lynch Cove at the head of Hood Canal in the Puget Lowland, and Discovery Bay on the Strait of Juan de Fuca near the entrance to Puget Sound (Figure 1.2C). Lynch Cove is a mesotidal salt marsh at the head of Hood Canal, a narrow (~2 km wide) channel in Puget Sound. The marsh at Lynch Cove is about one square kilometer in area, and has experienced minimal human modification. Lynch Cove was previously studied

because it preserves spectacular evidence of coseismic uplift and liquefaction from a local earthquake or earthquakes, about ~1,000 years ago, but the record of Cascadia subduction zone earthquake tsunamis and deformation preserved in the youngest sediments of Lynch Cove have not been previously studied.

The tidal marsh at Discovery Bay is similarly situated at the head of a narrow waterway. The marsh contains a long record of as many as nine tsunami deposits in the last 2,500 years. These tsunami deposits were studied and dated over a decade ago, and this study improves the dating of the tsunami events at the site, and improves our knowledge of Cascadia rupture behavior, earthquake recurrence, and allows individual deposits to be better correlated to other tsunami deposits, including those at Lynch Cove.

1.3 Significance of Dissertation Contributions

The goals of this study are to identify potential hazards from Cascadia tsunamis in Puget Sound, and to determine whether Lynch Cove records any Cascadia vertical deformation. Because there have been no Cascadia earthquakes in written history, we must rely on geological evidence to determine the effects these events had at various locations. Many studies along Cascadia's Pacific coastlines have helped to adequately assessed the local dangers of Cascadia earthquakes and tsunamis, and outer coast communities have begun to prepare for the eventual earthquakes and tsunamis. However, we still do not have a thorough understanding of how Cascadia tsunamis will affect the inland waterways of the Salish Sea, and where they will be the most hazardous.

This dissertation addresses these questions by focusing on the geologic evidence and ages of two past tsunamis. The tsunami simulations in this dissertation answer questions about the flow

depths, current speeds, and duration of tsunami events in the Strait of Juan de Fuca, and Puget Sound, and specifically in Hood Canal from different tsunami sources.

This study also provides an important "paleogeodetic" data point at an inland site that will help constrain the eastern limit of subduction zone deformation, and strong shaking during Cascadia subduction zone earthquakes. Vertical deformation that occurred on the surface, either during or between great earthquakes, yields clues to deformation occurring at depth on the subduction thrust. Vertical deformation can help define the downdip limit of the seismogenic zone, or area where seismic waves are generated, between the down-going Juan de Fuca plate and the overriding North America plate. Knowing the limits of the seismogenic zone is important because it defines the area of greatest hazard from shaking during subduction zone earthquakes. These limits can be applied to geophysical models of subduction zone deformation and studies of basin amplification of seismic waves, which is predicted in the deep sedimentary basins of the Puget Lowland. Together, this data influences earthquake hazard maps, emergency planning, and building codes.

This dissertation presents research that improves our knowledge of future earthquake hazards. The identification of paleotsunami deposits in Hood Canal identifies a hazard to Puget Sound from Cascadia tsunamis that was previously unknown. The tsunami simulations corroborate this geological evidence, and identify areas of greatest tsunami hazard. This study constrains the eastern limits of Cascadia deformation with geologic evidence. Collectively, this dissertation improves the knowledge of Cascadia earthquake hazards in the southern Salish Sea region.

1.4 GEOLOGIC SETTING

1.4.1 *Cascadia Subduction Zone*

Since the 1980s, tidal marshes along the coastlines of Vancouver, B.C. (Hutchinson and Clague, 2017; Clague et al., 2000, Hughes et al., 2002), Washington (Atwater et al., 2004; Atwater and Hemphill-Haley, 1997), Oregon (Kelsey et al., 2002; Nelson et al., 2006; Nelson et al., 2008a; Witter et al., 2003), and Northern California (Peterson et al., 2013) have yielded abundant paleoseismic evidence including buried soils and tsunami deposits. Tsunami deposits have been identified in coastal lakes in California and Oregon (Abramson, 1998; Garrison-Laney, 1998; Kelsey et al., 2005). Cascadia earthquakes are also recorded by turbidites in offshore submarine canyons and submarine slope failures near Vancouver Island (Goldfinger et al., 2012; Goldfinger et al., 2017; Blais-Stevens et al., 2011; Enkin et al., 2013). Cascadia tsunami deposits have been found in tidal marshes along the Strait of Juan de Fuca (Hutchinson et al., 2013; Williams et al., 2005), and on Whidbey Island in Puget Sound (Williams and Hutchinson, 2000). Along the Strait of Juan de Fuca there is evidence for modest amounts of coseismic subsidence from Cascadia earthquakes (Hutchinson et al., 2013).

Figure 1.2A shows the tectonic setting of Cascadia subduction zone (CSZ). On the Pacific coast of southwest Washington, paleoseismic evidence records a total of seven subduction thrust earthquakes over the last 3,500 years (Atwater and Hemphill-Haley, 1997; Atwater et al., 2004). The most recent earthquake was in A.D. 1700 (Jacoby et al., 1997; Yamaguchi et al., 1997; Atwater et al., 2005); and the penultimate earthquake is dated to between 793–913 cal yr BP (Atwater and Griggs, 2012).

1.4.2 *Puget Sound*

Puget Sound is in the forearc basin of the Cascadia subduction zone, and lies between the Olympic Coast Range and the Cascade volcanic arc. The Puget Lowland is subject to north-south compression with folding and thrust faulting on shallow roughly E-W oriented fault structures including the Seattle, Tacoma, Saddle Mountain, South Whidbey Island, and Olympia faults (Wells et al., 1998). These compressional faults, a result of northeast oblique subduction of the Juan de Fuca plate, have produced a series of up-thrown blocks and corresponding sedimentary basins in the Puget lowland that have been identified by seismic tomography (Brocher et al., 2001), seismic reflection (Johnson et al., 2004a; Johnson et al., 2004b), and magnetic anomaly mapping (Blakely et al., 2002; Johnson et al., 2004a). The Seattle fault (Figure 1.2C) had coseismic offset of up to 8 m during the "millennial earthquake series" of earthquakes about 1,100 years ago (Johnson et al., 1999; Nelson et al., 2014). Tsunami deposits attributed to the Seattle fault Restoration Point earthquake (Nelson et al., 2014) between A.D. 900–930 (Atwater, 1999) have been identified at Cultus Bay on Whidbey Island, at West Point in Seattle (Atwater and Moore, 1992), in the Snohomish River delta (Bourgeois and Johnson, 2001), and at Gorst at the head of Sinclair Inlet (Arcos, 2012).

Evidence for past earthquakes on the intraplate faults in the Puget Lowland includes fault ruptures, tsunami deposits, and turbidites. Paleoseismic evidence of late Holocene earthquakes from the Puget Lowland includes evidence from the Seattle, Tacoma, Saddle Mountain, South Whidbey Island, and Utsalady Point faults. Earthquakes on these faults (Figure 1.2C) have been identified from trenching studies of fault scarps (Nelson et al., 2003; Johnson et al., 2004b; Sherrod et al., 2008; Blakely et al., 2009; Witter et al., 2008a; Kelsey et al., 2012); coseismic uplift

(Bucknam et al., 1992; Sherrod et al., 2000; Sherrod et al., 2003); and coseismic subsidence (Sherrod, 2001; Bourgeois and Johnson, 2001).

The Puget lowland landscape is dominated by glacial landforms and deposits that are susceptible to slope failures. Steep shorelines are common in Puget Sound (Shipman, 2004; Schulz, 2007). Glacial sediments are particularly prone to generating tsunamigenic landslides (Tappin, 2010), and the fjords of Puget Sound, with deep water and steep slopes are a likely setting for submarine landslides (Masson et al., 2006). Earthquakes likely created subaqueous slope failures in Lake Washington (Karlin et al., 2004), Puget Sound (Smith, 2012), and Haro Strait (Blais-Stevens et al., 2011). While Cascadia and intraplate earthquakes are potential sources of these slope failures, the Puget Lowland also experiences frequent deep earthquakes from deformation within the subducting Juan de Fuca plate (Ludwin et al., 1991). In addition, large landslides commonly occur without seismic shaking, such the 2014 Oso landslide (LaHusen et al., 2015; Wartman et al., 2016).

Like the slope failures in Lake Washington and Puget Sound, some sites in Puget Sound and along the Strait of Juan de Fuca record evidence of coseismic land level change, tsunami, liquefaction, or slope failure from more than one earthquake source. One such site that likely records evidence of both intraplate and CSZ earthquakes is the tidal marsh at Lynch Cove, located at the head of Hood Canal (Figure 1.2C). In addition to the findings of this study, the tidal marsh at Lynch Cove also preserves sedimentary evidence of coseismic uplift from the intraplate earthquake or earthquakes between 895-975 cal yr BP (Bucknam et al., 1992; Bucknam et al., 1994); and a sand deposit that has been interpreted both as a tsunami deposit (Bucknam et al., 1992; Bucknam et al., 1994; Hemphill-Haley, 1996; Jovanelly and Moore, 2009), and more recently as vented sand (Martin and Bourgeois, 2012). The coseismic uplift at Lynch Cove lifted

tidal flats out of the intertidal zone, which were later colonized by upland forest and meadow plants. These forests and meadows began to be encroached by rising sea level by about 1200 A.D. (750 cal yr BP), and tidal marshes replaced upland. A few dead tree trunks remain sticking up out of the overlying tidal marsh deposits. Within the sequence of peaty tidal marsh sediments, there are two anomalous thin (< 4 cm) gray silt layers. These layers, which date to about 1200 A.D., and likely 1700 A.D., are described herein, with multiple lines of evidence to support the hypothesis that they are tsunami deposits.

Sixty kilometers to the north, at Discovery Bay (Figure 1.2C), the tidal marsh at the head of the bay contains a record of as many as nine tsunami deposits that span the last 2,500 years; more than the number of subduction zone earthquakes identified on the outer coast of Washington in that timespan (Williams et al., 2005; Atwater et al., 2004). These deposits are likely from both Cascadia tsunamis, local sources, and possibly transoceanic tsunami as well (Williams et al., 2005). Like Lynch Cove, the marsh at Discovery Bay is at the head of a narrow terminal embayment, a setting that amplifies tsunami waves. The low-lying areas at the head of Discovery Bay were flooded by the 1964 M 9.2 Great Alaskan earthquake tsunami, and a lamina of very fine sand, present in some parts of the marsh, was probably deposited during that event (Williams et al., 2005).

1.5 Synopsis of Dissertation Chapters

Chapter 2 is an examination of the stratigraphy and sedimentary characteristics of two silt layers in a tidal marsh at Lynch Cove that are probably tsunami deposits. The diatom paleoecology of the last ~1,000 years of tidal marsh deposits, and the two silt layers is examined. The chronology of the silt layers is compared to a refined chronology for tsunami deposits at Discovery Bay, and

local and regional earthquake and tsunami evidence that suggests that the silt layers at Lynch Cove are from Cascadia subduction zone tsunamis.

Chapter 3 compares five different tsunami simulations, and their predicted flow depths and speeds, at both Lynch Cove and Discovery Bay. The tsunamis generated by three different rupture styles of Cascadia earthquake, the 900-930 A.D. Seattle fault earthquake, and an earthquake within the rupture area of the 1964 Alaska earthquake are compared at both Lynch Cove and Discovery Bay, and evaluated as potential sources of tsunami deposits at both sites.

Chapter 4 is the development of a diatom-based transfer function. The transfer function compares diatoms preserved as fossils in the sediments of Lynch Cove to the distribution of modern diatoms in Puget Sound to those to determine the marsh elevation within the tidal zone over time. From this, using the suspected tsunami deposits as time-markers, a sea level history of the last ~1,000 years is reconstructed, to examine whether Lynch Cove preserves Cascadia interseismic vertical deformation.

Chapter 5 is a summary of the findings of the previous three chapters, and discusses the implications of the finding of this research and how that contributes to the understanding of Cascadia tsunami and earthquake hazards in Puget Sound. I also recommend further work that could clarify unanswered or uncertain findings of this research.

Chapter 2. **Tsunami Deposits at Lynch Cove and Discovery Bay, Washington**

2.1 INTRODUCTION

Since the 1980s, tidal marshes along the coastlines of Vancouver, B.C. (Hutchinson and Clague, 2017; Clague et al., 2000, Hughes et al., 2002), Washington (Atwater et al., 2004; Atwater and Hemphill-Haley, 1997), Oregon (Kelsey et al., 2002; Nelson et al., 2006; Nelson et al., 2008a; Witter et al., 2003), and Northern California (Peterson et al., 2013) have yielded abundant paleoseismic evidence of earthquakes on the Cascadia subduction zone, including buried soils, vented sediments, and tsunami deposits. In addition to those found in tidal marsh sediments, Cascadia tsunami deposits have also been identified in coastal lakes in California and Oregon (Abramson, 1998; Garrison-Laney, 1998; Kelsey et al., 2005). Additionally, tsunami deposits ascribed to Cascadia tsunamis have also been found in areas farther inland, including tidal marshes along the Strait of Juan de Fuca (Hutchinson et al., 2013; Williams et al., 2005), and on Whidbey Island in Puget Sound (Williams and Hutchinson, 2000).

While the hazard to Pacific coastlines from Cascadia tsunamis is well known, the hazard to inland waterways such as Puget Sound is less well understood. It is known that subduction zone tsunamis can travel hundreds of kilometers inland. Historical observations of subduction zone tsunami flooding inland waterways include examples from the Chile and Nankai subduction zones. The 1960 Chilean tsunami had wave heights of 1.6 meters at the mouth of Rio Aysen, over 100 km inland of the coast, and behind the Archipelago of Chonos (Sievers et al., 1963). In Japan, the 1707 Hoei earthquake on the Nankai subduction zone generated a tsunami that caused damage in the Bungo Channel (Hatori et al., 1983; Baranes et al., 2014), as well as along shorelines in the Seto Inland Sea (Hatori, 1988). The 1946 Nankai earthquake tsunami caused run-ups between 1–

3 meters along the Bungo Channel, and even greater run-ups of 3-4 meters were documented from the 1707 Hoei and 1854 Ansei tsunamis. In the Seto Inland Sea, tsunami run-ups reached 2-3 meters high in the eastern part, and 1.5 meters high in the western and central parts of the Seto Inland Sea where the tsunami caused damage to salt fields. The 1707 Hoei and 1854 Ansei tsunamis also caused increased current speeds in the Seto Inland Sea that were blamed for shipwrecks (Hatori, 1988). Figure 1.3 in Chapter 1 shows a summary of sites on the shorelines of the Seto Inland Sea with documented damage from both the 1707 Hoei and 1854 Ansei tsunamis.

Like the Seto Inland Sea, shorelines of Puget Sound have probably experienced flooding from Cascadia tsunamis. Along the Strait of Juan de Fuca near the entrance to Puget Sound, Discovery Bay has nine tsunami deposits spanning the last 2,500 years, some of which have been ascribed to Cascadia tsunamis (Williams et al., 2005).

While many of these deposits are likely from Cascadia tsunamis, because there are more tsunami deposits than there are number of known Cascadia earthquakes in the same time span, Discovery Bay must record tsunamis from other sources as well. Other potential tsunami sources include crustal faults, transoceanic tsunamis, or tsunamigenic slope failures. Because sites on or near the Strait of Juan de Fuca can record Cascadia tsunamis, sites farther away from the Cascadia deformation front may as well. One site that may record Cascadia tsunamis is Lynch Cove, a tidal marsh at the head of the Hood Canal arm of Puget Sound. There, two anomalous silt layers are candidate Cascadia tsunami deposits.

To test whether the silt layers at Lynch Cove are tsunami deposits, I examine the sedimentary characteristics, and diatom content of the layers. I compare the radiocarbon ages of the Lynch Cove deposits to the tsunami deposits at Discovery Bay, and to other earthquake evidence in the region. Collectively, the results of these lines of evidence suggest that the silt

layers at Lynch Cove are Cascadia tsunami deposits, and that Cascadia tsunamis are a greater hazard to Puget Sound shorelines than previously recognized.

2.2 SETTING

2.2.1 *The Cascadia Subduction Zone*

The record of earthquakes on the Cascadia subduction zone includes on land and offshore inventories of events. On the Pacific coast of southwest Washington, paleoseismic evidence from tidal marshes records a total of seven subduction thrust earthquakes over the last 3,500 years (Atwater and Hemphill-Haley, 1997; Atwater et al., 2004). Evidence for earthquakes includes coseismically buried soils, tsunami deposits, and vented sediments. The most recent and best dated Cascadia earthquake was in A.D. 1700 (Jacoby et al., 1997; Yamaguchi et al., 1997); and the penultimate earthquake is dated to between 793–913 cal yr BP (Atwater and Griggs, 2012).

The offshore turbidite record in the Juan de Fuca channel near Washington contains eight events in the last 3,500, one more than the onshore record in southwest Washington. The additional turbidite, T2, is radiocarbon dated between the two most recent earthquakes (Y and W) in southwest Washington. The T2 turbidite, which has been interpreted as a CSZ- wide event, has an averaged 2 sigma age of 448–548 cal yr BP, and when modeled in OxCal as part of the sequence of multiple events, an age of 320–610 cal yr BP (Goldfinger et al., 2012; Goldfinger et al., 2017). There is no known buried soil or tsunami deposit of T2's age preserved as a buried soil or tsunami deposit in any southwest Washington estuary, but there are but there are potentially correlative tsunami deposits from Vancouver Island at Deserted Lake, Tofino, and Ucluelet (Hutchinson and Clague, 2017; Clague and Bobrowsky, 1994a; Clague and Bobrowsky, 1994b; Guilbault et al., 1996); and from Oregon at Cannon Beach, Netarts Bay, and Yaquina

Bay (Witter et al., 2008b; Darienzo, 1991; Darienzo et al., 1994; Shennan et al., 1998; Graehl et al., 2015). There are also submarine slope failures close in age to T2 at Effingham Inlet, Saanich Inlet, Lake Washington, and Puget Sound (Enkin et al., 2013; Blais-Stevens et al., 2011; Karlin et al., 2004; Smith, 2012). Figure 2.1A shows the tectonic setting of Cascadia subduction zone (CSZ).

2.2.2 *The Puget Lowland*

The Puget Lowland is in the forearc basin of the Cascadia subduction zone, and lies between the Olympic Coast Range and the Cascade volcanic arc. The Puget Lowland is subject to north-south compression with folding and thrust faulting on shallow E-W oriented faults including the Seattle, Tacoma, Saddle Mountain, South Whidbey Island, and Olympia faults (Wells et al., 1998). These contractional faults, a result of northeast oblique subduction of the Juan de Fuca plate and resulting translation of crustal blocks in the forearc (Wells et al., 1998) have produced a series of upthrown blocks and corresponding sedimentary basins in the Puget Lowland that have been identified by seismic tomography (Brocher et al., 2001), seismic reflection (Johnson et al., 2004a; Johnson et al., 2004b), and magnetic anomaly mapping (Blakely et al., 2002; Johnson et al., 2004a). One of these upthrown blocks in the southern part of Puget Sound, the Seattle uplift, is bounded by the Tacoma fault zone to the south, the Seattle fault zone to the north, and the Saddle Mountain faults to the west (Figure 2.1C). This area, known as the Seattle uplift, is an area of about 1000 km^2 that was uplifted during the "millennial earthquake series," about 1,000 cal yr BP, and has coseismic uplifts up to 8 m south of the Seattle fault zone (Johnson et al., 1999; Nelson et al., 2014).

Evidence for past earthquakes on the intraplate faults in the Puget Lowland includes fault ruptures, tsunami deposits, and turbidites. Paleoseismic evidence of late Holocene earthquakes

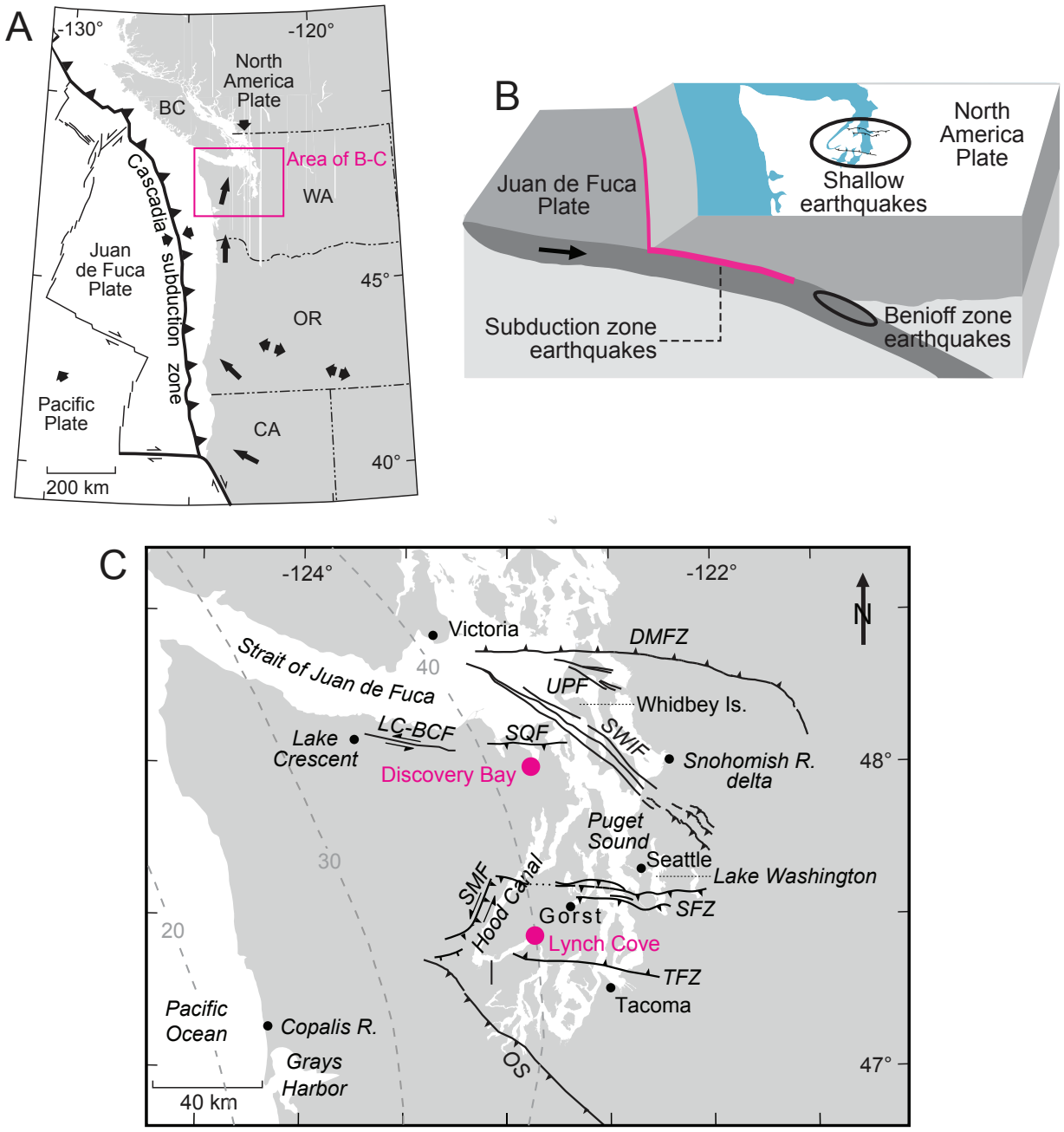

Figure 2.1. Tectonic setting of the Puget Lowland, and study site locations. (A) Tectonic setting of the Puget Sound region. Select Holocene faults in black (adapted from Blakely et al., 2009; Nelson et al., 2014). Labels as follows: LC-BCF—Lake Creek-Boundary Creek fault; DMFZ—Devils Mountain fault zone; UPF—Utsalady Point fault; SQF—Sequim fault; SWIF—South Whidbey Island fault; SFZ—Seattle fault zone; TFZ—Tacoma fault zone; SMF—Saddle Mountain faults; OS—Olympia structure. Gray dashed lines are depth (km) of Juan de Fuca slab (McCrory et al., 2012).

from the Puget Lowland includes evidence from the Seattle, Tacoma, Saddle Mountain, South Whidbey Island, and Utsalady Point faults (Figure 2.1C). Earthquakes on these faults have been identified from trenching studies of fault scarps (Nelson et al., 2003; Johnson et al., 2004b; Sherrod et al., 2008; Blakely et al., 2009; Witter et al., 2008a; Kelsey et al., 2012); coseismic uplift (Bucknam et al., 1992; Sherrod et al., 2000; Sherrod et al., 2003); and coseismic subsidence (Sherrod, 2001; Bourgeois and Johnson, 2001). Tsunami deposits attributed to the Seattle fault Restoration Point earthquake (Nelson et al., 2014) between 900–930 A.D. (Atwater, 1999) have been identified at Cultus Bay on Whidbey Island, at West Point in Seattle (Atwater and Moore, 1992), in the Snohomish River delta (Bourgeois and Johnson, 2001), and at Gorst at the head of Sinclair Inlet (Arcos, 2012).

The Puget Lowland landscape is dominated by glacial landforms and deposits that are susceptible to slope failures. Steep shorelines are common in Puget Sound (Shipman, 2004; Schulz, 2007). Glacial sediments are particularly prone to generating tsunamigenic landslides (Tappin, 2010), and the fjords of Puget Sound, with deep water and steep slopes are a likely setting for submarine landslides (Masson et al., 2006). Earthquakes likely created subaqueous slope failures in Lake Washington (Karlin et al., 2004), Puget Sound (Smith, 2012), and Haro Strait (Blais-Stevens et al., 2011). While Cascadia and intraplate earthquakes are potential sources of these slope failures, the Puget Lowland also experiences frequent deep earthquakes from deformation within the subducting Juan de Fuca plate (Figure 2.1B; Ludwin et al., 1991). In addition, large landslides also occur without triggering by earthquakes, such the 2014 Oso landslide (LaHusen et al., 2015; Wartman et al., 2016).

2.2.3 *Lynch Cove*

Lynch Cove is located at the head of Hood Canal, an arm of Puget Sound in the Puget Lowland (Figure 2.2). Hood Canal is a narrow (~2 km wide), deep, glacially-carved fjord, with an abundant sediment supply from unconsolidated and unstable glacial deposits. The tidal marsh at Lynch Cove is about one square kilometer in area (Figure 2.3A). Historical channeling has modified some of the natural channels in the marsh, but otherwise the marsh is largely unchanged since the time the area was first mapped in 1884 by the U.S. Coast Survey (Figure 2.4; Gilbert, 1884).

Relative sea level rise is apparent at Lynch Cove marsh. Snags of growth-position mature Western red cedar trees (*Thuja plicata*) are rooted in soils buried by tidal marsh deposits. There is also a fringe of more recently affected trees that are dying around the back edge of the marsh. A comparison of the modern tidal marsh with a georeferenced U.S. Coast Survey map (Gilbert, 1884) shows that the seaward edge of the marsh has eroded back as much as 20 meters in places, and the back edge of the central part of the marsh is correspondingly about 20 meters farther inland than it was in 1884 (Figure 2.4A-B); while in other parts of the marsh, the outermost and back edges of the tidal marsh remain similar to their position in 1884. Figure 2.4C-D shows a comparison of the current back edge of the marsh and the back edge in 1884 for the southern part of the marsh, as well as one of the cedar snags (Figure 2.4E). The position of the cedar snag (#399) in Figure 2.4E is plotted in Figure 2.4C & D, and based on the 1884 map, is in a similar position within, but near the back edge of the marsh as it was in 1884.

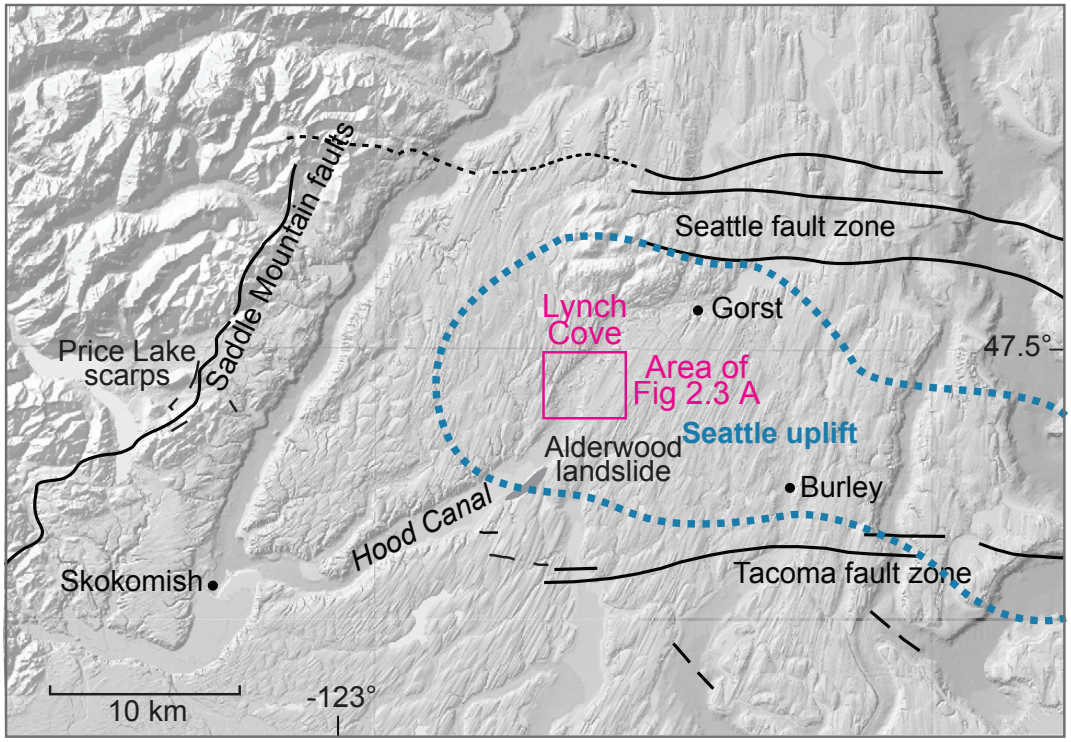

Figure 2.2. Tectonic setting of Lynch Cove in the southern Puget Lowland with select faults including the Seattle fault zone, Tacoma fault zone, and Saddle Mountain faults. Pink shaded area indicates approximate area of Seattle uplift (SU) (Bucknam et al., 1992; Johnson et al., 1999). Lidar map base of (Finlayson, 2005).

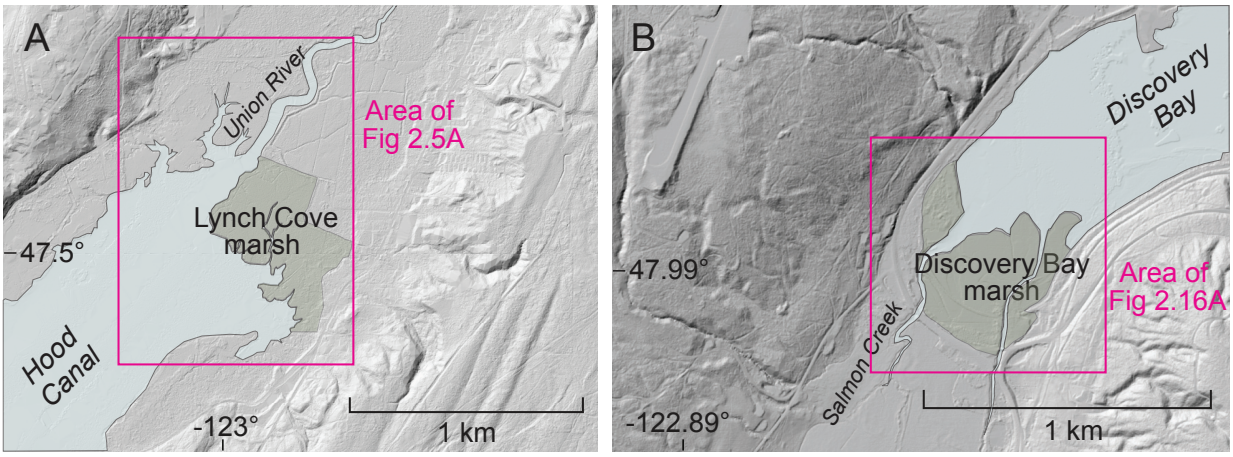

Figure 2.3. Detail of setting of Lynch Cove and Discovery Bay marshes. (A) Lynch Cove marsh study site. (B) Discovery Bay marsh study site. Lidar map base of (Finlayson, 2005).

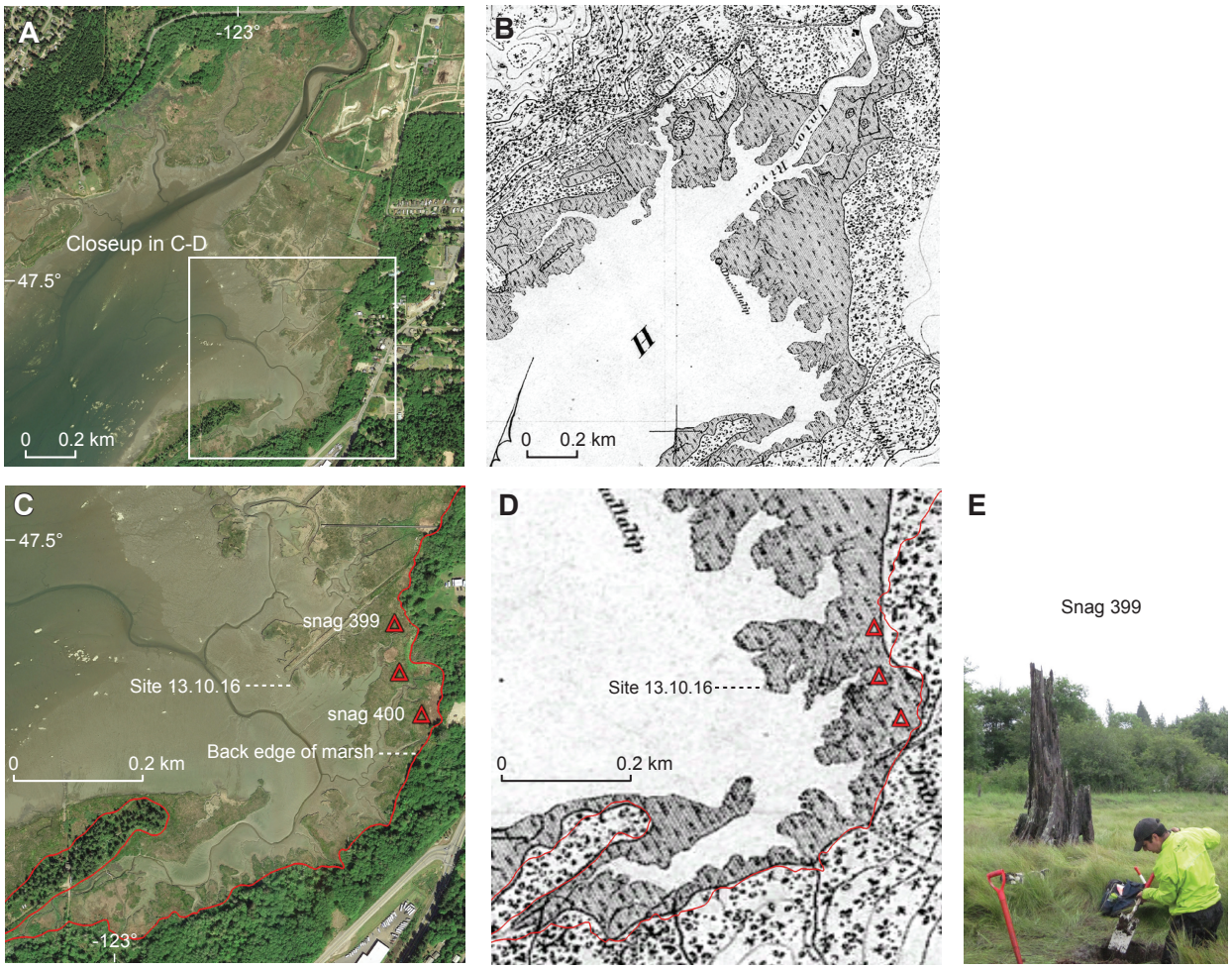

Figure 2.4. A comparison of recent and historical marsh extent at Lynch Cove. (A) 2013 Google Earth image and (B) U.S. Coast Survey map (Gilbert, 1884), (C) Locations of snags (red triangles) and back edge of tidal marsh (red line), (D) location of snags and back edge of 2013 marsh plotted in red on georeferenced 1884 map, (E) snag of Western red cedar (*Thuja plicata*) near back edge of tidal marsh.

2.2.4 *Previous Studies at Lynch Cove*

The marsh at Lynch Cove has been studied previously for evidence of local earthquakes, tsunamis, and liquefaction. The marsh sediments at Lynch Cove, at the southern part of the Seattle uplift (Figure 2.2) record coseismic uplift of at least 2 meters (Bucknam et al., 1992; Sherrod, 2001), and were uplifted during synchronous or closely-spaced earthquakes on the Seattle, Tacoma, and/or Saddle Mountain faults, part of a sequence of earthquakes known as the "millennial earthquake series" about 1,000 cal yr BP (Nelson et al., 2014). The uplift at Lynch

Cove has been dated between 895-976 A.D. (974-1055 cal yr BP) (Bucknam et al., 1992; Bucknam et al., 1994; Sherrod, 2001; Sherrod et al., 2004).

There is also evidence at Lynch Cove for liquefaction and a possible tsunami deposit associated with the uplift about 1,000 cal yr BP. A sand unit on top of the uplifted tidal flat forms a discontinuous layer as much as 80 cm thick, and has been interpreted both as a tsunami deposit (Bucknam et al., 1992; Hemphill-Haley, 1996; Bucknam et al., 1994; Jovanelly and Moore, 2009), and more recently as vented sediments (Jovanelly and Moore, 2009; Martin and Bourgeois, 2012). The deposit varies considerably in thickness and overall grain-size distribution, and has features such as source vents, intraclasts, and internal laminae that suggest the sand was vented from depth (Martin and Bourgeois, 2012). Previous workers considered the sand to be a tsunami deposit because of its extent, microfossil content, association with coseismic uplift, and because of an observation of the sand draping over a well-preserved log with bark (Bucknam et al., 1992; Bucknam et al., 1994; Jovanelly and Moore, 2009). In addition, the diatoms within the sand deposit correspond with those found living on the modern adjacent tidal flat (Hemphill-Haley, 1996). A potential source identified for the tsunami was the Alderwood landslide (Figure 2.2), ~ 4 km southwest of the marsh (Sarikhan et al., 2007). Other tsunami sources considered include a yet-unidentified submarine landslide, or possible rupture of the seafloor of Hood Canal by the Seattle fault (Blakely et al., 2002; Jovanelly and Moore, 2009).

2.2.5 *Discovery Bay*

Sixty kilometers to the north of Lynch Cove, on the Strait of Juan de Fuca, the tidal marsh at the head of Discovery Bay (Figures 2.1C, 2.3B) contains the longest record of tsunami deposits in Washington, with as many as nine Cascadia and/or intraplate tsunami deposits dating back 2,500 years (Williams et al., 2005). Like Lynch Cove, the marsh at Discovery Bay is at the head of a

narrow terminal embayment, a setting that amplifies tsunami waves. The low-lying areas at the head of Discovery Bay were flooded by the 1964 Mw 9.2 Great Alaskan earthquake Pacific Ocean tsunami, and 1-2 mm laminae of very fine sand, present in some parts of the marsh, were interpreted as possible deposits from that event (Williams et al., 2005).

Because there are more tsunami deposits at Discovery Bay than the number of subduction zone earthquakes identified on the outer coast of Washington during the last 2,500 years (Williams et al., 2005; Atwater et al., 2004), the deposits are likely from a combination of Cascadia tsunamis, local source tsunamis, and possibly transoceanic tsunamis as well (Williams et al., 2005). Discovery Bay Bed 1, the youngest tsunami deposit, was dated between 0–280 cal yr BP (minimum), and is assumed to be from the 1700 Cascadia tsunami. Beds 2 and 3, dated between 300–500 cal yr BP (maximum), and 540–790 cal yr BP (minimum), respectively; were ascribed to non-CSZ sources, such as tsunami from a crustal earthquake. Bed 4, dated between 960–1270 cal yr BP (close max), was considered to be from either the Cascadia W earthquake preserved on the Washington coast; or possibly from a tsunami or a tsunamigenic landslide triggered by the Seattle fault Restoration Point earthquake of 900–930 (Atwater, 1999; Williams et al., 2005; Nelson et al., 2014).

The tsunami deposits at Discovery Bay are similar in their appearance and geometry to the inferred tsunami deposits at Lynch Cove. Ages previously reported for the deposits at Discovery Bay have wide error bars, which hinders efforts assign individual tsunami deposits to a source. New radiocarbon ages for Discovery Bay tsunami deposits presented here improve correlations with other regional earthquake evidence, including the deposits at Lynch Cove. These results will help to differentiate between intraplate and CSZ events at Discovery Bay and Lynch Cove.

2.3 METHODS

2.3.1 *Field Methods*

The silt layers at Lynch Cove, herein named layer A (younger) and layer B (older), were mapped and described from channel bank exposures, dug pits, and gouge cores (25mm diameter) at more than 60 locations in the marsh. At each field location (Figure 2.5A), the absence or presence of each silt layer, layer thicknesses, depth from the surface, nature of upper and lower contacts, estimated grain size, sedimentary structures, and other notable characteristics were recorded. At the seaward edge of the marsh, where the sediment section of the last 1,000 years is thickest, two sediment monoliths were cut from the outcrop at a low tide bank exposure (Figure 2.5B, site 13.10.16). These monoliths were transported to the lab for detailed description and further sampling. Sediment samples from the adjacent tidal flat were also collected to compare to layers A and B.

2.3.2 *Grain Size Measurement*

Samples for grain size analysis were collected from layers A and B from outcrops and cores along the transect shown in Figure 2.5A. Fine sediment in the clay to coarse silt size range (14-5 φ) was measured in a solution of 0.05% sodium metaphosphate dispersant (NaO_3P) using x-ray analysis run on a SediGraphIII device. Grains coarser than very fine sand (4φ) were dry sieved in 1 φ increments. The coarse grain data was combined with the x-ray grain data for plotting.

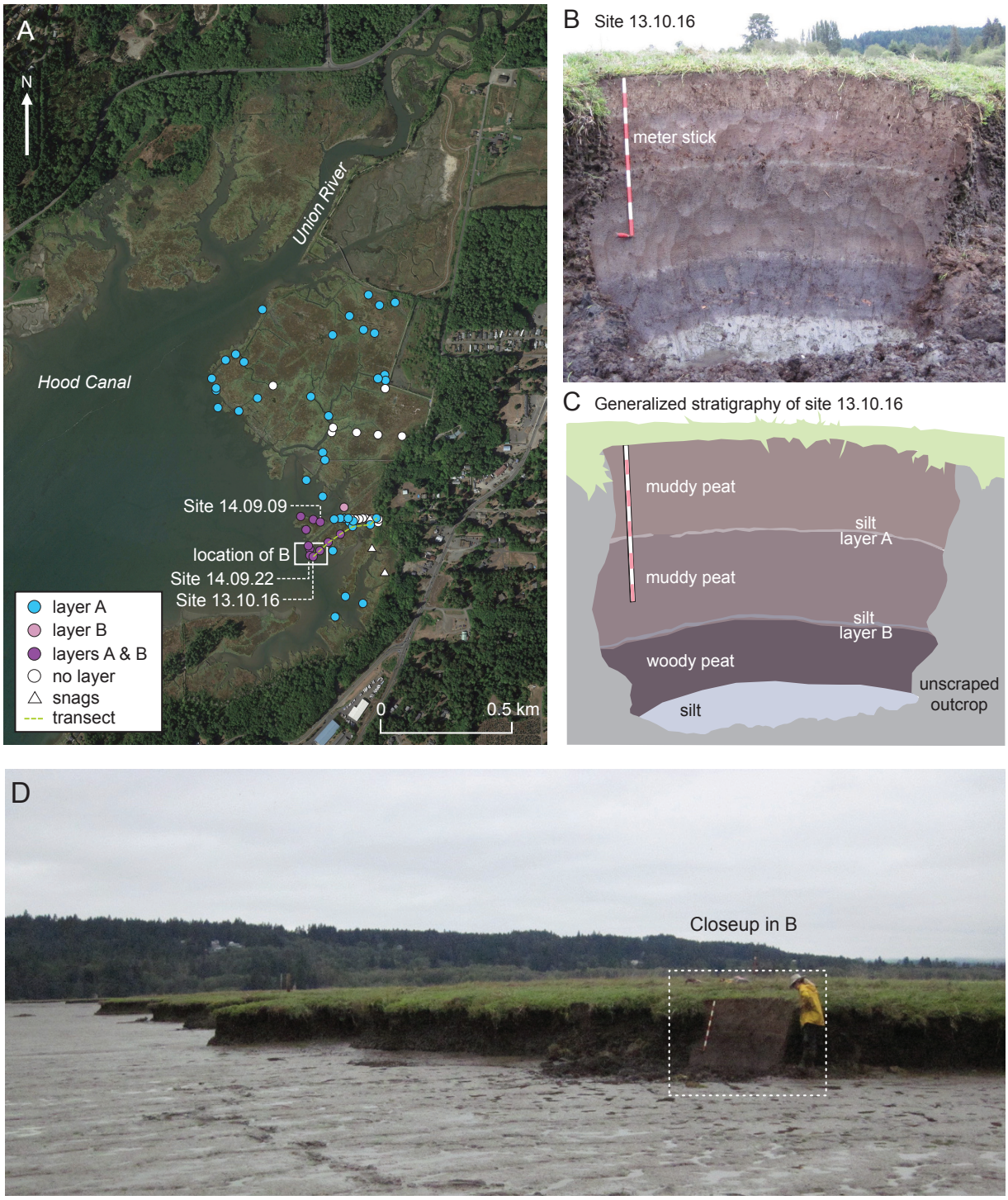

Figure 2.5. Locations of Lynch Cove marsh study sites and general stratigraphy of marsh. (A) Lynch Cove marsh study site showing locations of layers A and B, (B and C) outcrop and Generalized stratigraphy of site 13.10.16, with layers A (upper) and B (lower). There are between 3-5 cm of muddy peat below layer B. Layer B does not exactly coincide with the contact between the woody peat and the overlying muddy peat. (D) Eroding edge of marsh at location of (B) showing adjacent tidal flat.

2.3.3 *Diatom Collection and Sample Preparation*

Diatoms from layers A and B were compared to diatoms from peaty tidal marsh deposits directly above and below each layer. Diatoms from layers A and B were also compared to diatoms collected on the adjacent tidal flat, the potential sediment source area of A and B (seen in Figure 2.5D), and to diatoms collected at the site by Sherrod (1999). The diatom samples were sampled in the lab from the monoliths collected at outcrop location 13.10.16, the most expanded section in the marsh (Figure 2.5B).

Diatoms were sampled, prepared, and identified following standard methods. Samples were collected at ~10 cm intervals over the length of the 1.8 m section from location 13.10.16, with additional samples collected at closer intervals adjacent to two tsunami deposits. Diatom samples were prepared by reacting 1 cc of sediment with 100 ml of 35% H_2O_2 and gently heating to remove organics. Samples were rinsed with filtered water and centrifuged several times. Slides were made by allowing an aliquot of sediment and water to settle through a water column onto cover slips at the bottom of a 250-ml beaker for 8 hours (Warnock and Scherer, 2015). The coverslips were air dried, and then glued to slides with Meltmount mounting medium. Diatoms were counted to a minimum of 400 valves per slide at magnifications of 1000x, and 1500x as necessary for identification. Identifications were made using several widely-used diatom references (Hemphill-Haley, 1993; Hemphill-Haley and Lewis, 1996; Horn, 1987; Horn, 1992; John, 1983; Krammer and Lange-Bertalot, 1985; Krammer and Lange-Bertalot, 1986; Kramer and Lange-Bertalot, 1993; Krammer and Lange-Bertalot, 2001; Laws, 1988; Witkowski, 2000), and grouped into ecological assemblages following classification used in Oregon and Washington tidal environments (Hemphill-Haley, 1995; Sawai and Nagumo, 2003; Sawai et al., 2016; Sherrod, 1999), and from other studies of intertidal diatoms (Dura et al., 2015; Dura et al., 2016; Sawai et

al., 2017; Vos and de Wolf, 1993; Zong and Horton, 1998). A total of 109 diatom species were identified in 36 samples. Complete fossil diatom counts are in Appendix 4. A detailed statistical diatom environmental analysis and sea level reconstruction over the last 1,000 years at location 13.10.16 is described in Chapter 4.

2.3.4 *Radiocarbon Dating and OxCal Age Model*

Samples for radiocarbon dating were collected directly from outcrops in the field, or from slabs of outcrop sampled in the lab. Before submittal, radiocarbon samples were rinsed with water, picked clean under 30x magnification to remove any contaminating material, and allowed to air dry under an incandescent bulb. Dry samples were then re-examined under 30x magnification for contaminating material, and picked clean again as needed. Radiocarbon samples were submitted to Woods Hole (NOSAMS) for AMS analysis. Resulting ages were calibrated to cal yr BP using OxCal version 4.3.2 (Bronk Ramsey, 1995; Bronk Ramsey, 2009; Bronk Ramsey, 2017), and the IntCal 13 atmospheric curve (Reimer et al., 2013).

To constrain the ages of tsunami deposits, radiocarbon samples were selected strategically as either maximum or minimum ages. Twigs or other detrital material within tsunami deposits were treated as maximum ages, while marsh plant rhizomes or leaf bases above tsunami deposits were treated as minimum ages of the time of deposition. Marsh plant fossils submitted for radiocarbon dating were identified to the genus, and in some instances the species level to understand the typical position of the dated plant part with respect to the ground surface when in typical growth position. The leaf bases of the marsh plant *Triglochin maritima* were assumed to be at or near the paleomarsh surface when alive, so *Triglochin maritima* samples below the tsunami deposit were treated as maximum ages, while samples from above the tsunami deposit were treated as minimum ages. Plant rhizomes from above tsunami deposits were treated as minimum ages for

the deposit, but not as maximums when collected below a deposit, since they could be younger if the plant has deep rhizomes. Assigning ages as maximums and minimums guided the input of ages in an OxCal age model. A Bayesian sequence age model (Appendix 2) was constructed for both the Lynch Cove and Discovery Bay sites using OxCal software v 4.3.2 (Bronk Ramsey, 1995; Bronk Ramsey, 2009; Lienkaemper and Bronk Ramsey, 2009; Bronk Ramsey, 2017).

2.4 RESULTS

2.4.1 *Characteristics of Lynch Cove Layers A and B*

Figures 2.5B and 2.6 show how layers A and B typically appear in outcrop. Layers A and B are the same gray color as the adjacent tidal flat sediments, in contrast to the brown peaty mud deposits above and below. Both layers are thin, typically less than 3cm thick. Layer A is typically patchier than layer B, but B is also patchy in some outcrops. The patchy and thin layers are easily missed in narrow cores, but are visually distinct in outcrop. The layers have sharp basal and upper contacts. At two outcrops a fining upward grain size was observed in the field for both layers A and B, and at three other outcrops, the layer A was observed draping over woody roots. Some outcrops had what are possibly rip-up clasts associated with layer A, but these "chunks" are only in the back part of the marsh, in an area that may have been disturbed historically by cattle grazing. Appendix 1 contains Lynch Cove layer characteristics and outcrop locations. Figure 2.6 shows detailed stratigraphy and close-ups of the outcrop in Figure 2.5B.

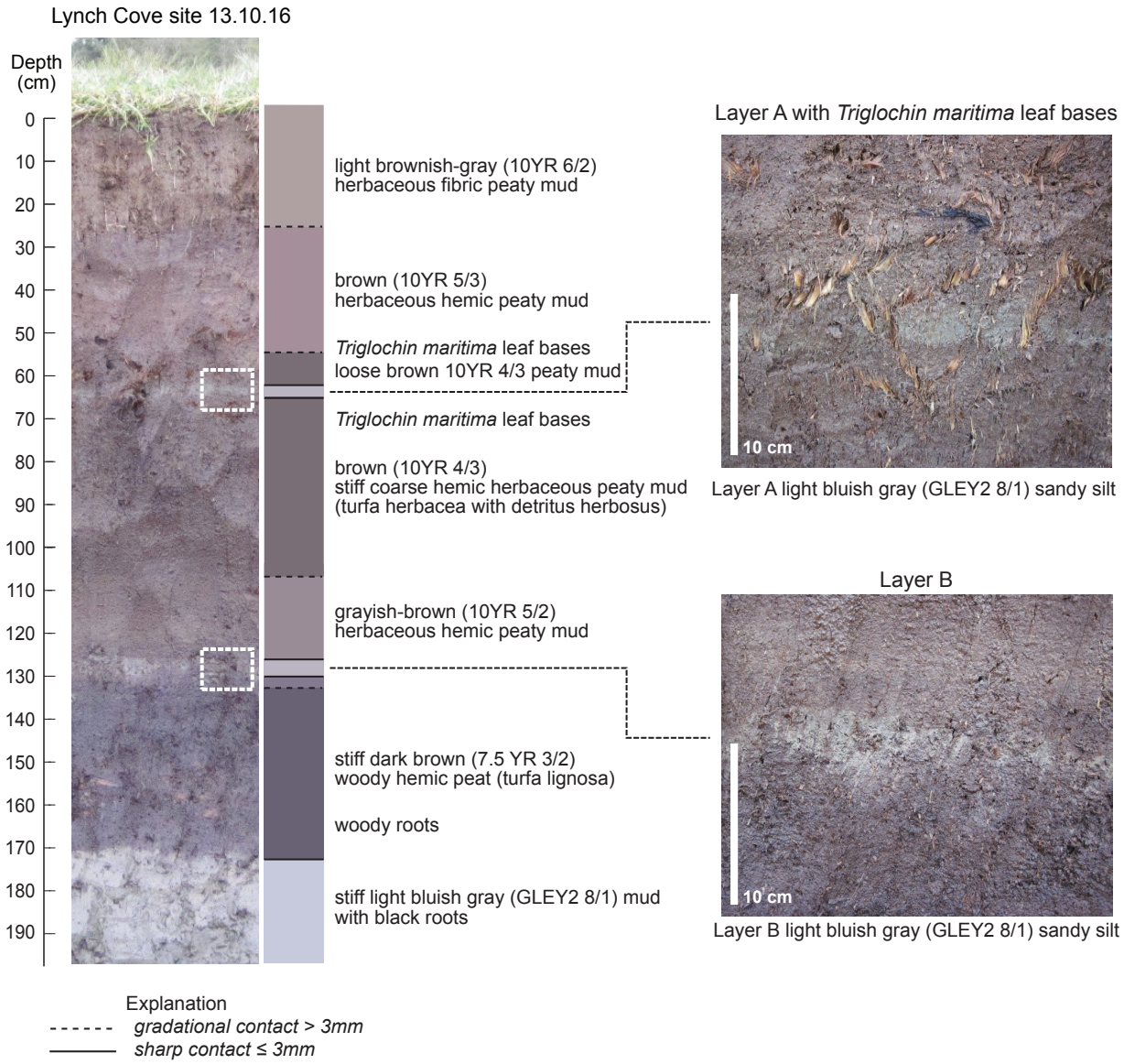

Figure 2.6. Stratigraphic section for Lynch Cove site 13.10.16. The base of the section is the tidal flat uplifted during an earthquake or earthquakes between 895–975 cal yr BP (Bucknam et al., 1994). Close-ups of layers A (top right) and B (bottom right) show detail of contacts and sediment color.

2.4.2 *Ages of Lynch Cove Layers A and B*

Lynch Cove radiocarbon samples were collected from outcrop locations 13.10.16, 14.09.09, and 14.09.22 (Figure 2.5A). Radiocarbon samples and calibrated ages from Lynch Cove are summarized in Table 2.1. Radiocarbon sample collection context and OxCal age model probability density functions for Lynch Cove samples are shown in Figure 2.7. The OxCal modeled age range for layer A is 1690–1830 A.D. (120–260 cal yr BP), and layer B is 1170–1230 A.D. (720–780 cal yr BP).

2.4.3 *Grain Size Data*

Both layers A and B have similar grain size, coarse silt with a small fraction of very fine sand. Both layers A and B display an overall fining inland trend (Figure 2.9). The clean silt in these layers differs in color and is coarser than the muddy peat marsh deposits above and below both layers, and is similar in color and grain size to the adjacent tidal flat sediments.

2.4.4 *Diatom Paleoecology*

Diatoms live in intertidal zone assemblages that, like marsh plants, are controlled by tidal exposure, salinity, and substrate (Hemphill-Haley, 1993; Dura et al., 2016). The Lynch Cove marsh intertidal zone is shown in Figure 2.10, with vascular marsh plants common to these zones, and tidal datums for the site. Figure 2.11 groups diatoms into intertidal affinities. Diatoms in each sample are plotted by ecological affinity to upper high marsh, lower high marsh to low marsh, and tidal flat environments. The most abundant species found in silt layers A and B include diatom species common on tidal flats including *Catenula adhaerens, Cocconeis scutellum*, *Dimeregramma minor*, *Fallacia oculiformis*, *Opephora pacifica*, *Seminavis eulensteinii,* and

Table 2.1. Lynch Cove Radiocarbon Samples

Sample number	Sample name	Laboratory number*	Laboratory reported age (^{14}C yr BP)	Calibrated age Cal AD (2 sigma probability)†	Calibrated age cal yr BP (before AD 1950)§	Material sampled, and context
1	03.09.23.03	Beta 192267	100 +/- 40	1680-1764 (30.8%) 1801-1939 (64.6%)	186-270	*Triglochin maritima* leaf base above A, minimum for layer A
2	13.10.16 RC9	NOSAMS 124763	100 +/- 20	1691-1730 (26.3%) 1810- 1925 (69.7%)	220-259	*Triglochin maritima* leaf base within A, minimum for layer A
3	03.09.23.01	NOSAMS 44820	80 +/- 40	1682-1738 (26.4%) 1758-1761 (0.5%) 1804-1937 (68.6%)	215-268	*Triglochin maritima* leaf base below A, maximum for layer A
4	13.10.16 RC4	Beta 400048	120 +/- 30	1679- 1765 (32.6%) 1800-1940 (62.8%)	185-271	*Triglochin maritima* leaf base 3.5 cm below A, maximum for layer A
5	13.10.16 RC8	NOSAMS 124762	165 +/- 20	1665-1695 (16.9%) 1726-1785 (46.2%) 1795-1814 (10.6%) 1838-1843 (0.5%) 1852-1868† (1.6%) 1917-1950† (19.7%)	255-285 165-224	*Triglochin maritima* leaf base 6.5 cm below A, maximum for layer A
6	15.05.08 RC2	NOSAMS 133045	330 +/- 15	1490-1603 (77.1%) 1613-1637 (18.3%)	347-460 313-327	*Triglochin maritima* leaf base 17.5 cm below A
7	15.05.08 RC1	NOSAMS 133044	400 +/- 15	1443-1491 (91.8%) 1602-1610 (3.6%)	459-507 340-348	*Triglochin maritima* leaf base 20 cm below A
8	14.09.22 RC4	NOSAMS 124767	800 +/- 20	1211-1270 (95.4%)	680-739	*Schoenoplectus sp.* rhizome within B, minimum layer B
9	14.09.22 RC3	NOSAMS 124766	860 +/- 20	1058-1075 (2.2%) 1153-1225 (93.2%)	875-892 725-797	*Schoenoplectus sp.* rhizome within B, minimum layer B
10	14.09.22 RC5	Beta 400047	870 +/- 30	1045-1095 (17.4%) 1120-1250 (78%)	855-905 700-830	*Schoenoplectus sp.* rhizome 1 cm above B, minimum layer B
11	14.09.09 RC3B	NOSAMS 124765	825 +/- 20	1170-1260 (95.4%)	690-780	Detrital twig in base of B, maximum layer B
12	14.09.09 RC2	Beta 400046	840 +/- 30	1059-1063 (0.4%) 1154-1264 (95%)	887-891 686-796	Detrital twig 1 cm below B, maximum layer B
13	14.09.09 RC3A	NOSAMS 124764	870 +/- 20	1052-1080 (7.8%) 1152-1220 (87.6%)	870-898 730-798	Detrital twig in base of B, maximum layer B
14	LYNCHCOVE 400	Beta 192266	260 +/- 50	(1492-1684) 1653-1845 (73.1%)# (1735-1806) 1896-1950 (17.2%)# 1931-1950 (5.1%)	256-458	Tree rings 3-6 from *Thuja plicata* snag, age of tree death#

*Laboratory name: Beta Analytic (Beta), National Ocean Sciences Accelerator Mass Spectrometry (NOSAMS).
†OxCal v4.3.2 Bronk Ramsey (2017); r:5 IntCal13 atmospheric curve (Reimer et al., 2013).
§Lynch Cove marsh mapped as tidal marsh in 1884 (Gilbert, 1884) with nearly the same extent as present day, limiting the younger end of calibrated age spans to pre-1884.
#Tree rings 3-6 (year of tree's life) dated out of 167 total in sample, with unknown number of outer (youngest) rings missing. Estimate of tree death requires adding 161 years to age obtained for rings 3-6

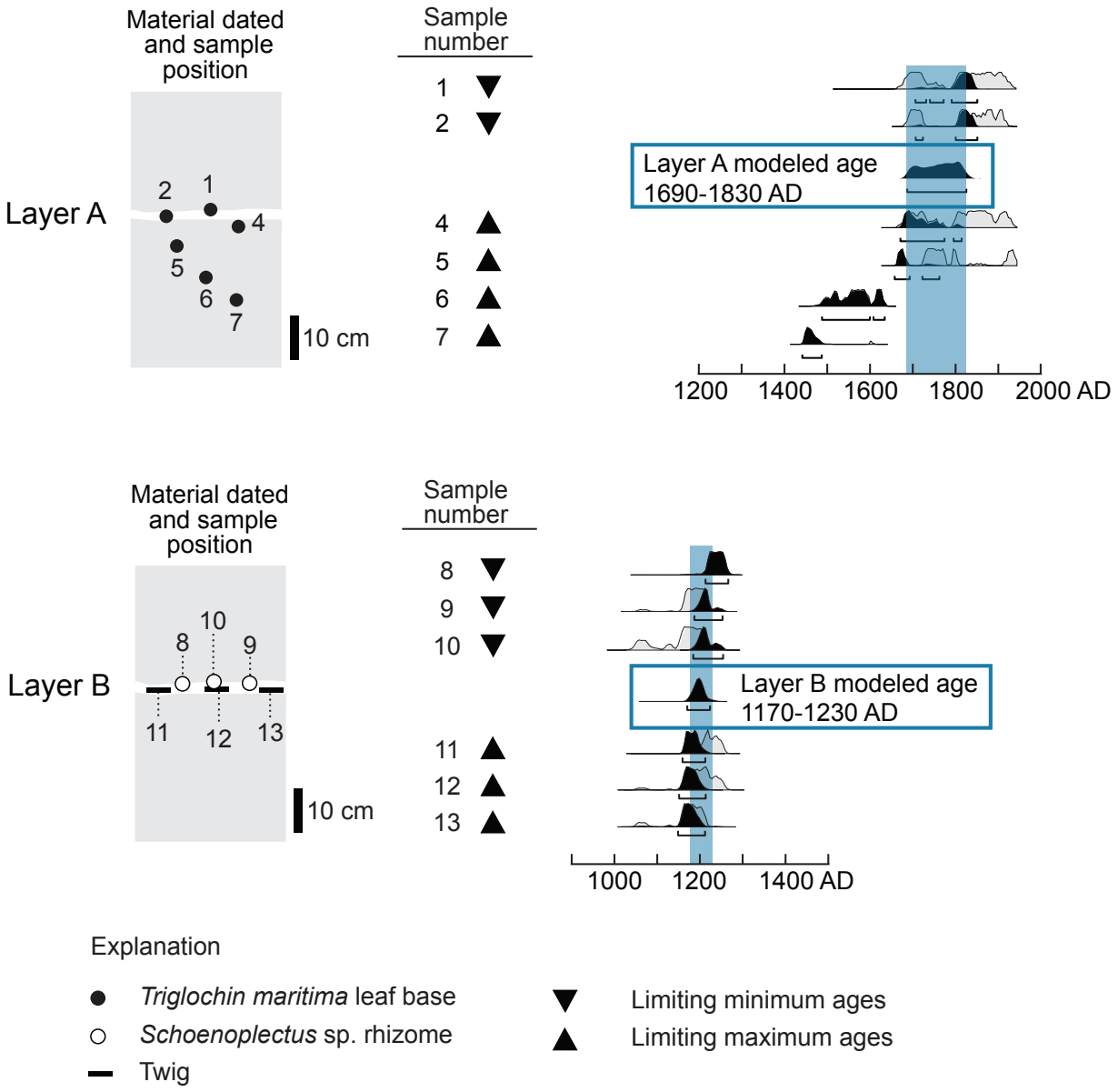

Figure 2.7. Schematic of radiocarbon sample positions relative to layers A and B and OxCal age model. Samples shown collected from the four outcrops labeled on Figure 2.4A. Sample numbers correspond to the samples in Table 2.1. Sampled material type indicated by symbols. Minimum and maximum ages noted by black triangles. OxCal model age probability density functions for layer A (above) and B (below). Individual radiocarbon sample calibrations are listed in Table 2.1. Modeled using OxCal version 4.3.2 (Bronk Ramsey, 1995; Bronk Ramsey, 2009; Bronk Ramsey, 2017), and calibrated with the IntCal 13 atmospheric curve (Reimer et al., 2013).

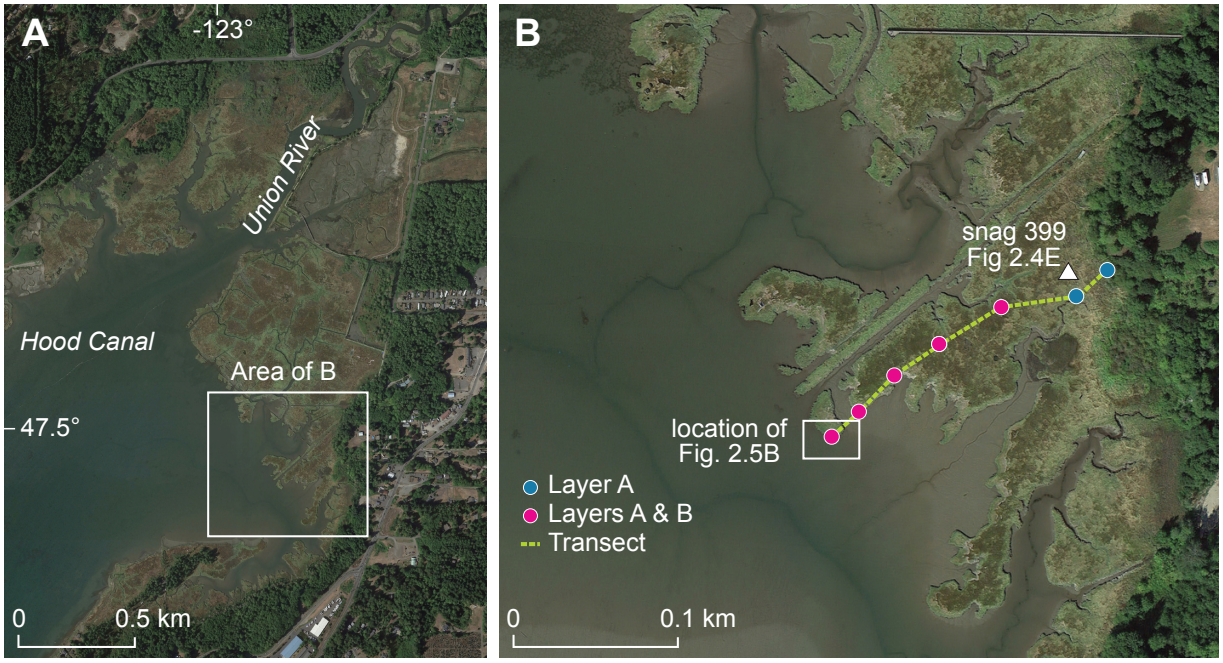

Figure 2.8. Lynch Cove grain size transect location. (A) Location of transect in Lynch Cove marsh, (B) Grain size transect line. Seaward edge of transect is at outcrop 13.10.16, as seen in Figure 2.4. Colored dots indicate either Layer A, or both Layers A and B were in the transect.

Tabularia fasciculata. These species differ from the abundant species both above and below each of these silt layers. Below layer B, upper high marsh diatoms including *Cosmioneis pusilla*, *Denticula subtilis*, and *Pinnularia lagerstedtii* are common. Above layer B, upper high marsh species decrease, and lower high marsh to low marsh species increase in relative percentage, including *Denticula subtilis, Diploneis interrupta, Diploneis pseudovalis, Caloneis bacillum, Luticola mutica,* and *Navicula peregrinopsis*. Above layer A, lower high marsh species are still abundant, but there is an increase in the percentage of diatoms that are common in the low marsh including *Navicula cincta, Navicula cryptotenella, Planothidium delicatulum, Pseudostaurosira brevistriata,* and *Staurosirella pinnata*. Figures 2.12-2.15 are photomicrographs of some of the species identified. Appendix 4 contains full diatom counts.

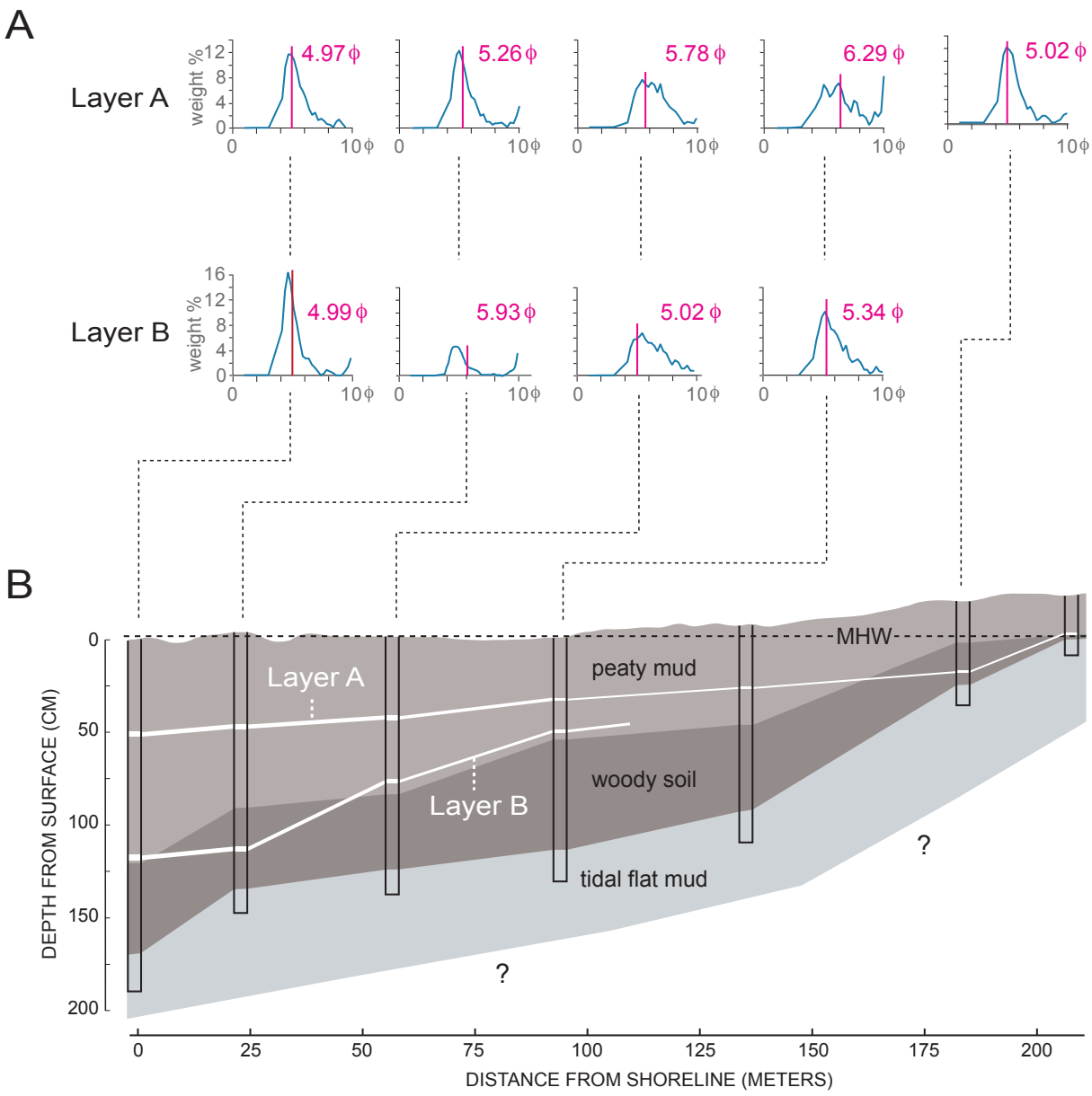

Figure 2.9. Lynch Cove grain size transect results for transect shown in Figure 2.8. (A) Grain size plots for layers A and B corresponding to cores and outcrops below in B. Mean grain size (in phi) for each sample is in pink. (B) Stratigraphy of cores and outcrops along transect. Depth from marsh surface on left axis, distance from shore inland to back edge of marsh on horizontal axis. MHW = elevation of modern mean high water datum.

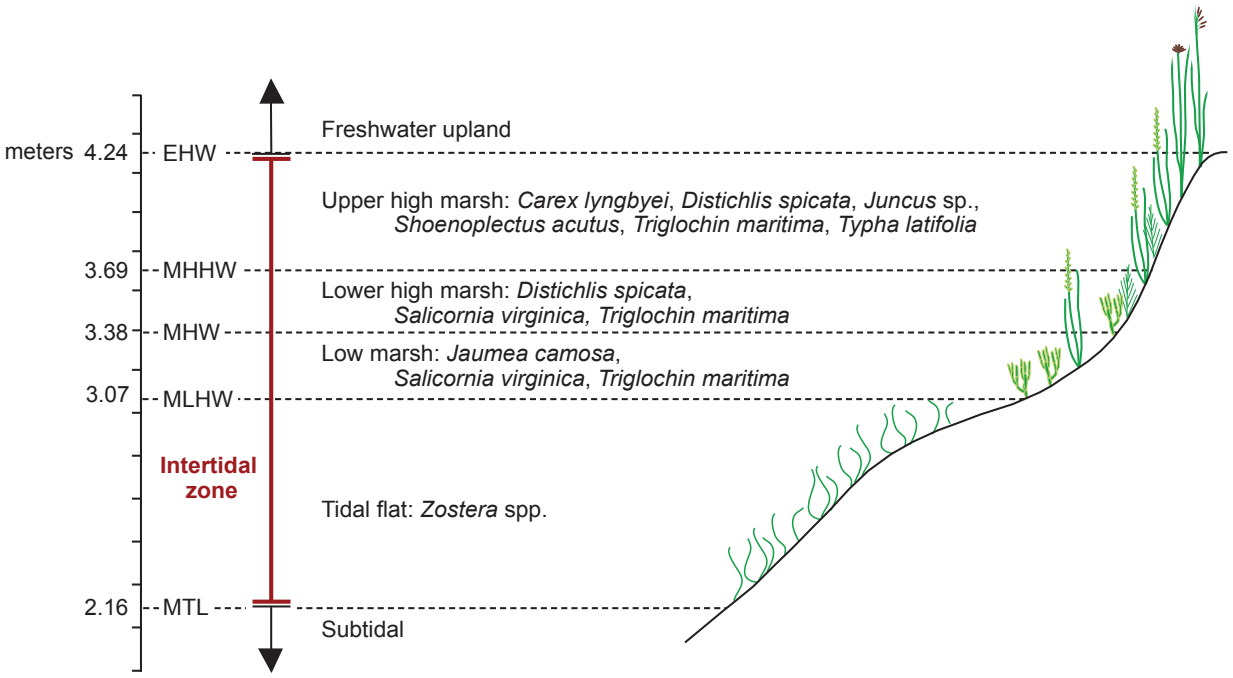

Figure 2.10. Lynch Cove tidal datums and vascular plant distribution in the intertidal zone. Drawing adapted from Witter et al. (2003), with plant distributions and tidal datums from Sherrod, 1999, and Lynch Cove Dock tide gauge.

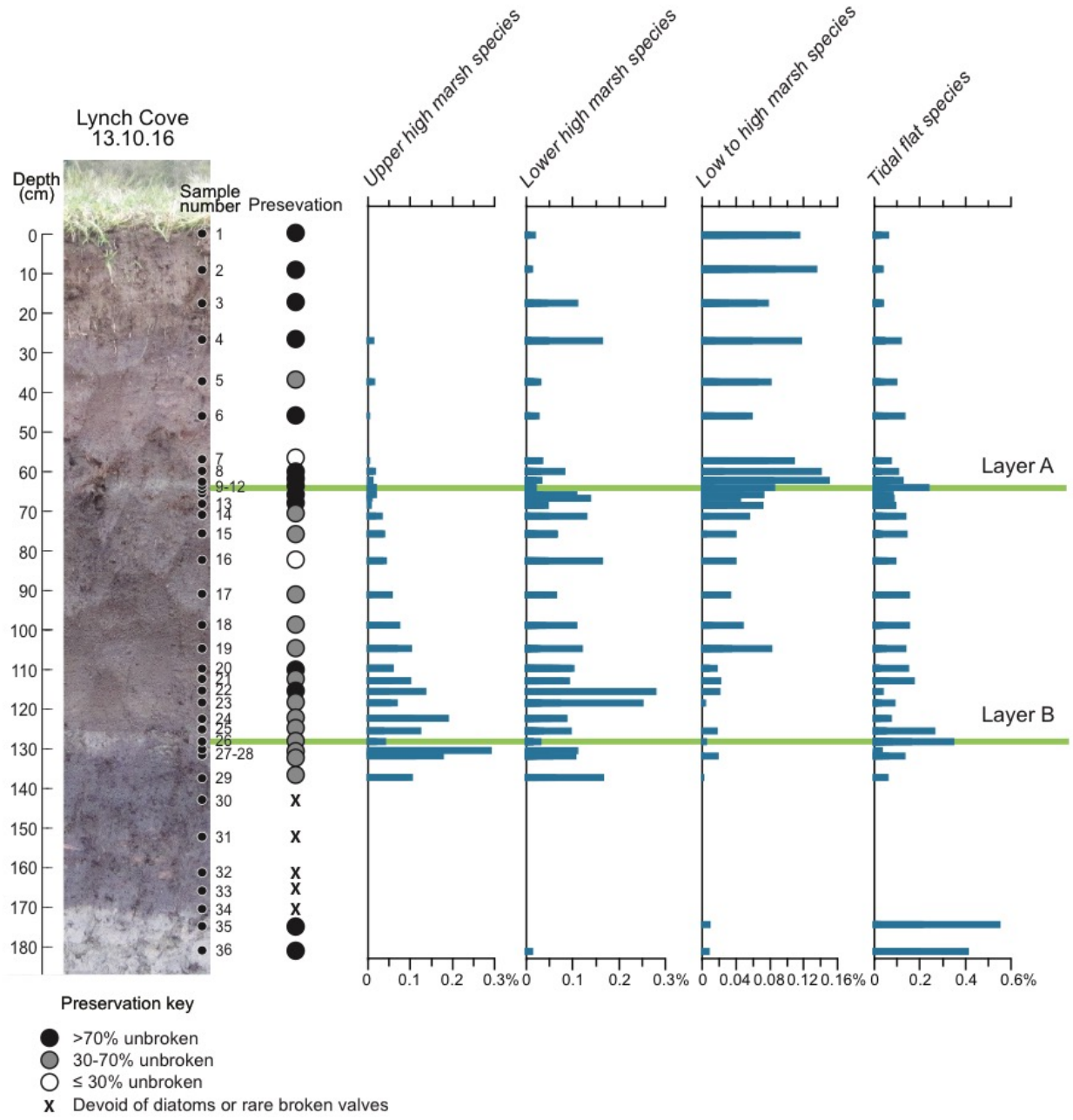

Figure 2.11. Lynch Cove diatom results for Lynch Cove outcrop 13.10.16 (location in Figure 2.5). Sample locations shown with numbered small black circles. Preservation is indicated by shaded circles where black is fewer broken, and white is most broken valves. Symbol X denotes samples with no or very few diatoms. On right, plots show select diatom species grouped by ecological affinity, and plotted as relative percentage of total species in each sample. Samples collected within layers A and B highlighted in green.

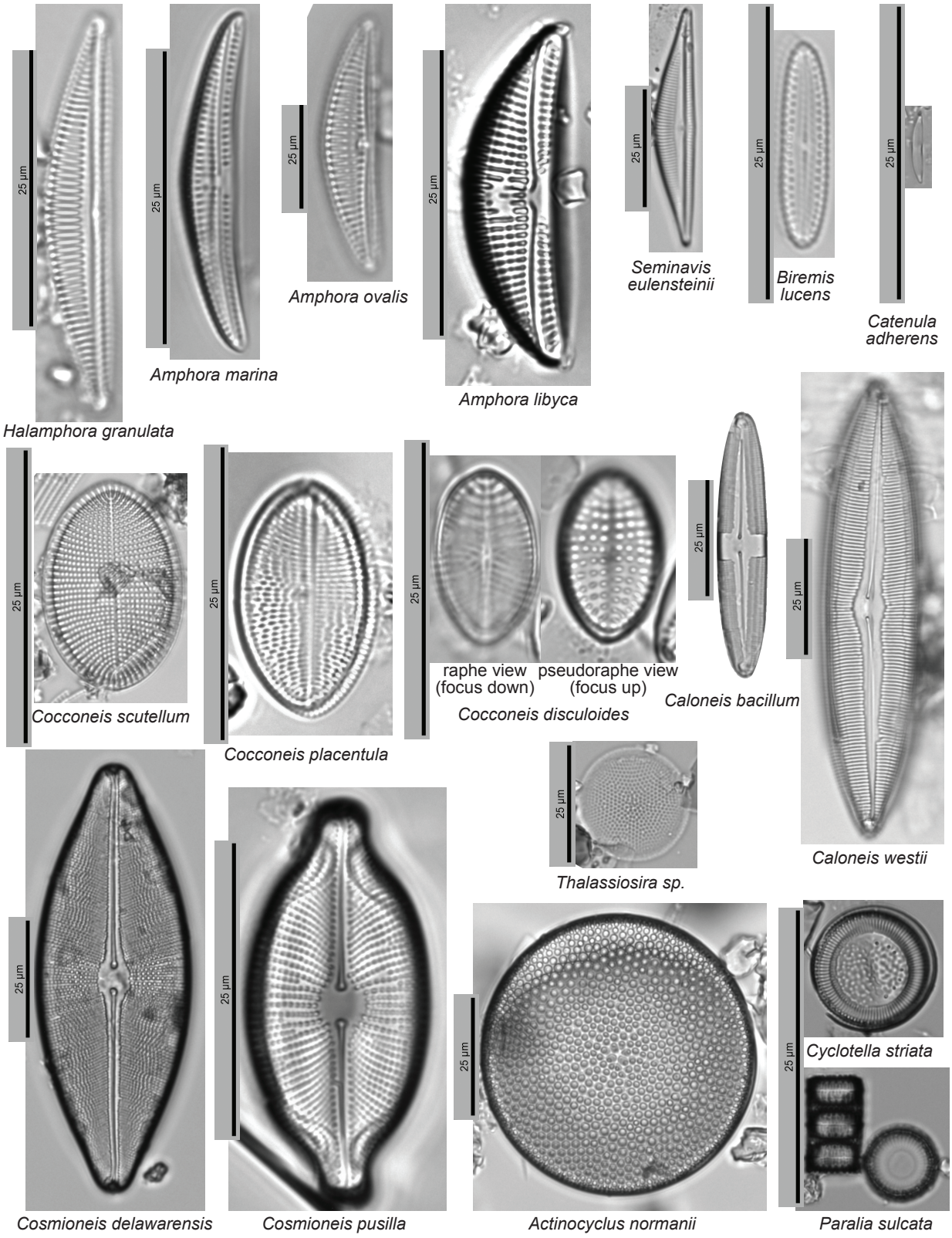

Figure 2.12. Diatom plate 1.

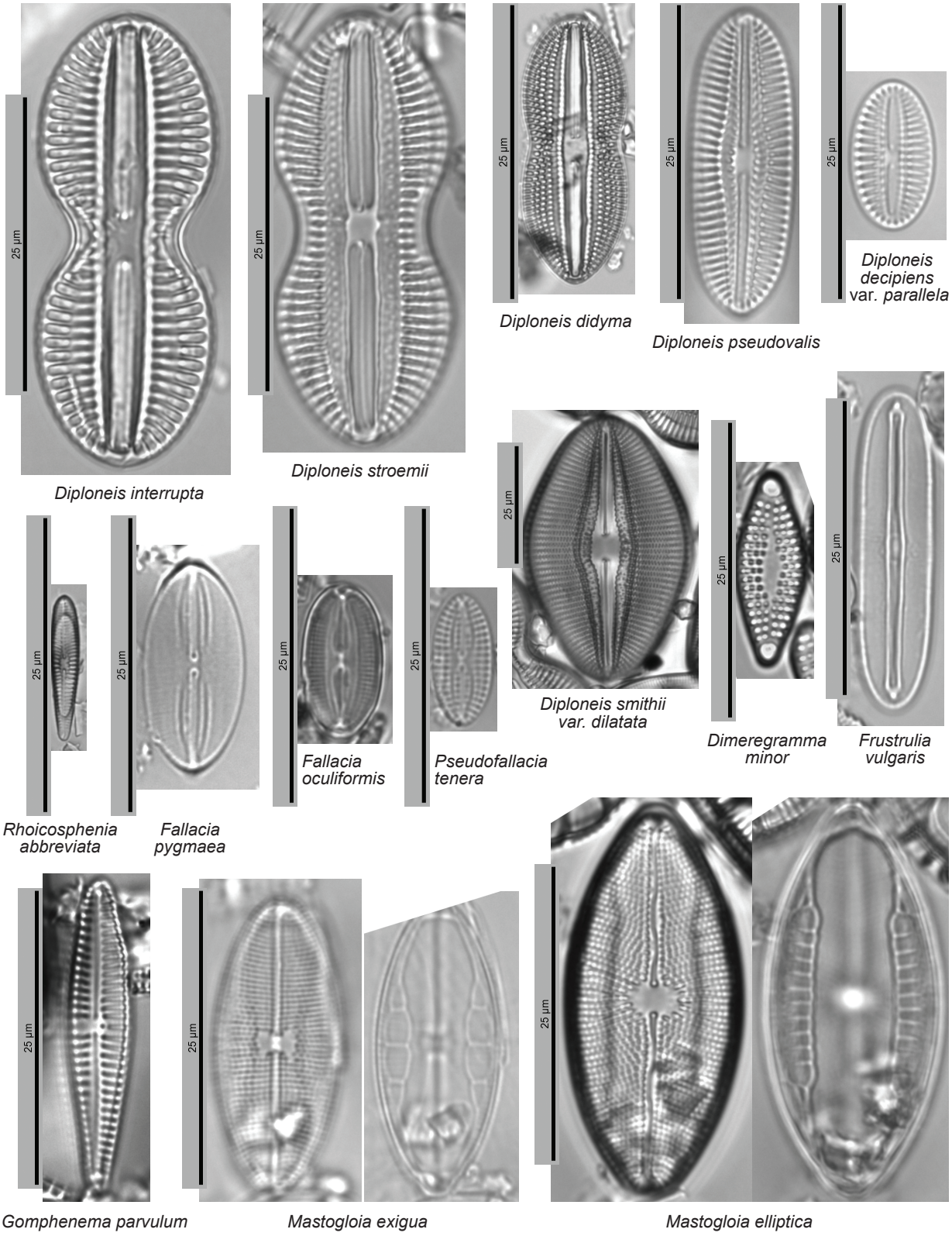

Figure 2.13. Diatom plate 2.

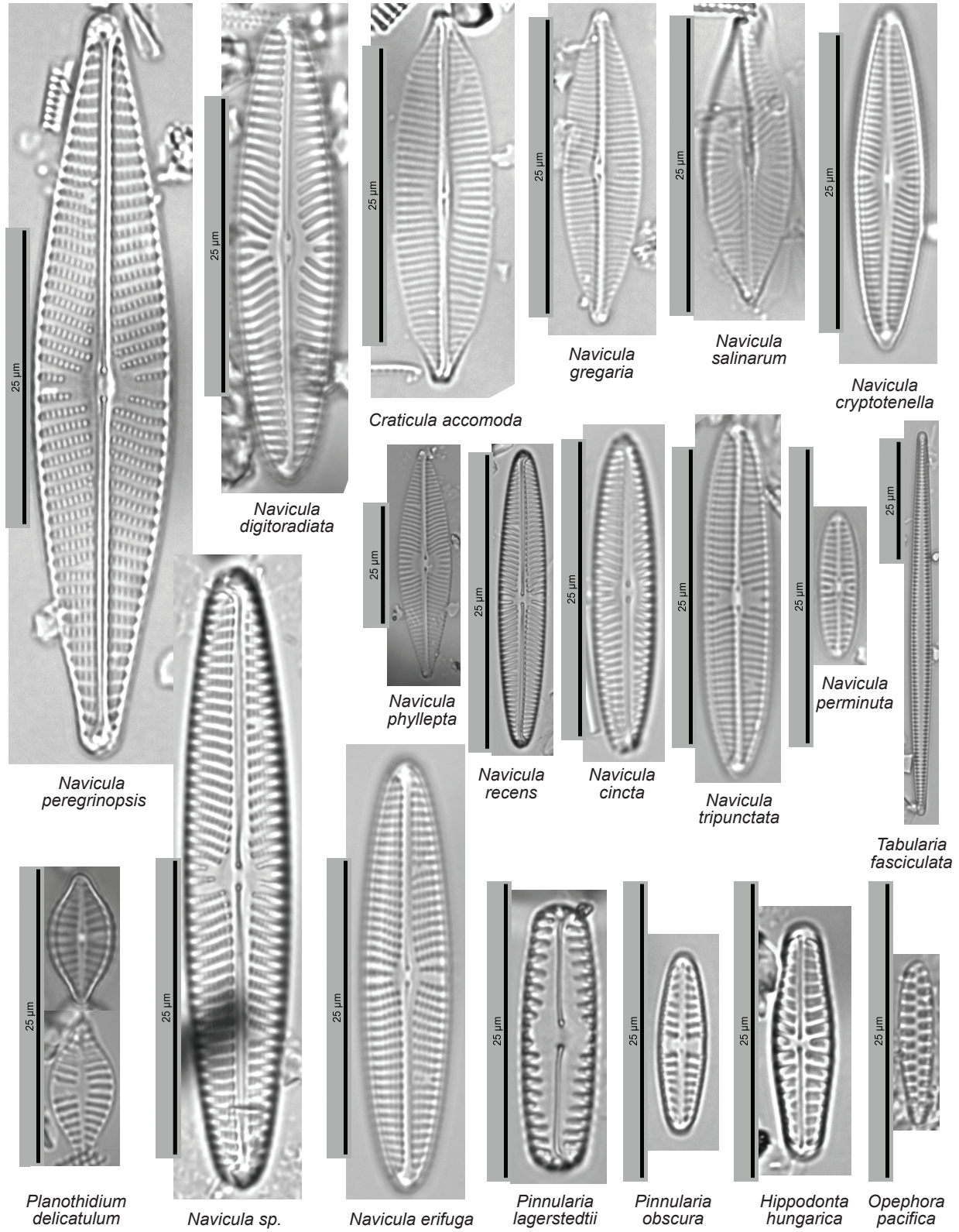

Figure 2.14. Diatom plate 3.

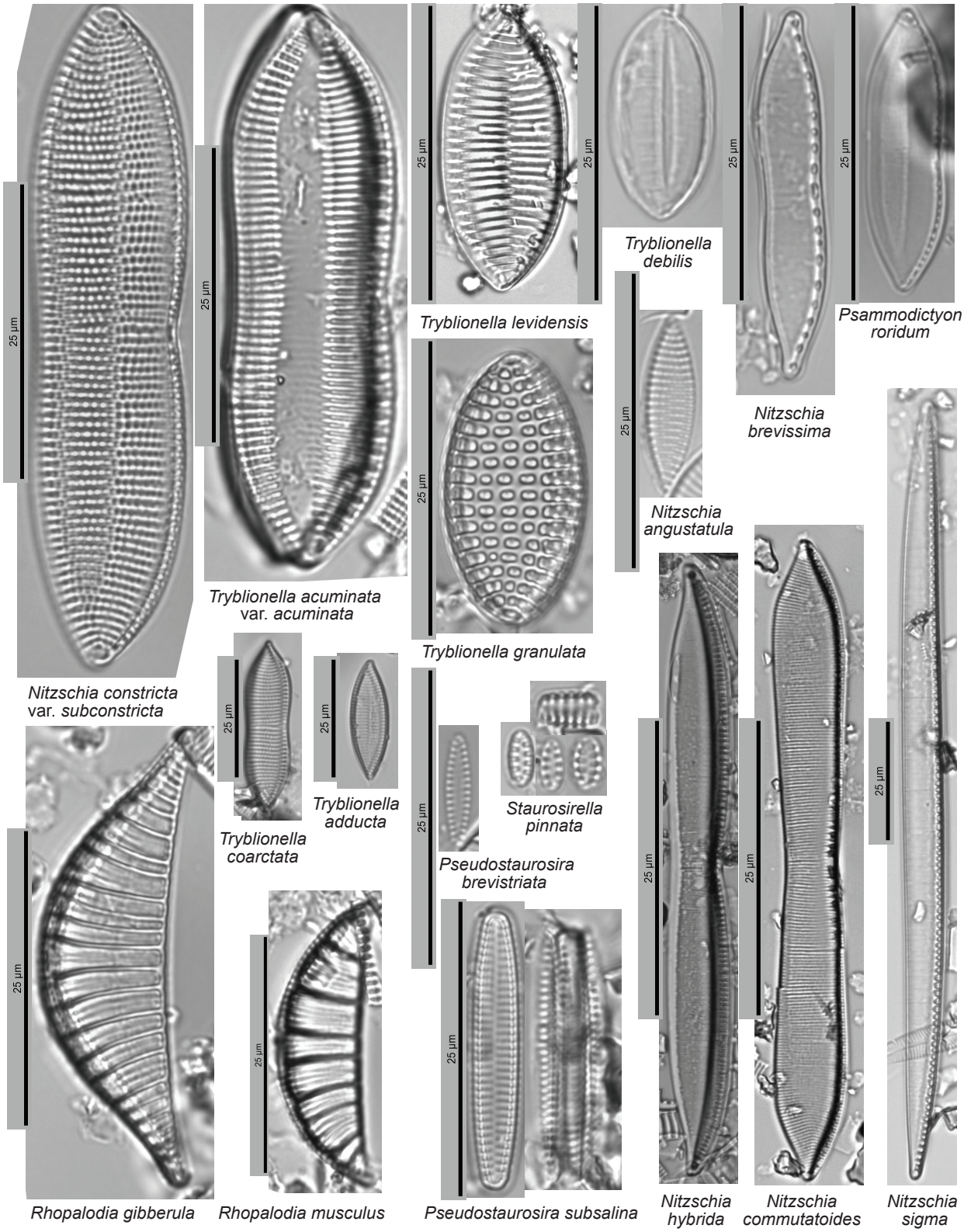

Figure 2.15. Diatom plate 4.

2.4.5 *Discovery Bay Beds 1-6 Ages*

To compare to ages from Lynch Cove, new samples from Discovery Bay were submitted for AMS radiocarbon dating for tsunami deposits Beds 2-6 at outcrops 16.06.17 (Figure 2.16), and 16.08.19 (Figure 2.17). A summary of samples collected and their calibrated ages is given in Table 2.2. The Discovery Bay OxCal model uses new AMS ages presented here combined with select ages from Williams et al. (2005). The sample collection context for Discovery Bay Bed 2 and the OxCal model probability functions for Beds 1-6 are shown in Figure 2.18. The OxCal modeled two sigma age ranges are as follows: Bed 1, 1585–1840 A.D. (110–1840 cal yr BP); Bed 2, 1319–1391 A.D. (559–631 cal yr BP); Bed 3, 944–1280 A.D. (670–1006 cal yr BP); Bed 4, 834–1195 A.D. (755–1116 cal yr BP); Bed 5, 658–745 A.D. (1205–1292 cal yr BP); and Bed 6, 321–677 A.D. (1273–1629 cal yr BP).

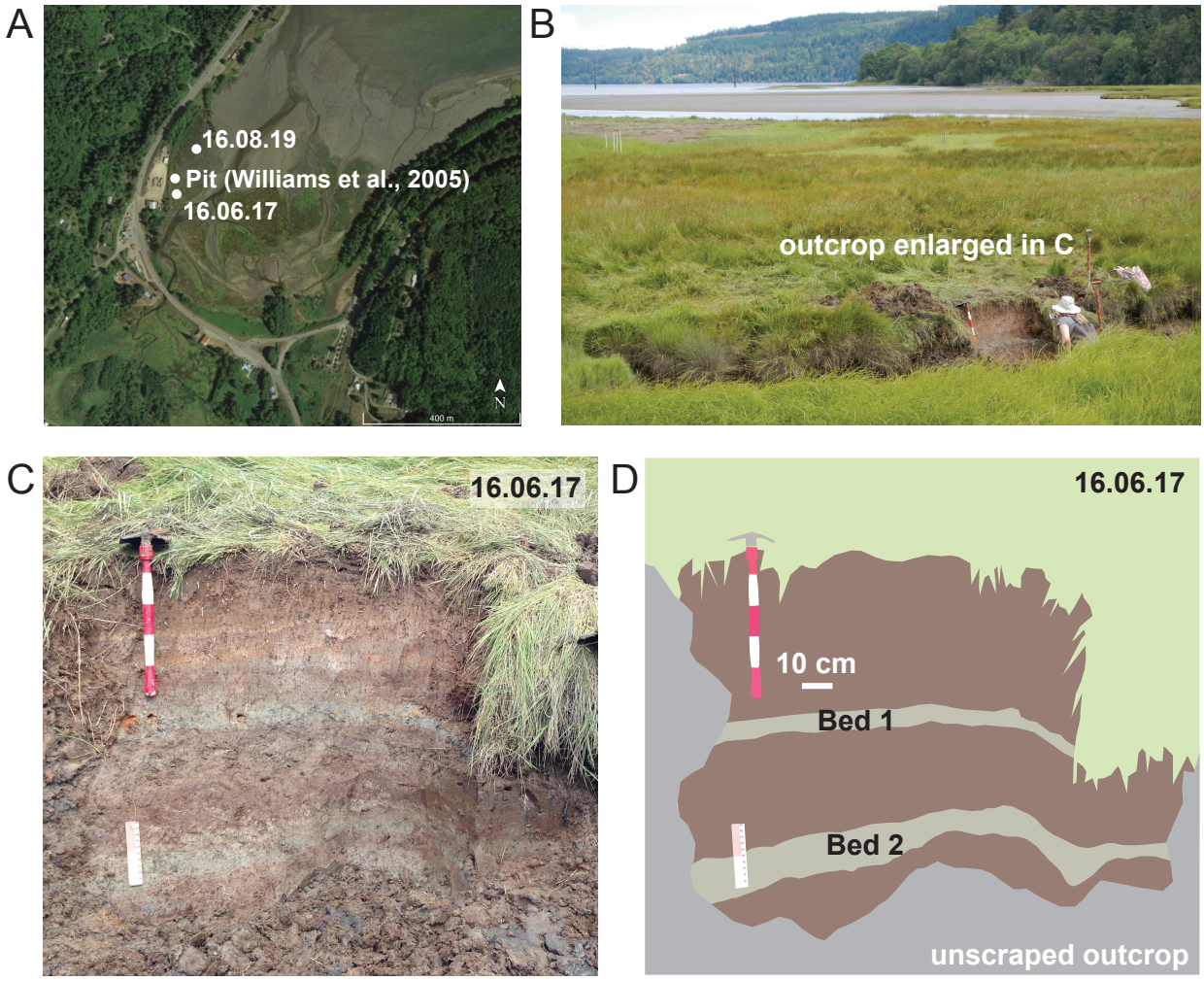

Figure 2.16. Discovery Bay field sites. (A) Location of outcrops. (B) overview of outcrop 16.06.17 looking to the northeast at low tide, with exposed tidal flat in the background, (C) close-up of outcrop 16.06.17 showing Beds 1 and 2, (D) interpretation of outcrop 16.06.07. Bed 1 is probably from the 1700 A.D. Cascadia tsunami.

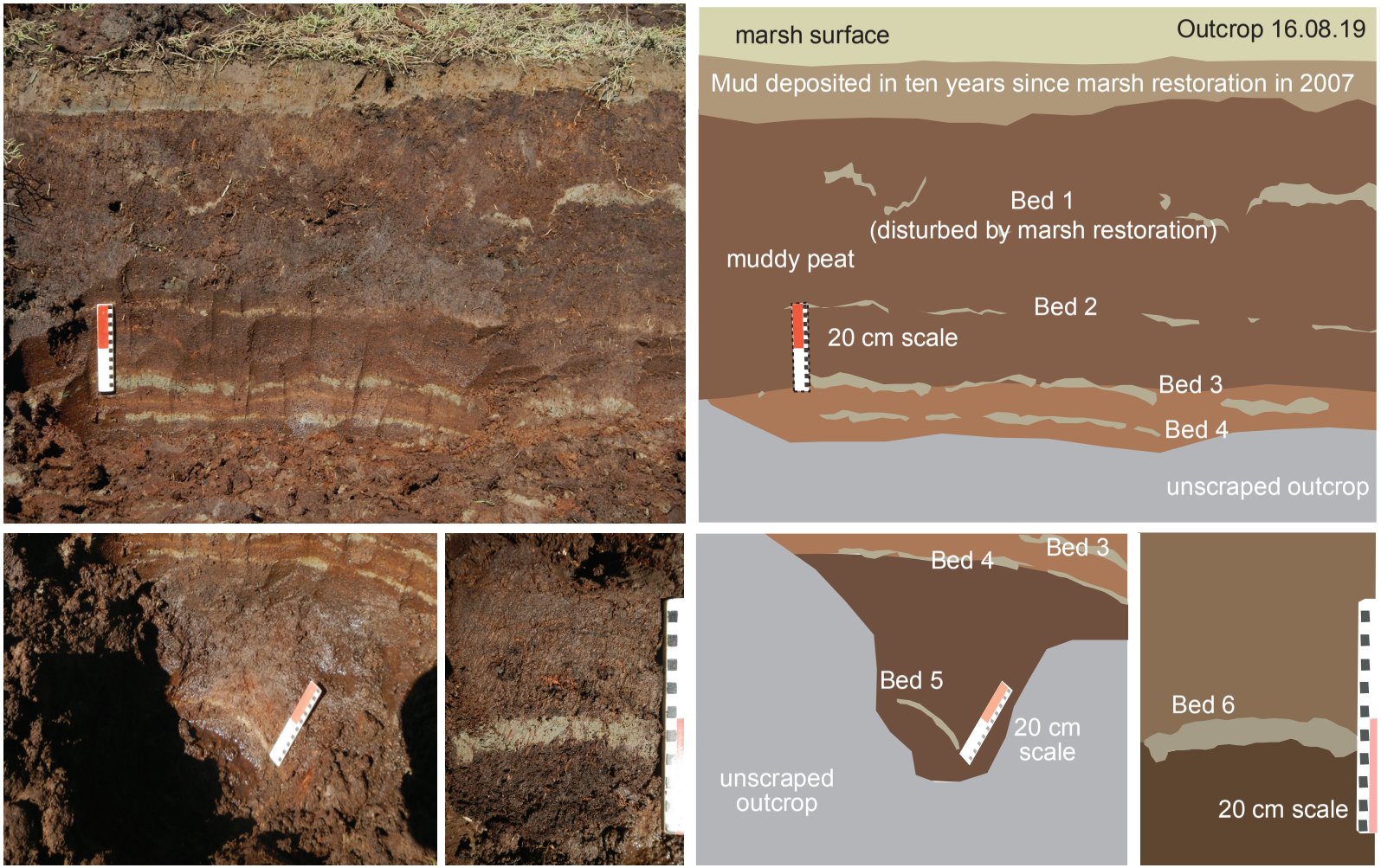

Figure 2.17. Discovery Bay Beds 1-6 at outcrop 16.08.19. Location of outcrop 16.08.19 shown in Figure 2.16A. Layer of mud on top of outcrop has aggraded on the marsh surface since it was restored in 2007. Scale bar in each panel is 20 cm Photographs on left, annotation on right.

Table 2.2. Discovery Bay Radiocarbon Samples

Sample number	Sample name	Laboratory number*	Laboratory reported age (^{14}C yr BP)	Calibrated age† Cal AD (2 sigma probability)	Calibrated age cal yr BP (before AD 1950)	Material sampled, and context
1	16.06.17 RC4	NOSAMS 139063	610 +/- 20	1298-1372 (75.5%) 1378-1400 (19.9%)	578-652 550-572	Triglochin maritima rhizome from the top of Bed 2, close minimum Bed 2
2	16.06.17 RC1	NOSAMS 139061	635 +/- 20	1288-1325 (38.5%) 1345-1394 (56.9%)	625-662 556-605	Triglochin maritima rhizome from within Bed 2, close minimum Bed 2
3	16.06.17 RC3	NOSAMS 139062	600 +/- 15	1304-1365 (75.2%) 1383-1403 (20.2%)	585-646 547-567	*Triglochin maritima* rhizome from within Bed 2, close minimum Bed 2
4	16.06.17 RC5	NOSAMS 139064	595 +/- 15	1305-1364 (73.6%) 1384-1405 (21.8%)	586-645 545-566	*Triglochin maritima* rhizome from 0.5 cm below Bed 2, close maximum Bed 2
5	16.06.17 RC2 A	NOSAMS 139061	685 +/- 20	1273-1305 (74.1%) 1364-1385 (21.3%)	645-677 565-586	*Triglochin maritima* rhizome from 2 cm below Bed 2, close maximum Bed 2
6	16.08.19 RC8A	NOSAMS 140212	590 +/- 20	1304-1365 (70.2%) 1384-1409 (25.2%)	585-646 541-566	*Triglochin maritima* rhizome from 6 cm below Bed 2
7	16.08.19 RC9	NOSAMS 140213	610 +/- 25	1297-1402 (95.4%)	548-653	*Triglochin maritima* rhizome from 11 cm below Bed 2
8	16.08.19 RC6	NOSAMS 140211	670 +/- 20	1278-1310 (56.3%) 1360-1388 (39.1%)	640-672 562-590	Herbaceous root cutting through Bed 3, close minimum for Bed 3
9	16.08.19 RC12	NOSAMS 140215	1180 +/- 20	772-893 (95.4%)	1057-1178	*Triglochin maritima* rhizome from 12 cm below Bed 4, maximum age Bed 4
10	16.08.19 RC10	NOSAMS 140214	1260 +/- 20	677-775 (95.4%)	1175-1273	Twig 15 cm below Bed 4, maximum age Bed 4
11	16.08.19 RC13	NOSAMS 140216	1300 +/15	665-718 (64.2%) 742-767 (31.2%)	1232-1285 1183-1208	*Bolboschoenus sp.* rhizome 20 cm below Bed 4, minimum for Bed 5 and maybe 4
12	16.08.19 RC17	NOSAMS 140217	1740 +/- 20	241-356 (92%) 366-380 (3.4%)	1594-1709 1570-1584	Twig 1 cm below Bed 6, close maximum Bed 6

*Laboratory name: Beta Analytic (Beta), National Ocean Sciences Accelerator Mass Spectrometry (NOSAMS).
†OxCal v4.2.4 (2013); r:5 IntCal13 atmospheric curve (Reimer et al., 2013).

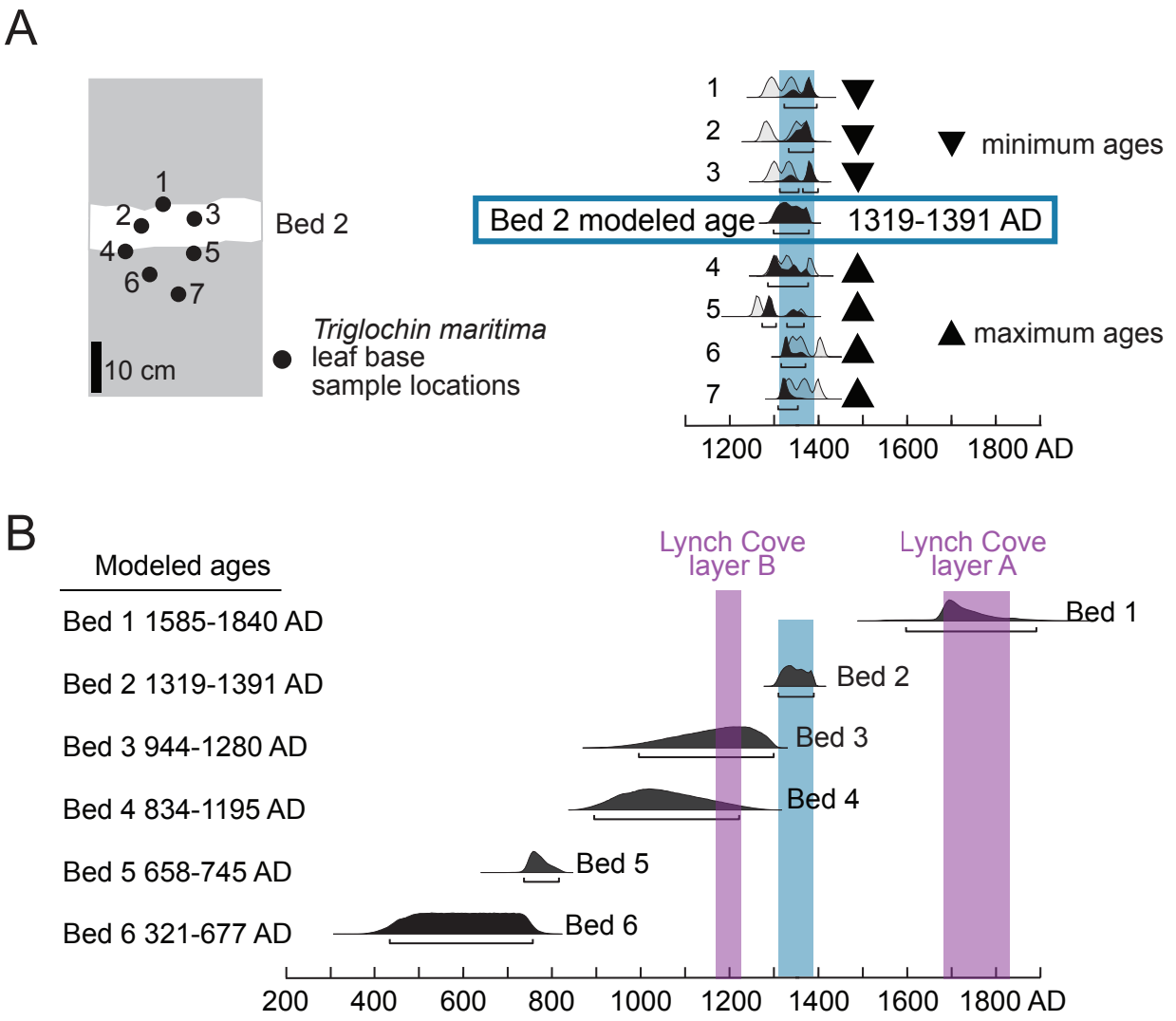

Figure 2.18. Radiocarbon dating results for Discovery Bay. (A) Sampling strategy for radiocarbon dating of Bed 2, composite from sites 16.07.17 and 19.08.19 shown in Figure 2.16A. Stratigraphic positions of radiocarbon samples of leaf bases of the marsh plant *Triglochin maritima* relative to Bed 2 indicated by numbered black dots. *Triglochin maritima* leaf bases grow at or near the marsh surface, so represent the age of a stratigraphic horizon from which they are collected. OxCal modeled age of Bed 2 with sample probability density functions (PDFs), minimum/maximum ages noted by black triangles. Sample numbers correspond to the samples in Table 2.2. (B) OxCal age model PDFs for Discovery Bay Beds 1-6 based on new radiocarbon dates from Table 2.2, and select ages for Beds 3, 4, 5, and 6 from Williams et al. (2005). Individual radiocarbon sample calibrations are listed in Table 2.2. Modeled using OxCal version 4.3.2 (Bronk Ramsey, 1995; Bronk Ramsey, 2009; Bronk Ramsey, 2017), and calibrated with the IntCal 13 atmospheric curve (Reimer et al., 2013).

2.5 DISCUSSION

2.5.1 *Are Layers A and B Tsunami Deposits?*

Layers A and B from Lynch Cove have characteristics common in tsunami deposits. Tsunami deposits are typically thin but patchy sheets distributed over a wide area, that thin and rise in elevation in the landward direction (Morton et al., 2007; Goff et al., 2004). Tsunami deposit sediments typically have sharp basal contacts, are either massive or normally graded, and exhibit landward grain size fining (Dawson and Shi, 2000; Tuttle et al., 2004; Morton et al., 2007). Layers A and B both have sharp basal contacts, and show a landward thinning, rising, and fining trend (Figure 2.9). The sediment grain size in tsunami deposits can range from very fine muds to boulders, and is dependent upon the grain size of the source material (Bourgeois, 2009). Most of the sediments of layers A and B are within the silt size range, and fine inland; with some deviation from this trend at the back edge of the marsh for layer A, and from the second sample from the seaward edge for layer B. Reasons for these deviations may include the relatively short transect of 212 meters that may not be long enough to adequately characterize the grain size trend. Additionally, a tsunami inundating the head of Hood Canal may produce eddies that could cause more variation in grain size distributions than deposits from open coastlines.

Layers A and B at Lynch Cove (Figure 2.5) are similar in appearance to the tsunami deposits at Discovery Bay (Figure 2.16, 2.17). They are slightly finer-grained than the tsunami deposits at Discovery Bay, which are in the silt to very fine sand range (Williams et al., 2005). This may reflect decreased energy of tsunami waves by the time they reach Lynch Cove, or it may be the result of a finer overall sediment source.

2.5.2 *Diatom Evidence of Tsunami*

Diatoms can help identify tsunami deposits when the deposits contain the same diatom assemblages as the sediments from the inferred source area (Hemphill-Haley, 1995; Hemphill-Haley, 1996; Horton et al., 2011; Dura et al., 2016). Diatoms from layers A and B contain many of the same tidal flat diatom species found in samples of older tidal flat sediments from the base of the section (Figure 2.11), and also contain species found on the adjacent tidal flat in this study and by Sherrod (1999). This suggests that the tidal flat silt was the source of the sediment in layers A and B. This supports deposition by a landward surge of water that both eroded the tidal flat sediments, and deposited the sediment on top of the tidal marsh, as would be consistent with deposition by tsunami.

Distinctive diatom assemblages occupy different intertidal elevation zones, and these distributions are cosmopolitan in temperate climates (Hemphill-Haley, 1995; Hemphill-Haley, 1996; Dura et al., 2016; Sawai et al., 2016; Sawai et al., 2017). There is a higher abundance of mid-to-high marsh diatoms above and below layers A and B, which indicates that layers A and B represent a change from usual diatom assemblages both before and after deposition (Figure 2.11). A similar lower proportion of tidal flat diatoms is seen in the high, mid-to-high, and low-to-mid marsh species between layers A and B. Note that tidal flat species are present in a relatively stable proportion throughout the section. This may be from tidal mixing, or it may show distribution being influenced by the muddy sediment input. Some studies suggest that substrate is an important control on species distribution as much as elevation in the tidal zone. In a study of diatom distribution in Washington and Oregon coast tidal marshes, Sawai et al. (2016) found that the presence of mud was the strongest control over diatom distribution. Elevation or tidal exposure, and salinity were found to be secondary influences of diatom distribution. Because the tidal marsh

at Lynch Cove is adjacent to a large muddy tidal flat, clay and silt sized grains are the dominant grain size in the sedimentary record of the last 1,000 years.

Because distinctive assemblages of diatoms occupy different levels in the intertidal zone, fossil diatoms from tidal marsh sediment records can be used to characterize paleoenvironment either by determining relative abundance of diagnostic species in fossil samples, or by employing statistical transfer function methods that compare the distribution of living diatoms with fossil diatoms. Using these quantitative methods, diatoms have been used to reconstruct paleo-sea level in tidal marsh sites as a way to determine coseismic land level change (Dura et al., 2015; Dura et al., 2016; Sawai et al., 2004a; Sawai et al., 2004b; Sawai, 2009; Shennan and Hamilton, 2006; Watcham et al., 2013; Wang et al., 2013). Chapter 4 contains a quantitative transfer function reconstruction of paleoenvironment and relative sea level over the last ~1,000 years at Lynch Cove.

2.5.3 *Comparison of Layers A and B Ages with Regional Paleoseismic Evidence*

Figure 2.19 compares ages of Lynch Cove layers A and B, the new Discovery Bay ages, and other paleoseismic evidence from the Puget Sound region from the last 1200 years. Sites are grouped by the source of the paleoseismic evidence preserved: intraplate earthquakes, Cascadia earthquakes, and sites that record evidence of both intraplate and Cascadia earthquakes including coseismic land level change, tsunamis, slope failures, or liquefaction.

The 2-sigma age range of layer A has an OxCal modeled age of 1690–1830 A.D. (Figure 2.7). Radiocarbon ages for the time period within about 300 cal yr BP calibrate to wide ranges in calendar years because of the broad flat plateau in the calibration curve for that time period (Reimer et al., 2013). Because the edge of the marsh where radiocarbon samples were collected for layer A is nearly unchanged since the marsh was first mapped in 1884 (Figure 2.4), the age of layer A is almost certainly closer to the older end of the modeled age range.

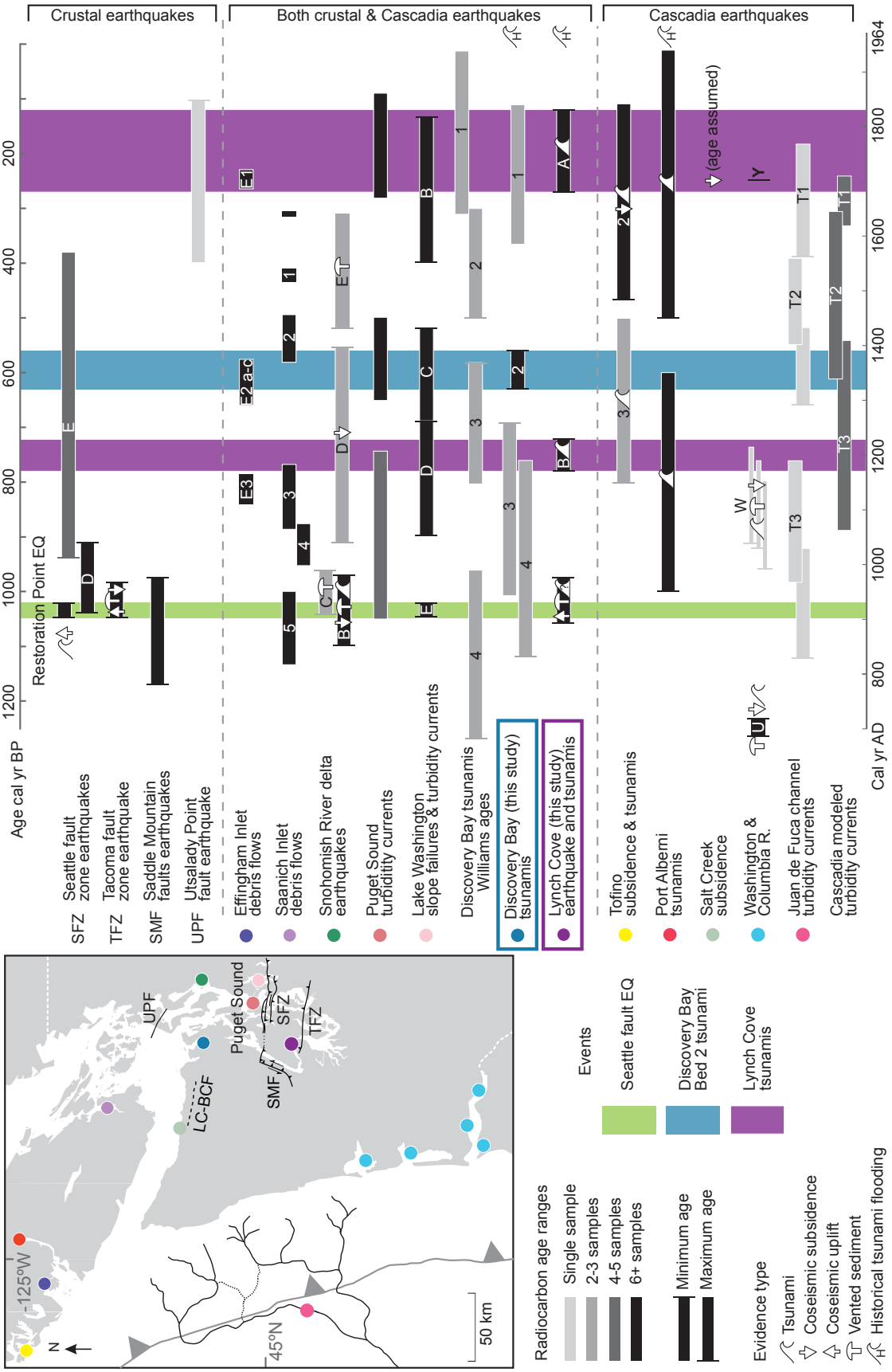
Crustal earthquakes
Both crustal & Cascadia earthquakes
Cascadia earthquakes
Age cal yr BP
Cal yr AD
1200
1000
800
600
400
200
800
1000
1200
1400
1600
1800
1964
Restoration Point EQ
(age assumed)
SFZ Seattle fault zone earthquakes
TFZ Tacoma fault zone earthquake
SMF Saddle Mountain faults earthquakes
UPF Utsalady Point fault earthquake
Effingham Inlet debris flows
Saanich Inlet debris flows
Snohomish River delta earthquakes
Puget Sound turbidity currents
Lake Washington slope failures & turbidity currents
Discovery Bay tsunamis Williams ages
Discovery Bay (this study) tsunamis
Lynch Cove (this study) earthquake and tsunamis
Tofino subsidence & tsunamis
Port Albemi tsunamis
Salt Creek subsidence
Washington & Columbia R. turbidity currents
Juan de Fuca channel turbidity currents
Cascadia modeled turbidity currents
-125°W
45°N
N
50 km
UPF
LC-BCF
Puget Sound
SMF
SFZ
TFZ
Events
Seattle fault EQ
Discovery Bay Bed 2 tsunami
Lynch Cove tsunamis
Radiocarbon age ranges
Single sample
2-3 samples
4-5 samples
6+ samples
Minimum age
Maximum age
Evidence type
Tsunami
Coseismic subsidence
Coseismic uplift
Vented sediment
Historical tsunami flooding

(Previous Page) Figure 2.19. Comparison of grouped radiocarbon ages for earthquakes from Puget Lowland intraplate faults (top), Cascadia subduction zone earthquakes and secondary effects (center), and events from sites that likely record both intraplate and Cascadia earthquakes (bottom). Colored dots on map correspond to colored dots next to place names on age plot. Symbols under "Evidence type" indicate type of evidence on age plot. Vertical shading shows the age of the Seattle fault Restoration Point earthquake (green), Lynch Cove layers A and B (purple), and Discovery Bay Bed 2 (blue). Horizontal age range bars are shaded to reflect the number of samples used to determine the range, and are bracketed as minimum or maximum ages where known. SFZ (Atwater and Moore, 1992; Bucknam et al., 1992; Atwater, 1999; Nelson et al., 2014); TFZ (Sherrod, 2001; Sherrod et al., 2004; Nelson et al., 2014); SMF (Witter et al., 2008a; Blakely et al., 2009; Barnett et al., 2015); UPF (Johnson et al., 2004b); Lake WA (Karlin et al., 2004); Puget Sound (Smith, 2012); Saanich Inlet (Blais-Stevens et al., 2011); Snohomish River delta (Bourgeois and Johnson, 2001); Effingham Inlet (Enkin et al., 2013); Discovery Bay (this study and Williams et al., 2005); Lynch Cove (this study, and Bucknam et al., 1992; Sherrod, 2001; Hemphill-Haley, 1996; Jovanelly and Moore, 2009; Martin and Bourgeois, 2012); Salt Creek (Hutchinson et al., 2013); Port Alberni (Clague et al., 1994; Clague and Bobrowsky, 1994a; Clague and Bobrowsky, 1994b); Tofino (Clague and Bobrowsky, 1994a; Clague and Bobrowsky, 1994b; Hughes et al., 2002); WA coast (Atwater, 1987; Atwater et al., 2004; event W plotted as three separate shrub root ages, Atwater and Griggs, 2012); Juan de Fuca and Cascadia turbidites (Goldfinger et al., 2012; Goldfinger et al., 2017, with both reported ranges plotted, maximum age ranges, and adjusted age ranges shifted to the right (younger); historical tsunami flooding (Seattle Daily Times, 1964; Port Townsend Leader, 1964). Appendix 3 summarizes sources used in Figures 2.19 and 2.20.

The thickness of the overlying marsh deposits above layer A, and a radiocarbon age below layer A also support an older age for layer A. A *Triglochin maritima* leaf base from 20 cm below layer A has a radiocarbon age of 1443-1610 A.D (Table 2.1). This age and depth give an accumulation rate between 1.6 to 2.4 mm/yr (80 cm of sediment, and using the present age as 1950 A.D.). Assuming a constant uninterrupted sediment accumulation rate, layer A, 20 cm above the fossil, should therefore be between 83-125 years younger. This suggests that layer A was deposited before 1735 A.D. Layer A may therefore record a tsunami either directly or indirectly caused by the 1700 A.D. Cascadia earthquake. Layer A probably correlates with Discovery Bay Bed 1 (Figure 2.19), also inferred to be a deposit of the 1700 A.D. tsunami (Williams et al., 2005).

Submarine slope failures in the Puget Lowland (Figure 2.19) have age ranges that include 1700 A.D., though these slumps and turbidites from Lake Washington and Puget Sound from around this time have wide age ranges (Karlin et al., 2004; Smith, 2012). Submarine slope failures from Effingham Inlet have narrower ranges, and event E1 (Figure 2.19) has a much narrower range and probably represents the 1700 A.D. Cascadia earthquake.

Another possible source for layer A is an earthquake on the Utsalady Point fault between 100–400 cal yr BP (1550–1850 A.D.). (Johnson et al., 2004b). It is unknown whether this earthquake was tsunamigenic, but if it had generated a tsunami, there should be tsunami deposits of that age in tidal marshes closer to Whidbey Island, but none have yet been identified.

Layer B's modeled age range of 1170–1230 A.D. (720–780 cal yr BP) overlaps with the age of 730-910 cal yr BP of a subduction zone earthquake on the Oregon coast (Nelson et al., 2008b), but does not overlap with a maximum age of 913–793 cal yr BP for earthquake W at the mouth of the Columbia River (Atwater and Griggs, 2012). Soil W is poorly-preserved and sometimes absent in southwest Washington tidal marshes, and has been difficult to date because of lack of datable material. It is therefore not as well-dated as other earthquakes in the southwest Washington estuary record (Atwater and Hemphill-Haley, 1997; Atwater et al., 2004). The Columbia River age is a high-precision age from three age-averaged samples of a shrub root. Already a maximum age for earthquake W, it may also be skewed older because one of the three root ages, which were averaged in the reported age range, is 95 years older than the youngest of the three dated pieces. Removing the oldest piece of shrub root from the age calculation, the age range shifts to 761-911 cal yr BP (1039-1189 A.D.), a range that overlaps with layer B. Each shrub root age is plotted individually in Figure 2.19.

The ages of regional secondary effects of earthquakes, including tsunamis and submarine slope failures, are in generally good agreement with the age of layer B at Lynch Cove (Figure 2.19). The ages of tsunami deposits from Port Alberni and Tofino in British Columbia overlap with layer B (Clague et al., 2000; Clague and Bobrowsky, 1994a; Clague and Bobrowsky, 1994b), as does the age of tsunami deposit Sand B from Alsea Bay, central Oregon coast (Nelson et al., 2006). Saanich Inlet debris flow 3 also agrees with the age for layer B (Blais-Stevens et al., 2011).

Offshore turbidite T3 has a Cascadia-wide OxCal modeled age range of 540–890 cal yr BP, as well as a single age from the more proximal lower Juan de Fuca canyon of 770–990 cal yr BP, both of which overlap with the modeled age of Lynch Cove layer B, 725–778 cal yr BP (Goldfinger et al., 2012; Goldfinger et al., 2017). The wide age range of subsidence event D at Snohomish River delta includes the age of layer B (Bourgeois and Johnson, 2001), but also overlaps with the new age of Bed 2 at Discovery Bay. Layer B is tentatively correlated to Discovery Bay Bed 3 (Figure 2.19).

2.5.4 *A New Age for Discovery Bay Bed 2*

The new OxCal modeled age for Discovery Bay Bed 2, 1319–1391 A.D. (560–630 cal yr BP) (Figures, 2.19, 2.20), is older than the previously published age for Bed 2 of 300–500 cal yr BP (Williams et al., 2005). Figure 2.20 shows the age ranges of Discovery Bay Bed 2 and Lynch Cove layer B plotted with age ranges of tsunamis, submarine slope failures, and subsidence for sites from Vancouver Island to Oregon. There are several sites that have potentially correlative tsunami deposits to Discovery Bay Bed 2 on Vancouver Island at Deserted Lake, Tofino, and Ucluelet (Hutchinson and Clague, 2017; Clague and Bobrowsky, 1994b; Guilbault et al., 1996); and from Oregon at Cannon Beach, Netarts Bay, and Yaquina Bay (Witter et al., 2008b; Darienzo, 1991; Darienzo et al., 1994; Shennan et al., 1998; Graehl et al., 2014). There are also submarine slope failures that are close to Bed 2's age at Effingham Inlet, Saanich Inlet, Lake Washington, and Puget Sound (Enkin et al., 2013; Blais-Stevens et al., 2011; Karlin et al., 2004; Smith, 2012), and a turbidite from Lake Crescent that dates between 510-640 cal yr BP (Pollen, 2016).

It is unclear whether Discovery Bay Bed 2 tsunami deposit is evidence of the same earthquake that formed turbidite T2. Turbidite T2, like Bed 2 at Discovery Bay, is radiocarbon dated between the two most recent earthquakes (Y, from 1700 A.D., and W, 913–793 cal yr BP)

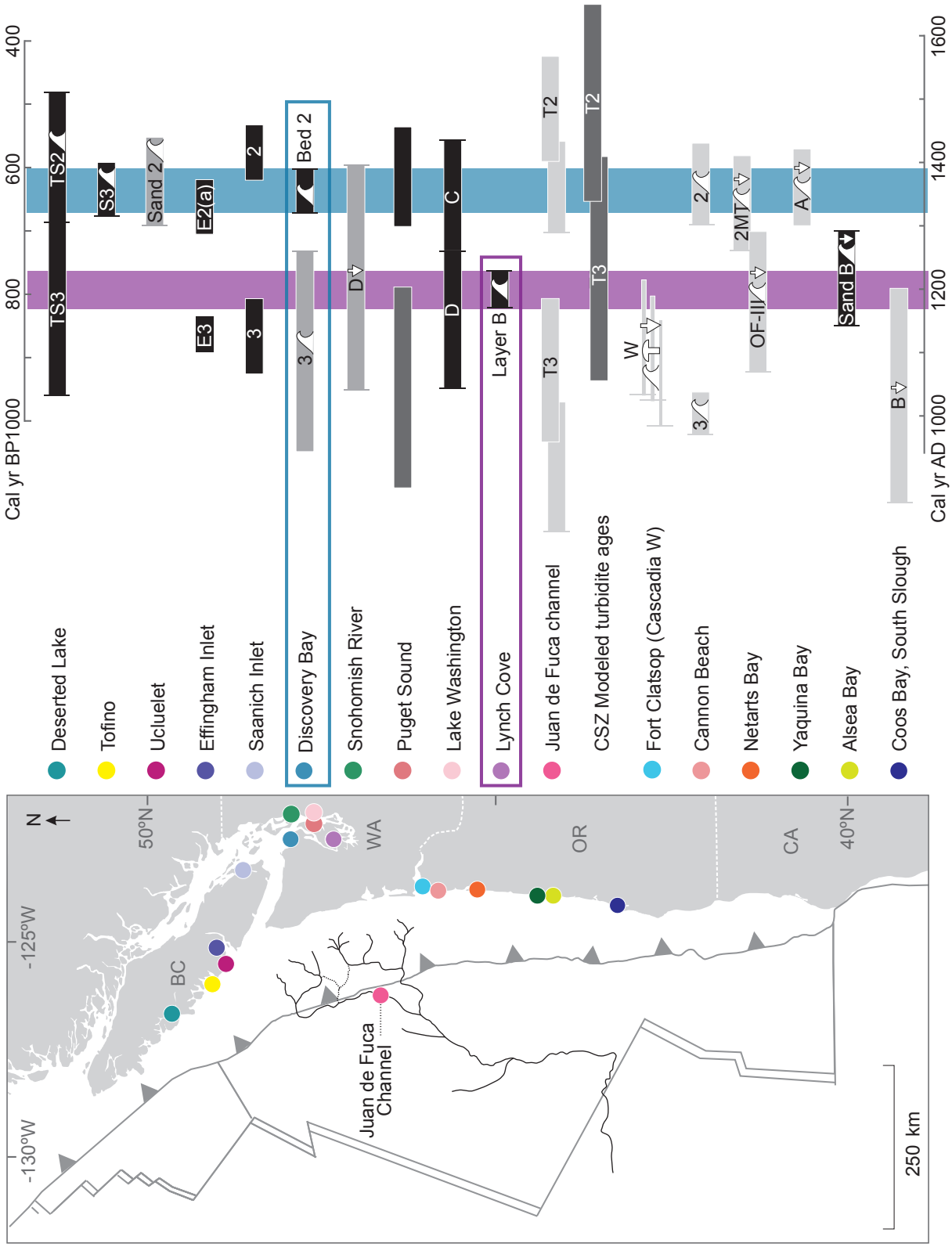
Cal yr BP1000
800
600
400
Cal yr AD 1000
1200
1400
1600
TS3
TS2
S3
Sand 2
E2(a)
2
E3
3
Bed 2
3
D
C
Layer B
T2
T3
T2
T3
W
2
3
2MT
OF-III
A
Sand B
B
Deserted Lake
Tofino
Ucluelet
Effingham Inlet
Saanich Inlet
Discovery Bay
Snohomish River
Puget Sound
Lake Washington
Lynch Cove
Juan de Fuca channel
CSZ Modeled turbidite ages
Fort Clatsop (Cascadia W)
Cannon Beach
Netarts Bay
Yaquina Bay
Alsea Bay
Coos Bay, South Slough
N
-130°W
-125°W
50°N
40°N
BC
WA
OR
CA
Juan de Fuca Channel
250 km

(Previous page) Figure 2.20. Comparison of ages for Lynch Cove layer B and Discovery Bay Bed 2, with select evidence: Deserted Lake cores 97-109 & 96-105 Ts2 (Hutchinson and Clague, 2017); Tofino Sand 3, (Clague and Bobrowsky, 1994a; Clague and Bobrowsky, 1994b); Ucluelet Sand 2, (Clague and Bobrowsky, 1994a; Clague and Bobrowsky, 1994b); Effingham Inlet E2 (Enkin et al., 2013); Saanich Inlet 2 (Blais-Stevens et al., 2011); Discovery Bay (this study); Snohomish River delta D (Bourgeois and Johnson, 2001); Puget Sound (Smith, 2012); Lake Washington C,D (Karlin et al., 2004); Lynch Cove (this study); Turbidity currents T2, T3 ages from Juan de Fuca Channel, both maximum (older range) and adjusted ages (younger range) are plotted as reported, in addition to modeled turbidite ages (Goldfinger et al., 2012; Goldfinger et al., 2017); Columbia River Fort Clatsop earthquake W, each of three root ages plotted (Atwater et al., 2004); Cannon Beach (Ecola Creek) Sands 2 and 3, (Witter et al., 2008b); Netarts Bay 2MT, (Darienzo, 1991; Darienzo et al., 1994) OF-III, (Shennan et al., 1998); Yaquina Bay buried soil A, (Graehl et al., 2015); Alsea Bay Sand B, (Nelson et al., 2008b); Coos Bay (Nelson et al., 2006). Key to radiocarbon age ranges and evidence type as in Figure 2.19. Appendix 3 summarizes sources used in Figures 2.19 and 2.20.

from estuaries in southwest Washington. However, these estuaries contain no known evidence of any earthquake or tsunami from about 600 cal yr BP. The T2 deposit closest to Discovery Bay in the mid Juan de Fuca channel (core M9907-11/-12, purple dot, Figures 2.19 and 2.20), is dated 390–550 cal yr BP (Goldfinger et al., 2012; Goldfinger et al., 2017), a range that does not include Bed 2. However, the OxCal modeled age of for the presumed full length T2 event which includes additional ages is 320-610 cal yr BP (Goldfinger et al., 2012; Goldfinger et al., 2017).

Collectively, the evidence plotted in Figure 2.20 around the age of Discovery Bay Bed 2 may record one full margin Cascadia earthquake, but could also represent one or more partial segment subduction zone earthquakes spaced closely in time. The limitations of radiocarbon dating (Nelson et al., 2006) preclude the possibility of determining whether only one, or more than one earthquake produced all of the evidence that includes Bed 2 at Discovery Bay, T2 offshore, and the evidence from Vancouver Island, the Strait of Juan de Fuca, Puget Sound and northern Oregon. Goldfinger et al. (2012) state that closely-spaced events should be preserved as separate turbidites because the coarsest sediments should be deposited within hours to days, and will be visible as separate flows, and no close pairs of turbidites have been observed in section of Bed 2 (Goldfinger, 2016 pers comm). However, if the turbidites are within weeks or months of each

other, they may appear as one event, especially if the finest grained sediments have not fallen out of suspension. (McHugh et al., 2011) observed a 600-m high plume of fine-grained sediment two months after the 2010 Haiti earthquake in the Canal du Sud basin.

Notably, the earthquake or earthquakes from around the time of Bed 2 failed to preserve coastal subsidence or tsunami deposits in any of the estuaries of southwest Washington (Atwater and Hemphill-Haley, 1997; Atwater et al., 2003). These estuaries (light-blue dots, Figure 2.19) record seven coseismically buried soils in the last 3500 yr, with tsunami deposits and liquefaction features accompanying some of the buried soils (Atwater and Hemphill-Haley, 1997; Atwater et al., 2003). The 1700 A.D. earthquake was dated, in part, by using tree rings of trees killed by coseismic subsidence in southwest Washington (Yamaguchi et al., 1997). One of the trees dated lived unscathed through the time of Bed 2 (snag GR-777 on the Columbia River, oldest ring dates to 1293 A.D., Yamaguchi et al., 1997). Two other trees from Grays Harbor (snag JN-560) and Willapa Bay (snag PX-783) had oldest sampled rings from 1379 and 1335 A.D., respectively. These trees, living through or within the age range of Bed 2 (1320–1390 A.D.), further attest to the lack of significant coastal subsidence in Washington during that time. If there was a single subduction zone earthquake at the time of Bed 2, it may have been smaller than the 1700 A.D. earthquake, with a relatively small amount of slip and minimal coastal subsidence, below the threshold for geologic preservation (Goldfinger et al., 2012; Goldfinger et al., 2016; Goldfinger et al., 2017).

Tsunami simulations of southern segment Cascadia earthquakes do not generate large waves on the coast of Vancouver Island (Cherniawsky et al., 2007), so it is probable that only full length or a shorter northern segment Cascadia earthquakes will leave tsunami evidence on Vancouver Island, along the Strait of Juan de Fuca, and farther inland in Puget Sound. The paucity

of coastal marsh sites in northern Washington, along the Strait of Juan de Fuca, and on Vancouver Island limits the onshore paleoseismic record for the northern part of the CSZ, and therefore the evidence and radiocarbon ages that would help clarify potential northern segment ruptures.

There is no Bed 2-aged tsunami deposit at Lynch Cove, which may indicate that the tsunami that deposited Bed 2 was smaller than the tsunamis that deposited Beds 1 or 3 at Discovery Bay, or layers A and B at Lynch Cove. If Bed 2, and layers A and B are all Cascadia tsunami deposits, there may be a threshold size of tsunami that can leave deposits at the head of Hood Canal, suggesting that the tsunami that deposited Bed 2 was smaller than the 1700 A.D. tsunami.

Another possibility is that some of the regional evidence from the time of Bed 2 is from an intraplate earthquake or earthquakes. Submarine slope failures in Puget Sound, turbidites in Lake Washington and Lake Crescent, and debris flows in Effingham and Saanich Inlet, all attest to strong shaking in the Puget Sound region around the time Bed 2 was deposited. Earthquake "E" in the Seattle fault zone has a very wide modeled age range that includes the age of Bed 2 (Nelson et al., 2014), but this earthquake or others on the Seattle zone, if tsunamigenic, would likely have dissipated before reaching Discovery Bay, as shown in Chapter 3. However, a Seattle fault or other crustal earthquake could have generated a tsunamigenic landslide near Discovery Bay.

An intraplate earthquake source that can be eliminated as a source of Bed 2 is the Utsalady Point fault (Figures 2.1, 2.19; Johnson et al., 2004b). The new age for Discovery Bay Bed 2 is too old to correlate the most recent Utsalady Point fault earthquake of 100–400 cal yr BP (Johnson et al., 2004b), which may also be the source of Event E liquefaction at the Snohomish River delta (Bourgeois and Johnson, 2001). There is no other known intraplate earthquake in the Puget Lowland from around 600 cal yr BP, and the coastal evidence from that time suggests that a CSZ earthquake tsunami is the likely source of Bed 2.

2.5.5 *Alternatives to Tsunami Deposition for Layers A and B*

2.5.5.1 Storm, Tide, or Flood Deposits

Storm waves can also deposit extensive sediment layers (Wallace et al., 2014), and distinguishing between tsunami and storm deposits in the sedimentary record is a topic that has received much research attention (Kortekaas and Dawson, 2007; Engel and Brueckner, 2011; Ramírez-Herrera et al., 2011; Richmond et al., 2011; Costa et al., 2017). Storm deposits and tsunami deposits may have similarities, but typically differ in a number of ways. Storm wave wash over forms a wedge-shaped deposit that is thickest near the shoreline, and tapers and disappears within tens of meters of the shoreline. Tsunami deposits are typically thin, widely-distributed sheets that can extend inland for hundreds of meters. Storm deposits are typically laminated or cross-bedded, while tsunami deposits are typically graded or massive deposits that have settled out of suspension (Morton et al., 2007; Goff et al., 2004). Layers A and B at Lynch Cove thin inland over more than 200 m, and are massive in all except two locations where the deposits display normal grading, suggesting deposition by tsunami.

Lynch Cove is unlikely to experience large storm waves comparable to cyclone or hurricane waves in the protected inland areas of Hood Canal. The eastern part of Hood Canal (Figure 2.2) has a fetch less than 20 km, limiting storm wave heights. Though Puget Sound does occasionally experience strong storms, none of the notable historic storms of the last century have left discernable deposits over the marsh at Lynch Cove. Therefore, it is less plausible that storm waves could leave behind extensive deposits over the marsh at Lynch Cove.

Extreme tides are not likely to leave deposits like layers A and B. The highest recorded tides since 1890 for Seattle (Lynch Cove tide gauge is subordinate) was less than one meter above mean higher high water (MHHW) for the hundred-year event (NOAA, 2015). A tide that high

would cause flooding comparable to flooding observed the night of the 1964 Alaska tsunami at Lynch Cove. There is no known sedimentary deposit from 1964 at Lynch Cove, so it is unlikely that even the highest tides would leave deposits like layers A and B over the marsh. Also, maximum tidal current speeds at Lynch Cove fluctuate between 0.0–0.05 m/s with occasional jumps to values approaching 0.1 m/s (Paulson et al., 2006), values too low to erode the tidal flat and transport silt over the marsh surface.

Flood deposits are also an unlikely source of layers A and B. The northwest edge of the marsh is next to the mouth of the Union River where it enters Hood Canal. The Union River drainage basin is less than 20 square miles, and has a peak predicted discharge of about 150 m^3/sec, with 185 m^3/sec the best estimate for the 100 year flood event (Kresch et al., 1998; Jackson, 2008). No overbank flood deposits of the Union River have been observed overtopping the marsh near the mouth of the river where it widens considerably as it enters Hood Canal (Jackson, 2008). If layers A and B were flood deposits, they would be expected to be thickest along the northwest side of the marsh near the Union River. However, they are thickest at the southern part of the marsh, the side of the marsh that would be directly inundated by a flow coming up Hood Canal (Figure 2.2).

2.5.5.2 Vented Sediments

There are vented sediments at Lynch Cove that are about 1,000 years old. A sand layer on top of the uplifted tidal flat has characteristics that suggest it was vented from below. Feeder dikes, intraclasts, laminae, and large variations in deposit thickness, all suggest venting as the mode of emplacement of this older sand, likely as the result of the earthquake that caused the tidal flat uplift (Bucknam et al., 1992; Martin and Bourgeois, 2012).

Layers A and B at Lynch Cove differ from the ~1,000 year old sand in thickness, geometry, sedimentary structures, grain size, and color. The older sand unit and layers A and B are both intermittent in their distribution, but the variation in deposit thickness is much greater for the older sand unit. Layers A and B are more common near the south (seaward) side of the marsh, while the older sand has thick concentrations in the center and back edge of the marsh (Jovanelly and Moore, 2009; Martin and Bourgeois, 2012) where layers A and B are largely absent. Layers A and B are both of similar thickness, typically between 1-3 cm, considerably thinner than the older sand, which is over 80 cm thick in places (Martin and Bourgeois, 2012). The older sand can vary in thickness over a few meters of outcrop from zero to tens of centimeters thick, while layers A and B maintain a more sheet-like geometry with a consistent maximum thickness over meters of outcrop. Layers A and B also do not have the sedimentary structures of vented sediments. In numerous observations of outcrops, dug pits, and cores, no feeder dikes were observed connected to either layer A or B, nor intraclasts, or other sedimentary structures suggestive of liquefaction. The grain size of layers A and B is overall much finer than the older vented sand. Layers A and B have mean grain sizes in the medium to coarse silt range (5-6 φ), while the older sand is noticeably coarser overall, with visible sand grains, and occasional pebbles. Sediment samples from the adjacent tidal flat are silt sized, and the same gray color as layers A and B. The source of the ~1,000 year old sand is inferred to be a sand deposit at an unknown depth, vented and fed to the surface by feeder dikes (Martin and Bourgeois, 2012), while color, grain size, and diatom evidence suggest that the source of layers A and B sediments was the adjacent tidal flat.

One notable similarity between the 1,000-year-old sand and layers A and B is that they contain similar tidal flat diatom species, including the species *Cocconeis scutellum*, and *Dimeregramma minor* (Hemphill-Haley, 1996). If the source of the ~1,000-year-old sand is an

older, buried tidal flat surface, it is not unexpected that some of the same diatom species would be in both deposits. The finer grained sediments of layers A and B contain a higher concentration of diatoms than found in the 1,000-year-old sand deposit. Because diatoms are silt-sized, it is not unusual for sandy tsunami deposits to be relatively low in diatoms, as a result of size sorting during transport and deposition (Hemphill-Haley, 1996).

The differences between the ~1,000-year-old sand deposit and layers A and B suggests different sediment sources and different modes of deposition. The older sand unit has several characteristics that suggest that most, if not all, of the deposit was vented onto the surface from below (Martin and Bourgeois, 2012). Overall, layers A and B differ enough in their geometry, grain size, and sedimentary structures from the 1,000-year-old sand deposit enough to conclude that they were deposited by different processes.

2.5.6 *Tsunamigenic Slope Failures as a Tsunami Source*

A possible source for the tsunami deposits at either of the sites is tsunamis generated by subaerial or submarine slope failures. Evidence for slope failure in the Puget Lowland includes the many slope failure deposits identified in Puget Sound and Lake Washington (Smith, 2012; Karlin et al., 2004). Some of these failures are within the age range of the local "millennial earthquake series" about 1,000 cal yr BP (Nelson et al., 2014), and earthquakes on the Utsalady Point fault (Johnson et al., 2004b); but some of these deposits may represent failures from shaking during subduction zone earthquakes. Events D and B in Lake Washington may be the result of shaking during the earthquakes that buried soils W and Y on the Washington coast (Karlin et al., 2004; Atwater and Hemphill-Haley, 1997; Atwater and Griggs, 2012). In Puget Sound, submarine failures are also recorded within the age ranges of Cascadia earthquakes W and Y on the

Washington coast, and there is also an additional set of failures from around the time of Bed 2 at Discovery Bay.

Delta failures, common in Puget Sound, are known to generate tsunamis when triggered by earthquakes or by oversteepening. In the minutes following the 1964 Alaska earthquake, failure of an inactive submarine delta generated a tsunami that destroyed the town of Chenega, AK (Brothers et al., 2016), and a similar submarine delta failure tsunami damaged Valdez, AK (Parsons et al., 2014). Local historic delta failures unrelated to earthquakes include a failure on the Puyallup river delta in Commencement Bay in 1894 and 1943; and the Duwamish river delta in 1986 (Gardner et al., 2001). A multibeam data survey of major deltas including the Nisqually, Puyallup, Duwamish, and Snohomish deltas following the 2001 M_w 6.8 Nisqually earthquake revealed evidence of submarine failures, and the 1894 Commencement Bay failure scarp was still visible (Gardner et al., 2001). Scans of the seabed in Hood Canal have identified potential slump blocks near the mouths of the Dewatto and Little Dewatto rivers (Walsh et al., 2009). These rivers differ from nearby rivers in that they do not have extensive deltas, so these blocks may be the remnants of failed delta fronts. Future multibeam surveys of the seafloor of Hood Canal may identify failures that could serve as candidate sources for the tsunami deposits at Lynch Cove, but will require additional high resolution bathymetric data.

Subaerial tsunamigenic landslides, may also occur either with or without seismic triggering. Above the southeast shoreline of Hood Canal, LIDAR imaging shows a head scarp from the Alderwood landslide about 4 km southwest of Lynch Cove marsh, Figure 2.2 (Sarikhan et al., 2007). A large landslide into Hood Canal could trigger a tsunami that could overrun the marsh at Lynch Cove. The age of the Alderwood landslide is estimated between 890–1040 A.D. (Sarikhan et al., 2007), too old to be the source of either layer A or B at Lynch Cove. The age of

the Alderwood slide suggests it may have been triggered during the "millennial earthquake series," coeval with the coseismic uplift of the tidal flat at Lynch Cove, and it is possible that the slide generated a tsunami in Hood Canal (Sarikhan et al., 2007; Nelson et al., 2014).

Earthquake-generated tsunamigenic landslides have historically occurred in Hood Canal. In 1949, a landslide near Tacoma days after the M_w 7.1 Olympia earthquake generated a tsunami that reached heights of ~2.5 meters locally (Chleborad, 1994). This earthquake was a deep earthquake caused by deformation within the subducting Juan de Fuca plate (Ichinose et al., 2006). There have been 10 deep earthquakes over M_w 6 in the last 100 years in the Puget Lowland (University of California Berkeley Seismological Laboratory et al., 2014). The frequency of these earthquakes compared to Cascadia and crustal fault events, in a geologic setting with steep and unstable shorelines, in addition to frequent non-seismic slides, makes either submarine or subaerial slope failures a likely source for tsunami deposits in the Puget Lowland. However, there are no identified landslides that could be candidate sources of layers A or B in Hood Canal. Older events such as the Alderwood landslide are clearly visible on LIDAR maps, so evidence of younger slides and scarps should still be visible. A search of LIDAR maps of Hood Canal shorelines failed to identify candidate source slides that could generate a tsunami.

2.6 CONCLUSIONS

Multiple lines of evidence support the hypothesis that layers A and B at Lynch Cove are tsunami deposits. Layers A and B have a sheet-like geometry, thin and rise landward, and possibly fine landward. Layers A and B contain tidal flat diatoms, and the sediment grain size and color is similar to the tidal flat adjacent to the marsh. This suggests that the source of the sediment in layers A and B was the adjacent tidal flat, and implies that layers A and B were deposited by a

landward surge of water that eroded tidal flat silts and deposited them on top of the marsh surface, as would be expected from a tsunami.

The radiocarbon ages of layers A and B are close to the age ranges of the past two Cascadia earthquakes preserved on the coast of Washington—earthquake Y in 1700, and possibly also earthquake W—though an averaged high-precision maximum age for this event of 913–793 cal yr BP from the Columbia River does not overlap with the layer B's age of 725–778 cal yr BP (Atwater and Griggs, 2012). This age, based on an averaging of three shrub root ages, two of which do overlap in age with the age of layer B.

Bed 2 tsunami deposit at Discovery Bay (560–630 cal yr BP) is of similar age to other tsunami deposits from Vancouver Island and Oregon, and submarine slope failures in Puget Sound and Lake Washington. The radiocarbon age for turbidite T2 from the Juan de Fuca canyon (Goldfinger et al., 2012; Goldfinger et al., 2017) is too young to correlate with Bed 2, though the wider OxCal modeled age for T2 does overlap with Bed 2's new age.

There is no event the age of Bed 2 at Lynch Cove or the coast of southwest Washington. The lack of preserved subsidence for an event of either T2 or Bed 2 age on the coast of Washington may be because the amount of slip was low, thus producing less coastal subsidence (Goldfinger et al., 2012; Goldfinger et al., 2017), or there may have been closely-spaced smaller CSZ segment earthquakes that produced little coastal subsidence. If Discovery Bay Bed 2 does represent either a narrow margin-long Cascadia earthquake or a smaller Cascadia segment earthquake, then Discovery Bay is a more sensitive recorder of CSZ tsunamis than Lynch Cove, and a larger threshold size tsunami may be needed to be recorded at Lynch Cove.

Lynch Cove, Discovery Bay, and potentially other sites in Puget Sound, particularly those situated at the terminuses of narrow waterways, are at a higher risk from Cascadia tsunamis than

previously known. These findings, which are particularly relevant to shoreline populations and infrastructure, suggest that further studies are needed accurately assess the hazard from Cascadia subduction zone tsunamis in Puget Sound.

Chapter 3. **Tsunami Simulations for Lynch Cove and Discovery Bay**

3.1 INTRODUCTION

Subduction zone tsunamis can travel hundreds of kilometers into inland waterways. Historical observations of subduction zone tsunamis flooding inland waterways include examples from the Chile and Nankai subduction zones. The 1960 Chilean tsunami had wave heights of 1.6 meters at the mouth of Rio Aysen, over 100 km inland of the coast, behind the Archipelago of Chonos (Sievers et al., 1963). In Japan, the 1707 Hoei earthquake on the Nankai subduction zone generated a tsunami that caused damage in the Bungo Channel (Hatori et al., 1983; Baranes et al., 2014), as well as along shorelines in the Seto Inland Sea (Figure 3.1; Hatori, 1988). The 1946 Nankai earthquake tsunami caused run-ups between 1-3 meters along the Bungo Channel, and even greater run-ups of 3-4 meters were documented from the 1707 Hoei and 1854 Ansei tsunamis. In the Seto Inland Sea, tsunami run-ups reached 2-3 meters high in the eastern area, and 1.5 meters high in the western and central areas, where the tsunami caused damage to salt fields. The 1707 Hoei and 1854 Ansei tsunamis also caused increased current speeds in the Seto Inland Sea that were blamed for shipwrecks (Hatori, 1988).

To improve the understanding of tsunami behavior and hazards in the Seto Inland Sea, a series of numerical simulation studies focused on the hazards to Seto Inland Sea shorelines from Nankai tsunamis. Simulations described tsunami propagation and estimated tsunami height and period for various points along the shorelines of the Seto Inland Sea (Kubo et al., 2007). Simulated tsunami heights were variable, and some areas saw locally amplified waves. Simulations also predicted that the largest waves were not always the first waves, and in some

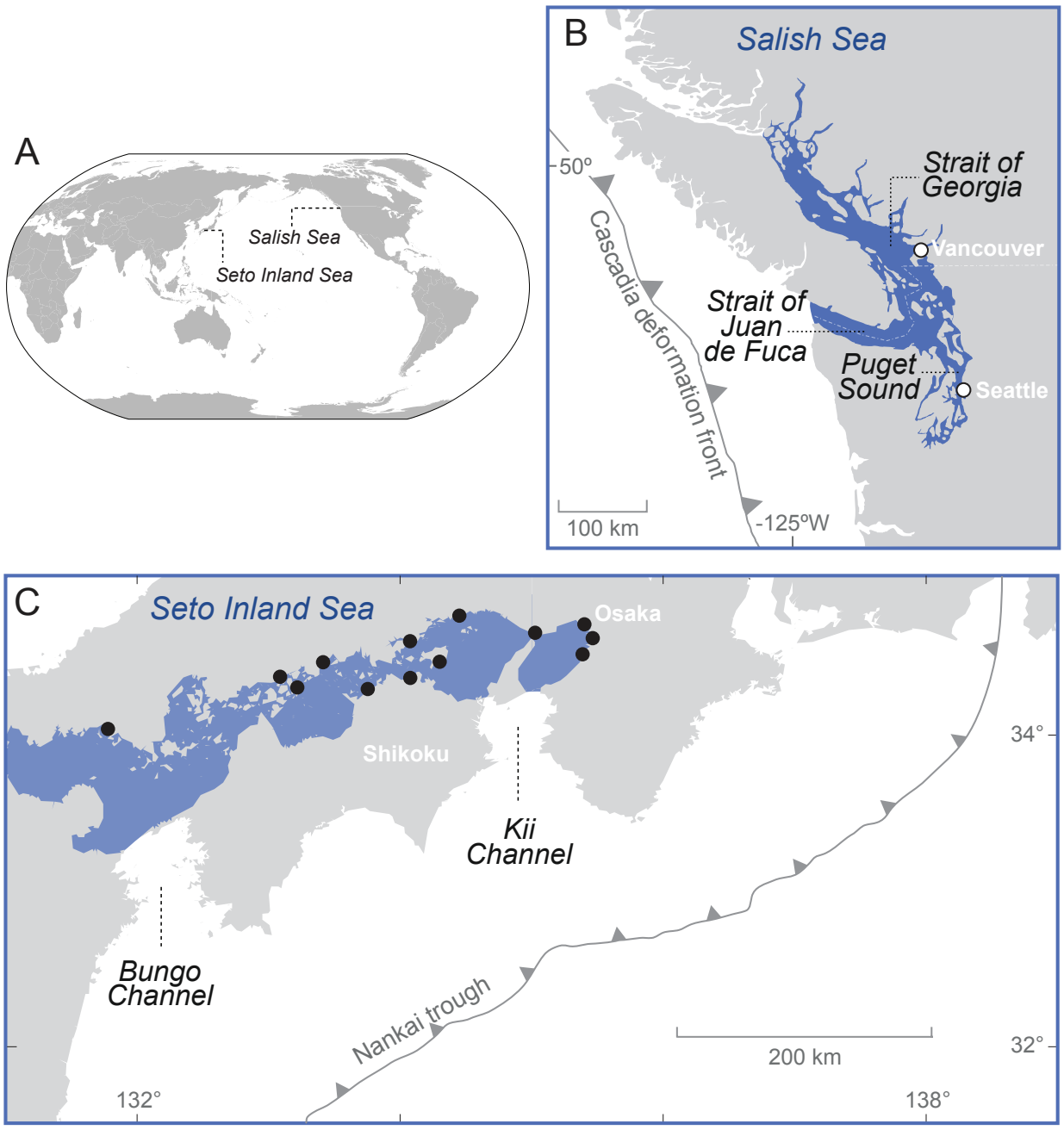

Figure 3.1. Seto Inland Sea north of Shikoku Island in southwest Japan. Map adapted from Lee et al., 2015. Black dots show locations of damage from 1707 Hoei tsunami (Hatori, 1988).

locations occurred 8-10 hours after the earthquake, and the tsunami wave decay time in the Seto Inland Sea was more than 20 hours. Kubo et al. (2007) concluded that the danger to Seto Inland Sea shorelines was greater than previously expected.

Yamanaka et al. (2009) simulated the 1854 Ansei Nankai earthquake (M_w 8.4) to study tsunami wave resonance amplification of waves in the Seto Inland Sea. Their simulations showed wave resonance in the long narrow Seto Inland Sea amplified tsunami waves, and wave amplification varied by location, as did current speeds. The highest simulated waves were about 2.3 meters high along the shoreline of Osaka Bay. The simulated wave heights and current speeds were summarized in a hazard map for different parts of the Seto Inland Sea, with a recommendation to improve tsunami hazard awareness in local communities (Yamanaka et al., 2009).

Motivated by the devastating 2011 Tohoku tsunami, Japanese tsunami hazard studies have revised hazard assessments for coastal regions, with attention to the Nanakai Trough region, which is expected to experience a large earthquake within the next 30 years (Lee et al., 2015). Using updated rupture and tsunami source areas for the Nankai-Tonankai-Tokai region, Lee et al. (2015) ran numerical models of the 1707 Hoei earthquake (M_w 8.4) to simulate a worst-case scenario tsunami for the Seto Inland Sea. These simulations, which included tidal effects, found that high tide increases wave height and shortens wave arrival times, and that areas with shallow water and greater tidal range increased tsunami wave heights the most. These simulations also predicted variation in wave height by location in the Seto Inland Sea, with notable wave heights as much as 3 meters high across from the Bungo Channel, and as much as 3.75 meters high across from the Kii Channel entrances to the Seto Inland Sea (Figure 3.1; Lee et al., 2015).

While the Japanese have focused attention on understanding the tsunami hazards in the Seto Inland Sea, Puget Sound, an inland waterway of the Salish Sea (Figure 3.1) in the forearc of the Cascadia subduction zone, has received less attention, and therefore the hazards to Puget Sound shorelines from Cascadia tsunamis remain largely unknown. Tsunami modeling studies in the early

2000s predicted inundation limits from Cascadia tsunamis for the cities of Port Angeles and Port Townsend on the Strait of Juan de Fuca (Walsh et al., 2002a; Walsh et al., 2002b); Whidbey Island on the eastern side of the Strait of Juan de Fuca (Walsh et al., 2005); and north of Whidbey Island in Bellingham (Walsh et al., 2004). While these studies provided a first estimation of tsunami hazards along the Strait of Juan de Fuca and nearby shorelines from Cascadia tsunamis, the results of these studies were limited by the availability of high-resolution topographic and bathymetric data. The complex waterways of Puget Sound, with varying water depths, current speeds, tidal ranges, and terminal waterways, will influence tsunami waves in ways that vary by location, as observed in the Seto Inland Sea. Because the Cascadia subduction zone is locked and has been accumulating stress since its last great earthquake in 1700, it is poised to release a great earthquake (Wang and Tréhu, 2016; Atwater et al., 2005), and therefore it is important to identify areas in heavily populated Puget Sound with the greatest hazard from Cascadia tsunamis.

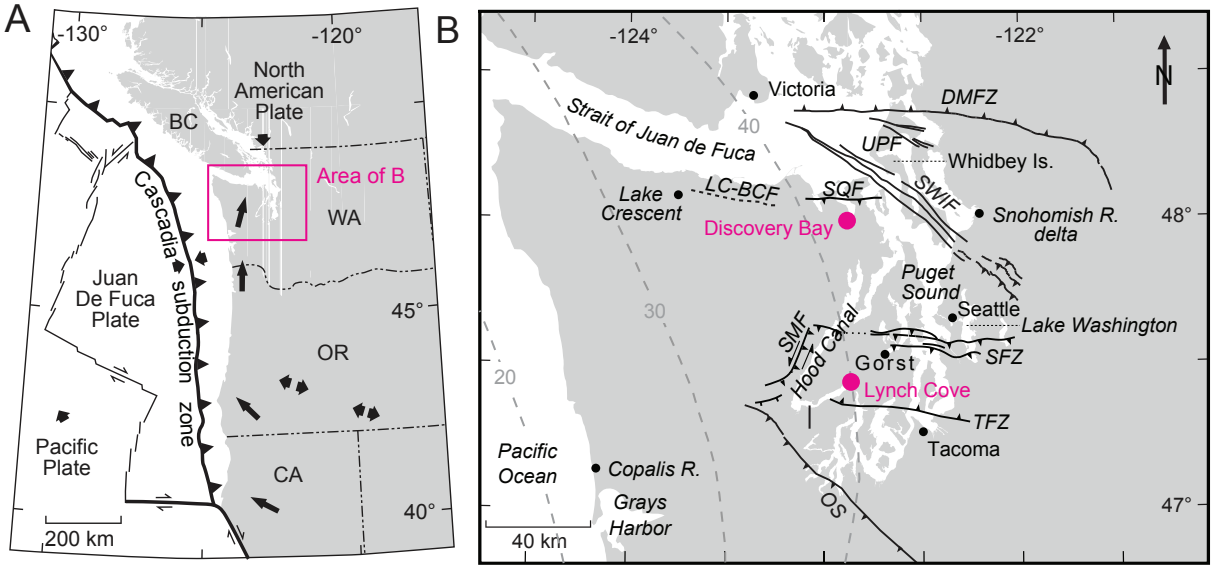

Figure 3.2. Tectonic setting (A) Tectonic setting of the Cascadia subduction zone. (B) The Puget Sound region, showing location of Lynch Cove and Discovery Bay. SFZ is the Seattle fault zone, TFZ is the Tacoma fault zone.

Two sites that geologically record evidence of past tsunamis, are Lynch Cove, at the head of Hood Canal in Puget Sound, and Discovery Bay, along the Strait of Juan de Fuca near the entrance to Puget Sound (Figure 3.2; 3.3). At Lynch Cove, layers of silt in peaty tidal marsh sediments record two episodes of tsunami inundation in the last 1,000 years—one at ~250 cal yr BP, and another at ~750 cal yr BP. Within the last 1,000 years at Discovery Bay, there are two similar-age tsunami deposits, that probably correlate to the Lynch Cove deposits, and there is also an additional deposit from ~600 cal yr BP.

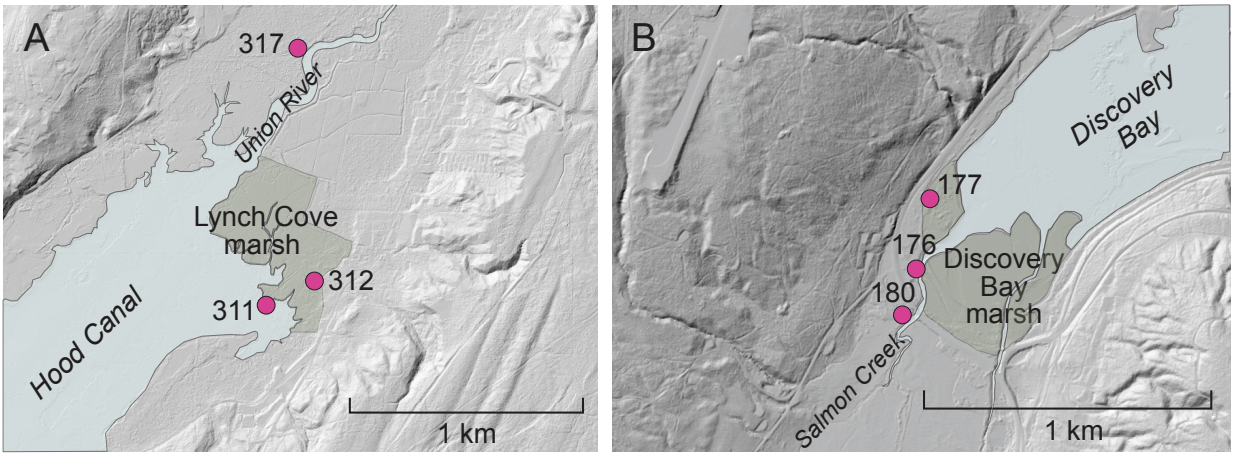

Figure 3.3. Map of study locations. (A) Lynch Cove marsh with tsunami simulation gauge positions. (B) Discovery Bay marsh with tsunami simulation gauge positions.

3.2 METHODS

Tsunami simulations for different tsunami-generating earthquake sources were run to compare tsunami run-ups at both Lynch Cove and Discovery Bay. Simulations were run for three great Cascadia earthquakes with different rupture styles, the 900–930 A.D. Seattle fault earthquake (Atwater and Moore, 1992; Atwater, 1999); and a hypothetical earthquake from Alaska, from within the rupture area of the 1964 Alaska earthquake (Figure 3.4). For each of these earthquake

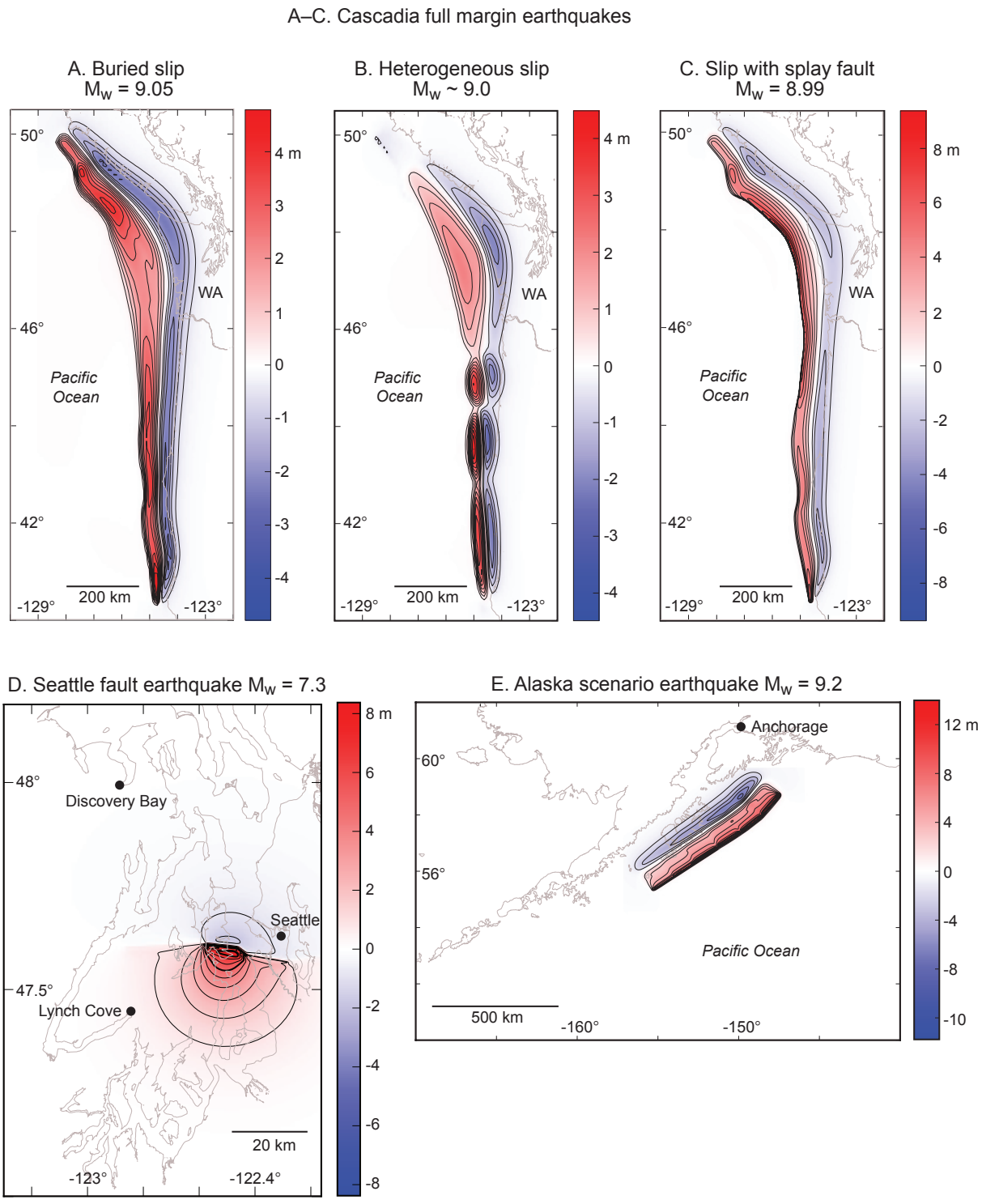

Figure 3.4. Seafloor deformation used as source inputs for GeoClaw tsunami simulations. Red shades indicate uplift, blues indicate subsidence. A-C, Cascadia full-margin earthquakes (A) buried slip that does not break the seafloor surface, (B) heterogeneous slip with patches of higher slip as an analog of the 1700 Cascadia earthquake, (C) slip with splay fault. (D) Seattle fault earthquake, (E) Alaska earthquake.

sources, flow depths and flow speeds are compared and evaluated as potential sources for the deposits at Lynch Cove and Discovery Bay.

Simulations were made using GeoClaw open source code (LeVeque et al., 2011; Berger et al., 2011; Clawpack Development Team, 2015). GeoClaw tsunami simulations use an initial three-dimensional fault dislocation model of sea floor deformation based on the Okada model (Okada, 1985). GeoClaw uses high-resolution finite volume methods to solve the depth-averaged two-dimensional shallow water equations using adaptive mesh refinement to follow wave propagation and zoom in on coastal regions. These simulations predict fluid flow onto dry land surfaces for areas of interest at high resolution. The topography and bathymetry DEM data used for the Puget Sound area is 1/3 arc-second resolution, 10-meter cell size, with mean high water (MHW) as zero elevation (Carnigan et al., 2014). In the simulation, the DEM was coarsened for areas farther away from the study sites, and then refined ahead of wave arrival up to 2/3 arc-second resolution in grids around the Lynch Cove and Discovery Bay sites. Both simulations grids cover a wider area around the marsh areas shown in Figure 3.3. Simulations were all run with constant (non-fluctuating) tidal level. All simulations use a Manning's formula bottom friction coefficient of 0.025 (bare Earth), so simulate flows onto a bare landscape.

To approximate sea levels at the time of each earthquake source, adjustments were made based on the assumption of 1 meter of sea level rise over the last 1,000 years in northern Puget Sound (Eronen et al., 1987; Beale, 1991). To account for this sea level rise in the tsunami simulations, the Cascadia simulations were run at -0.33 meters below current MHW, the Seattle fault simulations were run at -1.0 meters below current MHW, and the Alaska earthquake was run at modern MHW. Because the simulations are run at MHW, or an adjusted paleo-MHW, these simulations represent "worst case" scenarios, where tsunami waves coincide with high tide. The

sea level adjustments, and additional simulation inputs for each earthquake source are summarized in Table 3.1. Alaska and Cascadia tsunami source simulations were run for 12 hours after the earthquake at 10 minute intervals, the Seattle fault simulation was run for four hours after the earthquake at 5 minute intervals.

The simulations include gauges that monitor and plot flow depths and current speeds at select locations during the simulation. All simulations were run using three gauges each at Lynch Cove and Discovery Bay (pink dots in Figure 3.3). At Lynch Cove, gauge 311 was placed at the seaward edge of the marsh, on the modern tidal flat surface. Gauge 312 was placed at the back edge of the marsh next to snag 399 (Chapter 2), close to the landward limit of layer A. Gauge 317 was placed on a road near the bank of the Union River. This location was chosen because flooding attributed to the 1964 Alaska tsunami was observed there about 4.5 hours after the earthquake. At Discovery Bay, gauge 177 is located at the "Pit" site of Williams et al. (2005), a location where there are at least six tsunami deposits, and traces of sand that may be deposits of the 1964 Alaska tsunami (Williams et al., 2005). Gauge 176 is located on top of the river bank next to Salmon Creek. There is also a thin lamina (2-3 mm) of sand at this location that may be a deposit of the 1964 Alaska tsunami. Gauge 180 was placed at a residence that experienced two waves of flooding from the 1964 Alaska tsunami (Port Townsend Leader, 1964).

Table 3.1. Tsunami Simulation Sources

Earthquake source	Source reference	Rupture length (km)	Rupture width (km)	Slip (m)	Magnitude M_w	Simulation sea level, in relation to MHW	Simulation length, time step
Cascadia whole margin with buried slip	Gao, 2016, Figure 4.5d	full length	distributed up to ~100	up to 20, distributed	9.05	MHW-0.33 m	12 hours, 10 minute
Cascadia whole margin with patchy heterogeneous slip, 1700 earthquake analog	Gao, 2016, Figure 4.16c	full length	distributed up to ~75	up to 20, distributed	~9.0	MHW-0.33 m	12 hours, 10 minute
Cascadia whole margin slip with splay-fault	Gao, 2016, Fig 4.7d	full length	distributed up to ~75	up to 18, distributed	8.99	MHW-0.33 m	12 hours, 10 minute
Seattle fault 900-930 earthquake	Chamberlin et al., 2015 Table 1, Scenario A	60	35	30, distributed over 6 segments	7.3	MHW-1.0 m	4 hours, 5 minute
Alaska earthquake within deformation area of 1964 earthquake	González et al., 2009; Tsunami Pilot Study Working Group (TPSW), 2006 Table 1, Source 3	600	100	15-30, distributed over 12 segments	9.2	MHW	12 hours, 10 minute

3.3 Simulation Results

3.3.1 *Cascadia Earthquake Simulations*

Three simulated great Cascadia earthquake sources are shown in Figure 3.4A-C. The buried slip earthquake (3.4A) has distributed buried rupture that does not break the surface (Gao, 2016). The Cascadia heterogeneous slip earthquake (Figure 3.2B) is based on seafloor deformation as calculated from microfossil evidence of coseismic subsidence from the 1700 Cascadia earthquake, with four rupture patches of higher slip (Wang et al., 2013). The Cascadia splay fault earthquake (Figure 3.2C), has a surface-rupturing splay fault (Gao, 2016). All three Cascadia earthquake sources used to simulate tsunamis in this study use a revised Cascadia fault geometry created by Gao (2016).

Figures 3.5 and 3.6 summarize the results of the tsunami simulations of the three Cascadia sources at Lynch Cove and Discovery Bay, respectively. These figures show maximum flow depths in shades of blue over the 2/3 arc-second resolution grids, and gauge plots of flow depths (m) in blue, and flow speeds (m/s) in red, for each of the three simulation gauge points at each site over 12 hours of simulation time.

3.3.2 *Seattle Fault Earthquake Simulation*

Tsunami deposits from four tidal marsh sites in Puget Sound have been attributed to the tsunami formed by the intraplate Restoration Point earthquake on the Seattle fault between 900–930 A.D (Atwater and Moore, 1992; Atwater, 1999; Nelson et al., 2014). This tsunami left deposits in Cultus Bay on the south end of Whidbey Island, West Point in Seattle, the Snohomish River delta, and Gorst, at the head of Sinclair inlet (Atwater and Moore, 1992; Bourgeois and

Johnson, 2001; Arcos, 2012). Earthquakes from the "millennial earthquake series" in Puget Sound were also considered as a potential source of the sand unit that lies atop the uplifted tidal flat surface at Lynch Cove (Hemphill-Haley, 1996; Jovanelly and Moore, 2009; Nelson et al., 2014). The Restoration Point earthquake was rejected as the source of Bed 4 at Discovery Bay by Williams et al. (2005), though other intraplate faults were considered potential sources (Williams et al., 2005).

The Restoration Point earthquake (Figure 3.4D) was simulated using the tsunami source of Chamberlin et al., (2015) to test whether this intraplate earthquake tsunami reached either Lynch Cove or Discovery Bay. This earthquake source was designed to be a maximum credible earthquake for the Seattle fault (Chamberlin et al., 2015). Figure 3.7 summarizes the results of the Seattle fault source simulation for both Lynch Cove and Discovery Bay.

3.3.3 *Alaska Earthquake Simulation*

The 1964 Alaska tsunami caused flooding and damage along the west coast of the United States (Lander et al., 1993), including flooding at both Lynch Cove and Discovery Bay (Seattle Daily Times, 1964; Port Townsend Leader, 1964). The Alaska earthquake simulation uses an earthquake source (Figure 3.4E) that overlaps part of the area of deformation that accompanied the 1964 Great Alaska Earthquake (González et al., 2006; González et al., 2009; Plafker and Kachadoorian, 1966), and was used in a probabilistic tsunami hazard assessment for Crescent City, CA (González et al., 2014). Figure 3.8 summarizes the Alaska tsunami simulation for both Lynch Cove and Discovery Bay, and compares the simulated results with the eyewitness observations from the location of gauge 317 at Lynch Cove where roadway flooding was observed, and gauge 180 at Discovery Bay, where a residence was flooded.

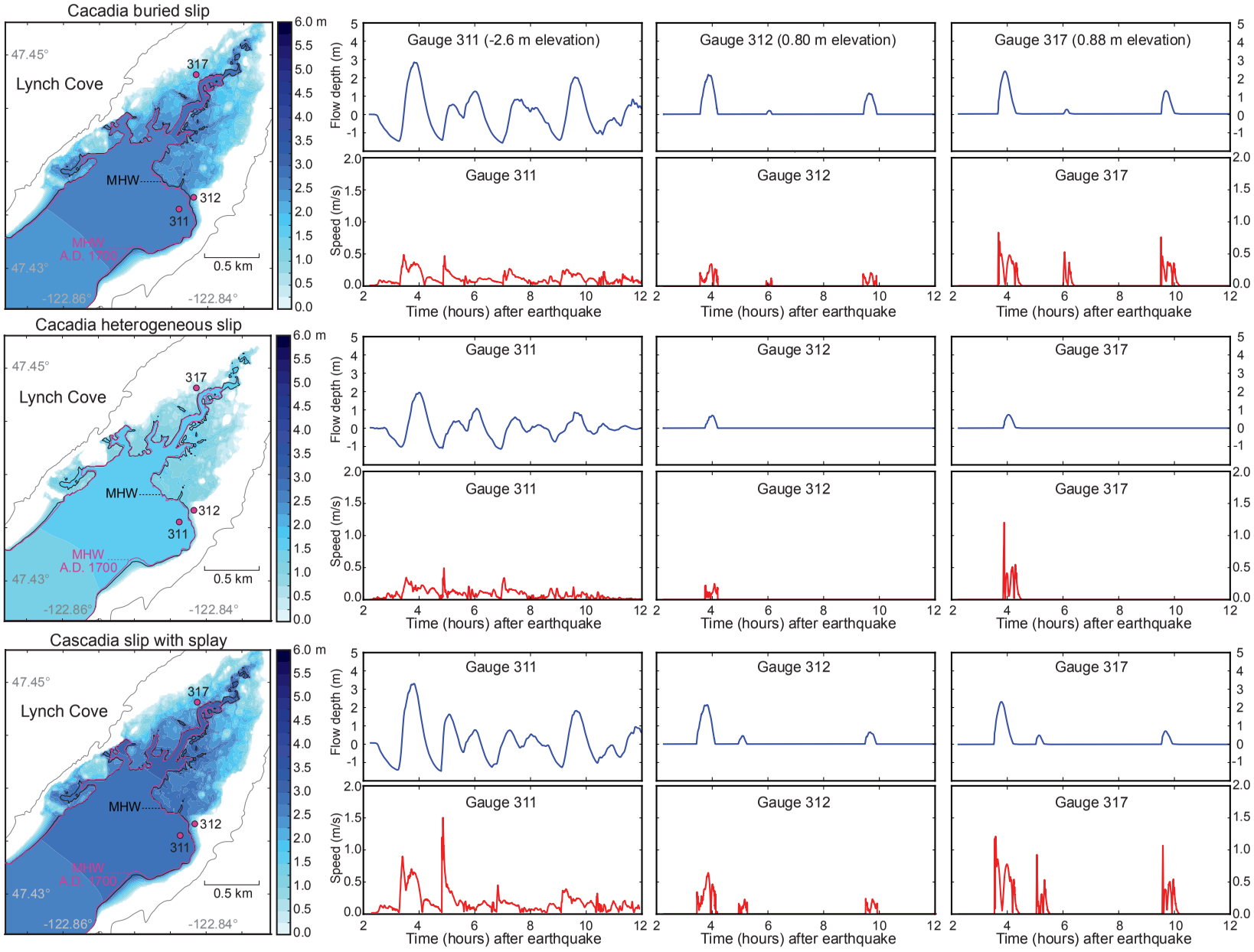
Cacadia buried slip
Cacadia heterogeneous slip
Cascadia slip with splay
Lynch Cove
47.45°
47.43°
-122.86°
-122.84°
317
312
311
MHW
MHW
A.D. 1700
0.5 km
6.0 m
Flow depth (m)
Speed (m/s)
Gauge 311 (-2.6 m elevation)
Gauge 312 (0.80 m elevation)
Gauge 317 (0.88 m elevation)
Gauge 311
Gauge 312
Gauge 317
Time (hours) after earthquake

(Previous page) Figure 3.5. Lynch Cove Cascadia tsunami simulations. Each row shows the simulation grid of maximum flow depths above mean high water (MHW) on the left, and corresponding point gauge plots (pink dots) on the right. The simulation grid shows modern MHW datum in black, and the 1700 A.D. adjusted sea-level MHW in pink (-0.33 m relative to modern MHW). The top row is the buried slip source, the middle row is the heterogeneous slip source (analog of the 1700 A.D. earthquake), and the bottom row is the splay fault source. The numbered gauge plots on the right correspond to gauge locations in the simulation grid on the left. Gauge elevations and flow depths are with respect to the MHW datum. Blue are flow depths (m); red lines are flow speeds (m/s).

(Next page) Figure 3.6. Discovery Bay Cascadia tsunami simulations. Each row shows the simulation grid of maximum flow depths above mean high water (MHW) on the left, and corresponding point gauge plots (pink dots) on the right. The simulation grid shows modern MHW datum in black, and the 1700 A.D. adjusted sea-level MHW in pink (-0.33 m relative to modern MHW). The top row is the buried slip source, the middle row is the heterogeneous slip source (analog of the 1700 A.D. earthquake), and the bottom row is the splay fault source. The numbered gauge plots on the right correspond to gauge locations in the simulation grid on the left. Gauge elevations and flow depths are with respect to the MHW datum. Blue are flow depths (m); red lines are flow speeds (m/s).

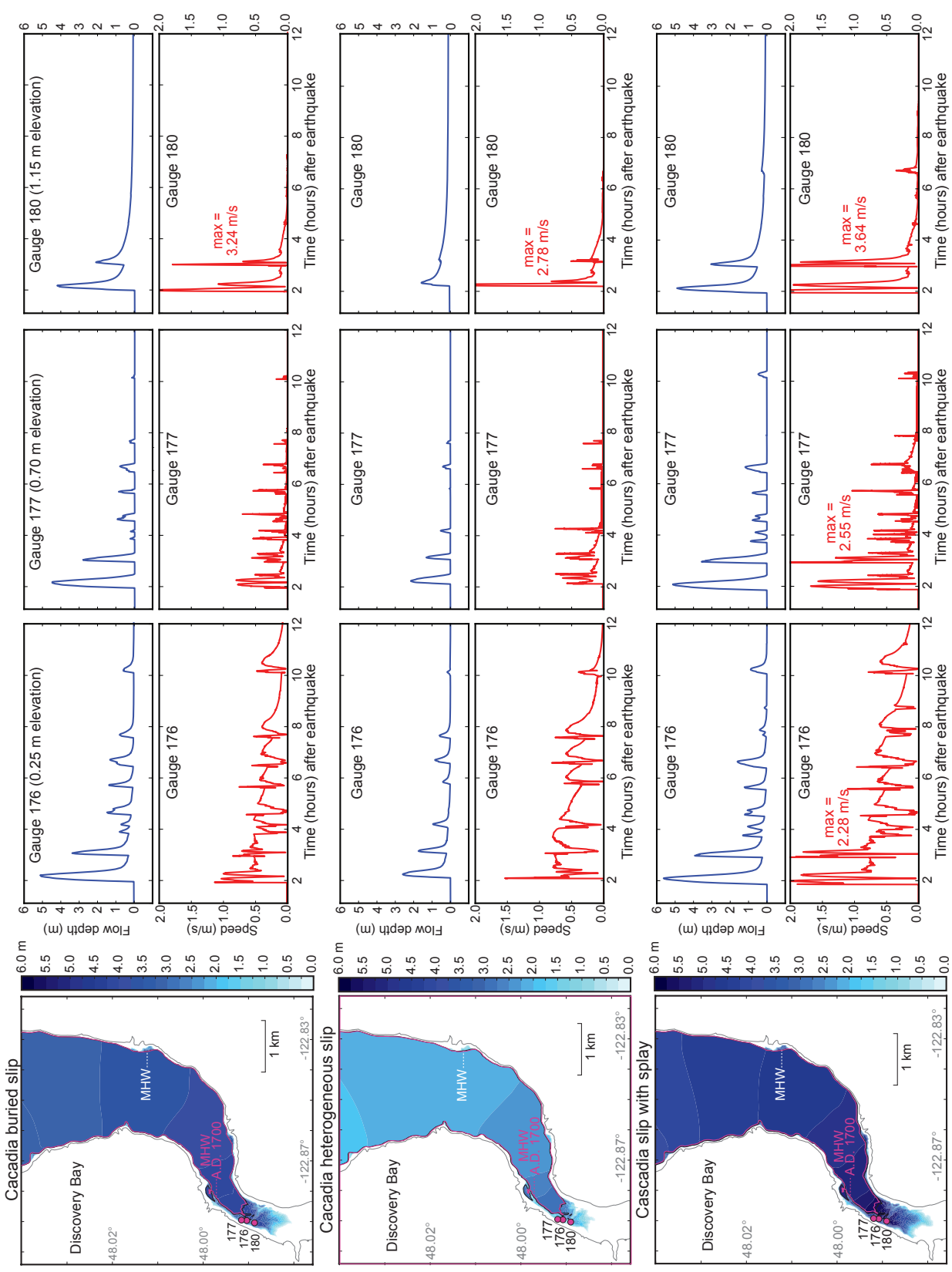
Cacadia buried slip
Cacadia heterogeneous slip
Cascadia slip with splay
Discovery Bay
MHW
MHW A.D. 1700
1 km
48.02°
48.00°
-122.87°
-122.83°
177
176
180
6.0 m
Gauge 176 (0.25 m elevation)
Gauge 177 (0.70 m elevation)
Gauge 180 (1.15 m elevation)
Gauge 176
Gauge 177
Gauge 180
Flow depth (m)
Speed (m/s)
Time (hours) after earthquake
max = 3.24 m/s
max = 2.78 m/s
max = 2.28 m/s
max = 2.55 m/s
max = 3.64 m/s

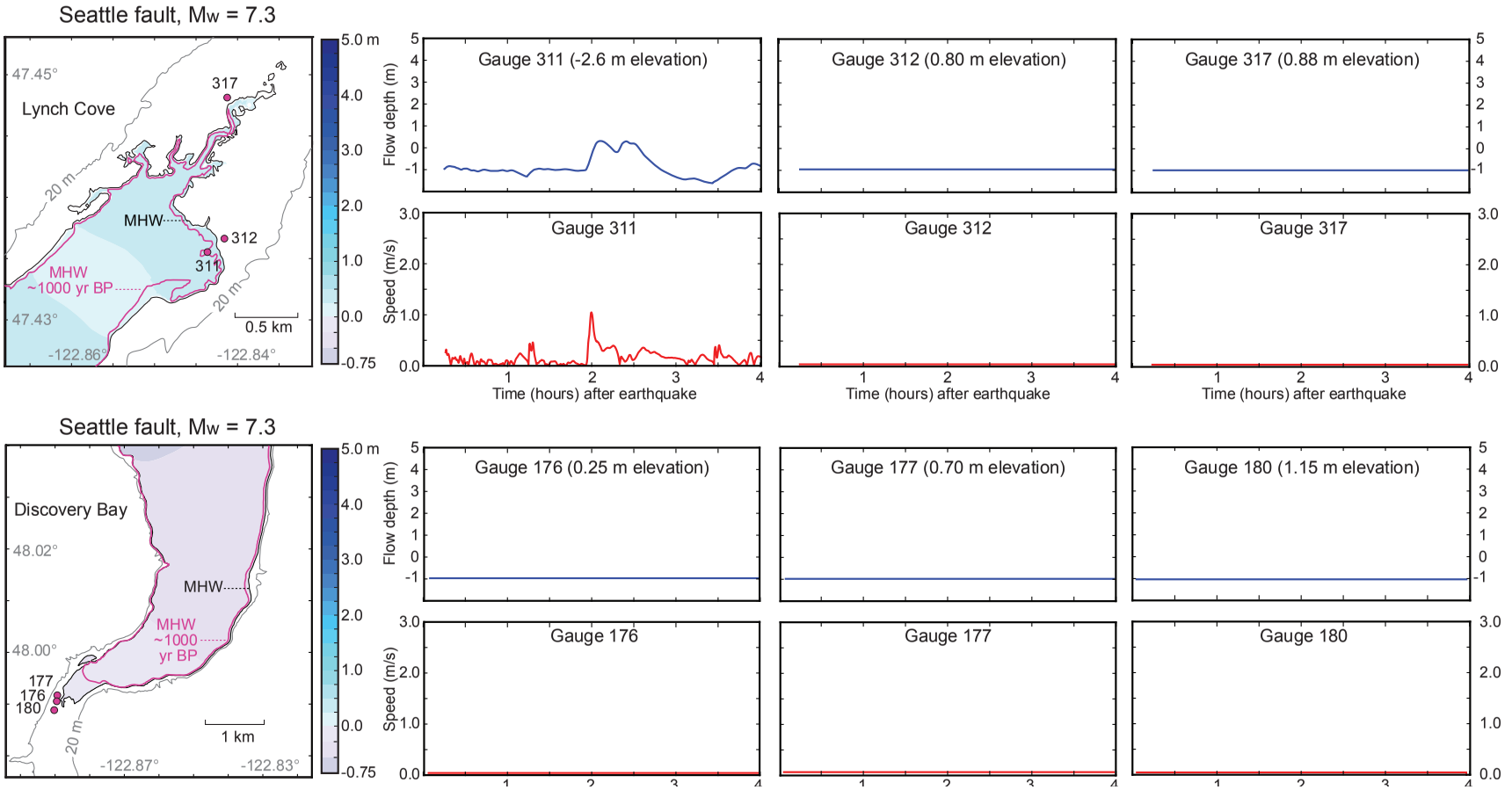

Figure 3.7. Seattle fault earthquake GeoClaw tsunami simulation results for Lynch Cove (top row) and Discovery Bay (bottom row). The simulation grid shows modern mean high water (MHW) in black, and adjusted MHW from 1,000 years ago (-1m) in magenta. The numbered gauge plots on the right correspond to gauge locations in the simulation grid on the left. Gauge elevations and flow depths are with respect to a MHW datum. Plots in blue are flow depths (m), and plots in red are flow speeds (m/s).

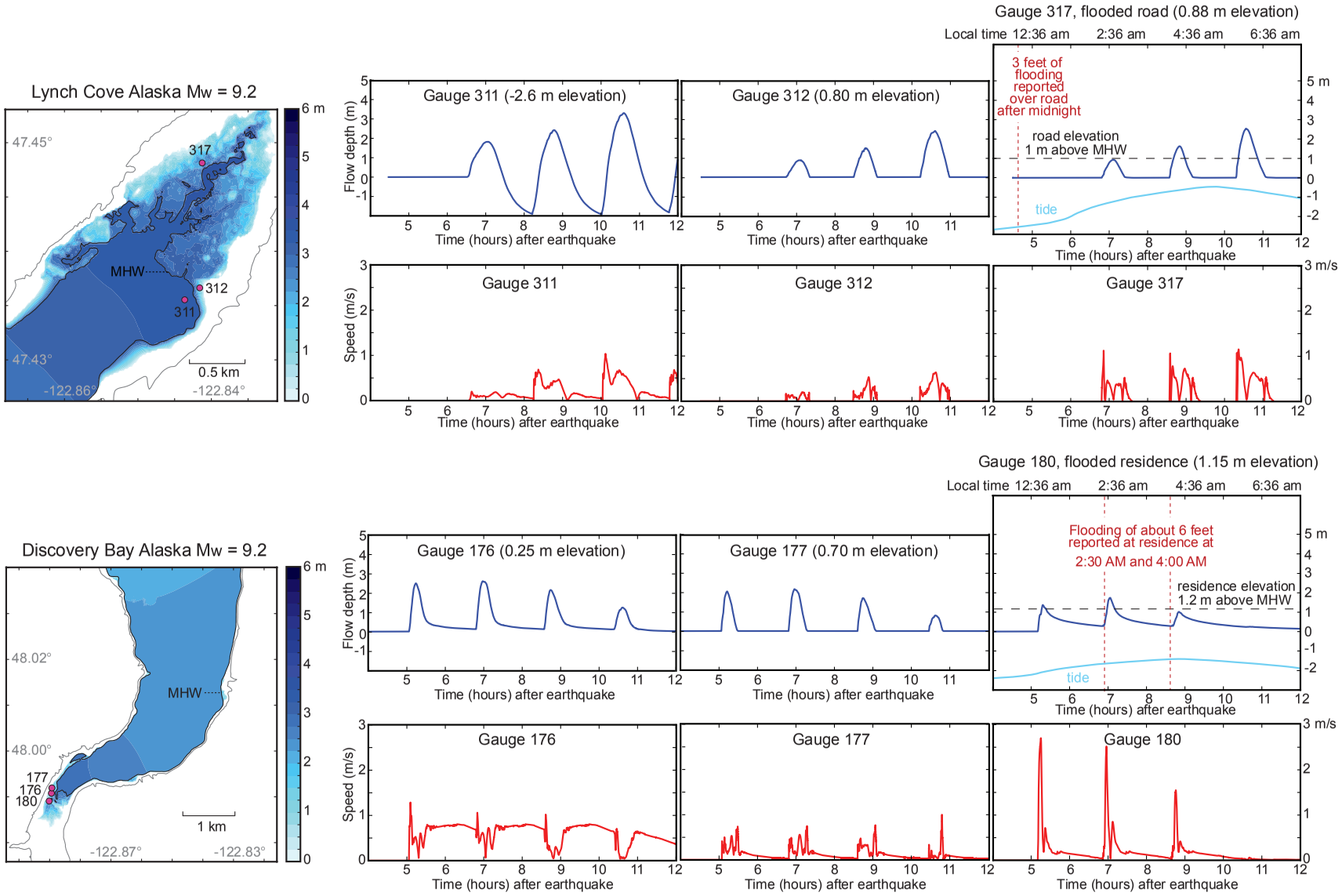
Lynch Cove Alaska Mw = 9.2
47.45°
47.43°
-122.86°
-122.84°
317
312
311
MHW
0.5 km
6 m
Gauge 311 (-2.6 m elevation)
Gauge 312 (0.80 m elevation)
Gauge 317, flooded road (0.88 m elevation)
Local time 12:36 am
2:36 am
4:36 am
6:36 am
3 feet of flooding reported over road after midnight
road elevation 1 m above MHW
tide
Flow depth (m)
Time (hours) after earthquake
Gauge 311
Gauge 312
Gauge 317
Speed (m/s)
3 m/s
Discovery Bay Alaska Mw = 9.2
48.02°
48.00°
-122.87°
-122.83°
177
176
180
MHW
1 km
Gauge 176 (0.25 m elevation)
Gauge 177 (0.70 m elevation)
Gauge 180, flooded residence (1.15 m elevation)
Flooding of about 6 feet reported at residence at 2:30 AM and 4:00 AM
residence elevation 1.2 m above MHW
Gauge 176
Gauge 177
Gauge 180

(Previous page) Figure 3.8. Alaska earthquake GeoClaw tsunami simulation results for Lynch Cove (top row) and Discovery Bay (bottom row). The simulation grid shows modern mean high water (MHW) in black. The numbered gauge plots on the right correspond to gauge locations in the simulation grid on the left. Gauge elevations and flow depths are with respect to a MHW datum. Plots in blue are flow depths (m), and plots in red are flow speeds (m/s). Alaska earthquake occurred at 3:36 UTC (5:36 pm Alaska Standard time; 7:36 pm Pacific Standard Time). Light blue tide curve shows vertical tidal difference in 1964 in the hours after the earthquake, but its position on the y-axis is arbitrary.

3.4 DISCUSSION

Simulated tsunami waves are variable in Puget Sound, where they are controlled by complex channel morphology, refraction by islands, and varying water depths ranging from 250-meter-deep glacially-carved fjords, to expansive shallow tidal flats. Narrow, deep fjords common in Puget Sound have been recognized as amplifiers of tsunami waves (Fine et al., 2008). The tidal marshes at Lynch Cove and Discovery Bay, both at the head of narrow terminal channels, are flooded in all tsunami simulations except the Seattle fault simulation, and the tsunami deposits preserved at these sites are evidence of past tsunami inundations.

3.4.1 *Cascadia Tsunamis Flood Both Lynch Cove and Discovery Bay*

The tidal marshes at both Lynch Cove and Discovery Bay experience flooding from the simulated Cascadia tsunamis. At Lynch Cove, the buried rupture and splay fault sources produce the highest waves, while the heterogeneous slip source, a potential analog of the A.D. 1700 earthquake (Wang et al., 2013), produces the lowest. GeoClaw tsunami simulations of all three Cascadia rupture styles produce tsunamis with flow depths higher than adjusted MHW (-0.33 m below present) at all gauges. The buried rupture and splay sources predict similar flow depths between 2.0–2.25 m over MHW at the back edges of the marsh at gauges 312 and 317. Gauge 311, on the seaward edge has the greatest flow depths for all three Cascadia sources. The

heterogeneous slip source predicts flow depth 1 m over MHW at gauges 312 and 317, and the buried and splay ruptures predict over flow depths over 2 m above MHW at gauge 312 and 317. At Lynch Cove, the simulated current speed at the gauge 311 has spikes between 0.5–1.5 m/s for all three Cascadia simulations (Figure 3.3). The maximum simulated speeds for the Lynch Cove grid exceed the values calculated at the gauges for all three the Cascadia sources, with highest speeds occurring in the channel of the Union River. Appendix 5 contains plots of maximum speeds within each site's grid. The simulated speeds exceed typical tidal current maximum speeds at Lynch Cove, which fluctuate between 0.0–0.05 m/s with occasional jumps to values approaching 0.1 m/s (Paulson et al., 2006), and exceed current speeds capable of eroding muddy tidal flats (Houwing, 1999). Simulated current speeds rise and drop to zero over the 12 hours of the simulations for all three Cascadia sources. Current speeds must drop to nearly zero to deposit 5 φ (0.3 mm) silt-sized particles, and the variation in speed seen in the gauge plots for all three Cascadia sources suggests that current speeds vary from speeds sufficient to erode and transport silt grains then slow between waves, allowing deposition of silt.

The heterogeneous rupture earthquake source was created to approximate the A.D. 1700 earthquake based on estimates of greatest slip amount of coastal subsidence derived from paleoseismic studies (Wang et al., 2013; Gao, 2016). While this source has lower flow depths than either the buried rupture or splay earthquake sources, the heterogeneous slip source still produces a tsunami that covers the marsh at Lynch Cove, implying that a deposit could be left behind by a similar flow, given sufficient flow speeds. This model used coseismic subsidence values that were less than estimates previously made using diatoms and vascular plants (Hemphill-Haley, 1995; Atwater and Hemphill-Haley, 1997), so it may underestimate the actual coseismic subsidence in A.D. 1700.

Variations in tides may affect wave height and whether tsunamis leave deposits. Back calculations of tides indicate that the tide was low on the coast of Washington at the time of the 1700 Cascadia earthquake (Mofjeld et al., 1997). Using Mofjeld et al.'s (1997) calculated tidal level for Victoria, BC after the 1700 earthquake, and then comparing modern tidal offset between Victoria and Lynch Cove, suggests that the tide was low, but rising, when the first wave would have arrived at Lynch Cove, about four hours after the earthquake. Lynch Cove has a tidal range of 3.7 meters, so a low tide would reduce flow depths significantly. However, simulated tsunamis waves, once in Hood Canal, oscillate back and forth between Lynch Cove and Dabob Bay for at least 12 hours after the earthquake, and that timeframe could potentially include two high tides (Cascadia simulation URL in Appendix 5). Such oscillations were also described from simulations of tsunamis in the Seto Inland Sea, where tsunami waves resonated for over 20 hours, and tsunami heights did not decline for over 10 hours (Kubo et al., 2007).

Each of the three Cascadia sources produce greater flood depths and flow speeds at Discovery Bay than at Lynch Cove. As at Lynch Cove, the heterogeneous slip source produces the smallest run-ups and flow speeds. In addition to greater flow depths and speeds, Discovery Bay shows different wave behavior than Lynch Cove. Discovery Bay simulations show an initial large wave followed by a sequence of smaller, decreasing waves. This differs from Lynch Cove, where later waves are sometimes higher than earlier waves. Current speeds at gauge 180 at Discovery Bay are the highest observed in any of the three Cascadia simulations at either site. This is likely caused by constriction of the flow as it moves up Salmon Creek. Because Discovery Bay flow depths are always higher than Lynch Cove flow depths in the simulations, it is possible that there is a threshold size of tsunami that would leave deposits at Discovery Bay, but not Lynch Cove.

3.4.2 *Seattle Fault Tsunami Dissipates Before Reaching Lynch Cove or Discovery Bay*

The simulation of the 900–930 A.D. Seattle fault earthquake produced measurable flow depths at only the single lowest elevation gauge, the tidal flat gauge 311 at Lynch Cove (Figure 3.3, 3.7). This suggests that the Restoration Point earthquake's tsunami (Nelson et al., 2014), as simulated, was extremely unlikely to be geologically recorded at either study site, eliminating this earthquake's tsunami as a source of deposits at either Lynch Cove or Discovery Bay. If the 900–930 A.D. Seattle fault zone rupture had extended west and offset the seafloor in Hood Canal (Lamb et al., 2012), there would likely have been a tsunami generated that may have reached Lynch Cove, but if the seafloor offset remained east of Hood Canal, the resulting tsunami, as simulated, was negligible.

Previous simulations of a Tacoma fault tsunami generated tsunamis an order of magnitude smaller than Seattle fault tsunamis at Gorst (Figure 3.2B) in Sinclair Inlet (Arcos, 2012). Because Gorst is closer to the Seattle fault, and a tsunami generated by the Tacoma fault would have to travel even farther to get to Lynch Cove or Discovery Bay, it unlikely that the Tacoma fault could be a source of deposits at either Lynch Cove or Discovery Bay.

Because the simulation was run using modern topography and bathymetry, the simulation may not reflect the conditions 1,000 years ago, as changes in the morphology of Lynch Cove or Discovery Bay would likely influence tsunami behavior. Also, for the Seattle fault simulation, sea level was lowered by 1 m from modern MHW, which would also influence the simulation, because when sea level fluctuates, the location of large shallow tidal flats and marshes shifts.

3.4.3 *Alaska Tsunami Floods Both Discovery Bay and Lynch Cove*

3.4.3.1 Discovery Bay 1964 Eyewitness Account

The 1964 Alaska tsunami caused two distinct waves of flooding at a residence at the head of Discovery Bay, near the bank of Salmon Creek (Port Townsend Leader, 1964; Lander et al., 1993). The timing of the flooding and the flood depths were recalled by the homeowner. The first wave of flooding was at about 2:30 AM, and the receded after about 20 minutes. A second wave of flooding occurred at about 4:00 AM. The homeowner estimated the depth of the flooding to be about 6 feet (~2 m) above the normal level of Salmon Creek (Port Townsend Leader, 1964; Lander et al., 1993). Simulation gauge 180 at Discovery Bay is at the location of the flooded residence (Figure 3.8).

3.4.3.2 Discovery Bay Alaska Simulation

The Alaska tsunami simulation produced maximum flood depths and wave arrival times that agree with the eyewitness observations of flooding at Discovery Bay. The first simulated wave arrives at about 12:30 AM, earlier than any flooding was observed in 1964, but a wave arriving at that time would have coincided with low tide, and therefore may not have been observed. The second and third waves have simulated arrival times that agree with 1964 observation of 2:30 AM and 4:00 AM (Figure 3.8). The simulated flood depths also agree with observations from 1964. Gauge 180 is at an elevation of 1.2 m above MHW, and in the simulation, the second wave reaches nearly 2 m above MHW, consistent with the observation that the water was about 6 feet (~2m) above normal level for Salmon Creek. The timing of the third simulated wave at 4:00 am agrees with the observations from 1964. The simulation predicts a smaller third wave than second wave. A wave arriving at 4:00 am in 1964 would have coincided with high tide, and therefore could have caused similar flooding as earlier higher waves that arrived at lower tides

(Figure 3.8). Simulations were run with a constant sea level held at MHW, and therefore do not reflect the tidal fluctuations that would have influenced the actual 1964 flow depths.

3.4.3.3 Lynch Cove 1964 Eyewitness Account

The 1964 Alaska earthquake tsunami was reported to be the cause of localized flooding north of the marsh at Lynch Cove (Seattle Daily Times, 1964; Lander et al., 1993). According to eyewitness observations, flooding occurred shortly after midnight on March 28, 1964. The flooding covered a road north of Lynch Cove marsh and the water was estimated to be 3 feet (~1 m) higher than normal. It was also observed that there was debris, including trees, floating in Hood Canal at the time of the flooding.

3.4.3.4 Lynch Cove Alaska Simulation

The simulation results for Lynch Cove are inconsistent with the historical observations of time of flooding. In the simulation, the arrival of the first wave at Lynch Cove is about 7 hours after the earthquake, about 2:40 AM local time. This is inconsistent with the observation of flooding of the road around midnight (Seattle Daily Times, 1964). Another discrepancy is that the simulation predicts increasing wave heights, with the largest wave at about 6:30 AM on March 28; however, there are no known observations of any flooding other than that of the road around midnight.

The simulation arrival times of the first waves at Neah Bay, Seattle, and Discovery Bay, agree with tide gauge records, and the wave arrival times at Port Alberni, Canada (Clague et al., 1994). In 1964, the first wave arrived at Port Alberni at 12:20 AM. In the simulation, the first wave reaches Discovery Bay after 12:30 AM. By sea, Lynch Cove is over 330 km away from the entrance to Alberni Inlet, on a path along the Strait of Juan de Fuca past Discovery Bay, into the entrance to Puget Sound, and then along the length of Hood Canal to Lynch Cove. In all the

tsunami simulations (except the Seattle fault simulation) the first wave arrival time at Discovery Bay is about 1 hour and 20 minutes earlier than at Lynch Cove. Both the observed and simulated first wave arrival times at these closer to the Pacific suggest that either there must be a different source for the flooding observed after midnight at Lynch Cove, or that the eyewitness reported time of flooding was inaccurate by nearly three hours.

If the time of the flooding of the road was accurately reported, the flooding must have been caused by something other than the Alaska tsunami. Tidal records from 1964 indicate that the tide would have been low around midnight at Lynch Cove. The tide gauge at Lynch Cove was not in operation until 1978, but tidal highs and lows at Lynch Cove are nearly synchronous with those at the Seattle tide gauge. Records for the Seattle gauge, plotted onto the Gauge 317 plot in Figure 3.8, show that the tide at Lynch Cove would have nearly coincided with the lower low tide of the 24-hour semidiurnal tidal cycle at midnight. The tide would have been rising at the arrival time of the first wave, predicted by the simulation to arrive at ~2:40 AM; near peak high tide level at the arrival of the second wave at ~ 4:30 AM; and lowering at the arrival of the third wave at ~6:15 AM. The incoming tsunami, which would have been in the Strait of Juan de Fuca around midnight, may have influenced the tides in the narrow waterway of Hood Canal (~100 km long, and an average of 2 km wide), possibly preventing complete tidal drainage of Hood Canal. However, at Alberni Inlet, a similar narrow inlet, tides did fluctuate during the tsunami on the night of March 27-28, 1964, despite the arrival of three tsunami waves (Clague et al., 1994).

If tidal fluctuations in Hood Canal were not affected by the tsunami, another possible source of the observed flooding is a seismic seiche in Hood Canal. The 1964 Alaska earthquake generated seismic seiches around the world, including at the Snohomish River delta and in Lake Union in Seattle (McGarr and Vorhis, 1968). The tsunami simulation animation (Appendix 5)

shows that tsunami waves oscillate between Lynch Cove and Dabob Bay for hours following the arrival of the first waves in Hood Canal. It appears that this oscillation may have an additive effect on the height of later waves, because at Lynch Cove, simulated waves do not follow a pattern of decreasing height over time as they do at Discovery Bay. This simulated wave behavior may also mirror seiche behavior in Hood Canal, with oscillations and increasing wave heights over time, resulting in the flooding over the road near midnight. If oscillating waves washed debris into the water in the hours following the earthquake, this may also explain the observation in 1964 of trees and brush in the water near Lynch Cove (Seattle Daily Times, 1964).

3.4.3.5 Comparing Alaska and Cascadia Simulations

As simulated, the Alaska tsunami produced flow depths comparable to the Cascadia buried rupture and splay fault simulations at Lynch Cove (Figure 3.5). At Discovery Bay, the 1964 Alaska simulation is comparable to the Cascadia heterogeneous slip source, but smaller than the buried rupture or splay fault simulations (Figure 3.6). These comparisons suggest that the 1964 Alaska simulation source used overestimates tsunami wave flow depths, at least at Lynch Cove. The 1964 Alaska earthquake source is a simplified geometry of true rupture from the 1964 Alaska earthquake (González et al., 2014). A study using this source for Crescent City, CA suggests that it may produce greater inundation distances than were historically observed, although the exact inundation limits are not well known for all areas affected (González et al., 2014).

Another way to compare Alaska and suspected Cascadia tsunamis at Lynch Cove and Discovery Bay is by their respective tsunami deposits. No tsunami deposits from the 1964 Alaska tsunami have been observed at Lynch Cove. At Discovery Bay, two thin (1-2 mm) discontinuous sand laminae were interpreted as potential deposits from the 1964 Alaska and 1960 Chile earthquakes (Williams et al., 2005). If the 1964 Alaska tsunami left no or only trace tsunami

deposits, then layers A and B at Lynch Cove, and Beds 1-6 at Discovery Bay, which are much thicker, are unlikely to be the deposits of transoceanic tsunamis. Therefore, it is more likely that these thicker deposits are either from Cascadia earthquakes, intraplate earthquakes, or landslide-generated tsunamis.

3.5 CONCLUSIONS

GeoClaw tsunami simulations of three Cascadia great earthquake sources—buried slip, heterogeneous slip, and slip with an accompanying splay fault—all produce tsunamis that reach both Lynch Cove and Discovery Bay with flow depths and current speeds capable of producing tsunami deposits. The heterogeneous slip source, an analog of the 1700 Cascadia earthquake produces the smallest of the three Cascadia tsunamis, while the buried slip earthquake produces the largest. The 900–930 A.D. Restoration Point Seattle fault earthquake produces a tsunami that fails to register at 5 of the 6 gauges used in the simulations. In the simulation of a tsunami from the area of deformation of the 1964 Alaskan earthquake, the marshes are overtopped at both Lynch Cove and Discovery Bay, and the simulation likely overestimates flood depths, though the wave heights and arrival times agree well with eyewitness observations of flooding at Discovery Bay. The tsunami wave arrival times at Lynch Cove probably went unobserved, but early flooding before the predicted first wave arrival time may have been the result of a seiche in Hood Canal triggered by seismic waves from the Alaska earthquake.

Chapter 4. A Diatom-Based Transfer Function for Lynch Cove in Puget Sound—An Aid to Studying Relative Sea Level Change and Cascadia Subduction Zone Dynamics Over the Last ~1,000 Years

4.1 INTRODUCTION

Lynch Cove marsh in the Hood Canal arm of Puget Sound lies in the forearc basin of the Cascadia Subduction zone (CSZ), about 240 km inland of the deformation front (Figure 4.1). Geophysical models of CSZ earthquake deformation predict coastal subsidence of varying inland extents (cf. Figure 3.4A-C), and some of these models calculate nonzero values for areas as far inland as Lynch Cove (Figure 4.2). The inland extent of earthquake cycle deformation for Cascadia is not precisely known, and determining this is important to assessing seismic hazards (Petersen et al., 2014). Cascadia earthquake deformation has not been quantified at sites as far inland as Puget Sound. The tidal marsh sedimentary record at Lynch Cove spans over 1,000 years, a time span that includes at least two, and probably three Cascadia subduction zone earthquakes (Atwater and Hemphill-Haley, 1997; Atwater et al., 2004; Goldfinger et al., 2012; Goldfinger et al., 2017), and has two tsunami deposits that serve as markers for two of these earthquakes (Chapter 2). Because few margin-normal data points exist for Cascadia, determining the presence or absence of vertical deformation at Lynch Cove will help constrain the easternmost edge of subduction zone deformation and seismic locking (Wang and Tréhu, 2016), provide an important "paleogeodetic" data point for models of subduction zone dynamics, improve the estimation of seismic hazards, and refine long-term rates of local sea-level rise.

Tide gauge and leveling data has been used to study interseismic vertical deformation for Cascadia (Alba et al., 2011; Burgette et al., 2009; Burgette et al., 2012; Verdonck, 2006). Tide gauge records that span over a century in Seattle and other southern Puget Sound sites with shorter

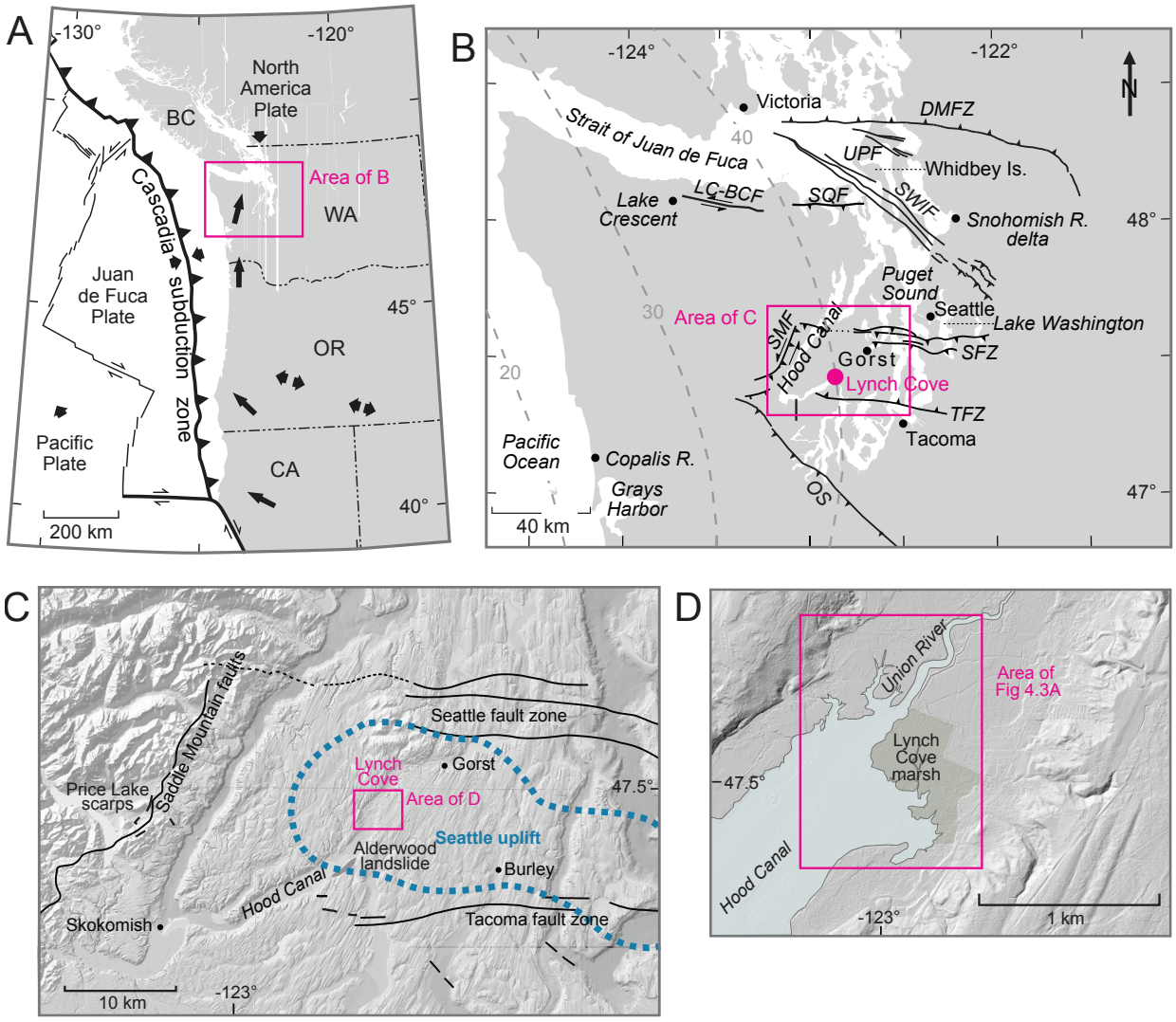

Figure 4.1. Tectonic setting of the Puget Lowland, and study site location. (A) Tectonic setting of the Puget Sound region. Holocene faults in black (adapted from Blakely et al., 2009; Nelson et al., 2014), labeled as follows: SFZ—Seattle fault zone; TFZ—Tacoma fault zone. Gray dashed lines are depth (km) of Juan de Fuca slab (McCrory et al., 2012). (C) Setting of Lynch Cove in the southern Puget Lowland and Hood Canal. Blue dotted area is approximate area of Seattle uplift from ~1,000 years ago (Bucknam et al., 1992; Johnson et al., 1999). Lidar map base of (Finlayson, 2005).

histories were used in combination with vertical GPS data to estimates an absolute sea level rise of 1.3 ± 0.7 mm/yr, in southern Puget Sound. When added to local tectonic subsidence, the overall rate of relative sea level rise is estimated to be 2.2 ± 0.01 mm/yr (Mazzotti et al., 2008). Another study using tide gauge data combined with leveling surveys also find a greater relative sea level

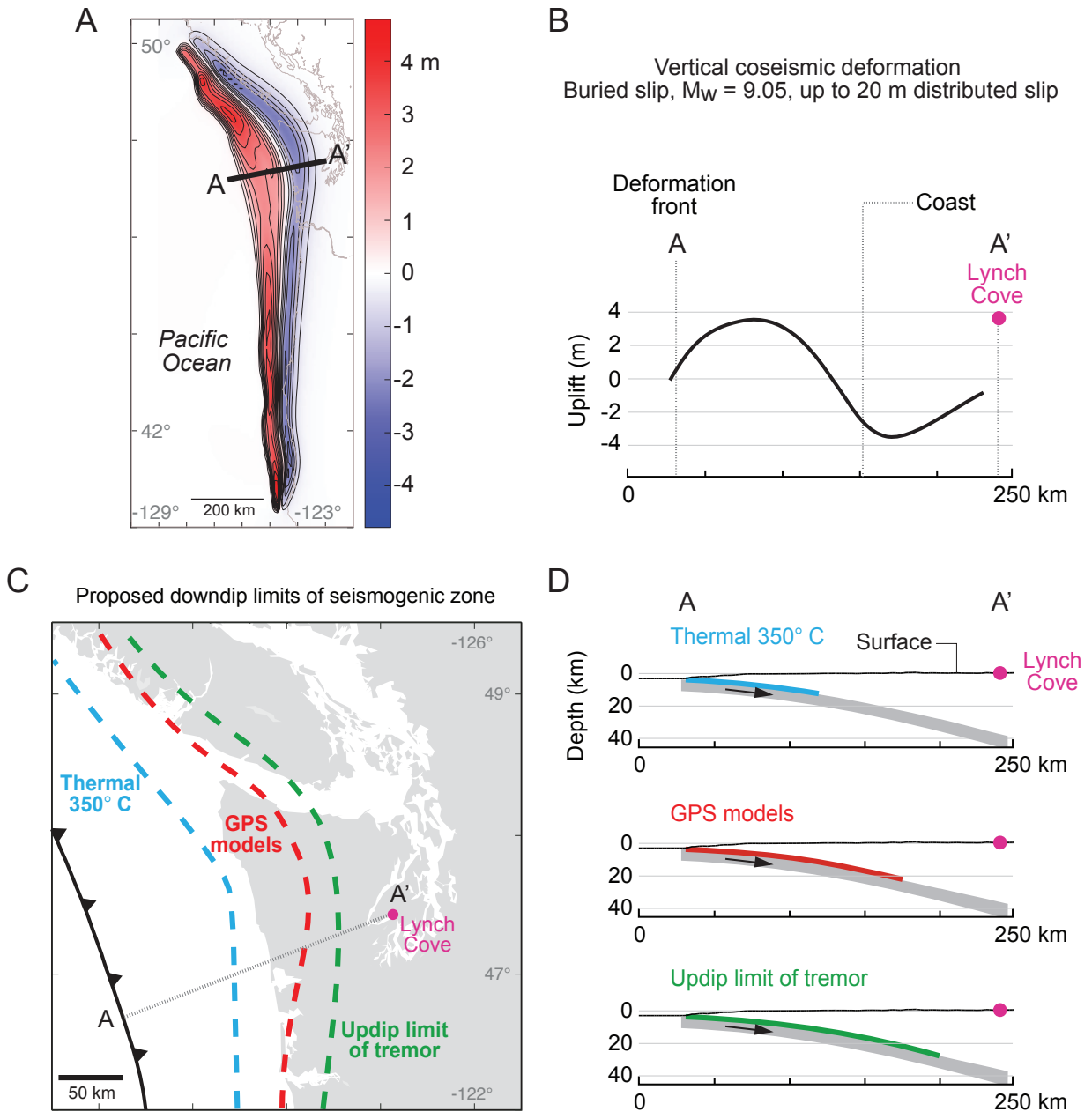

Figure 4.2. Cascadia coseismic deformation and downdip rupture limits. (A) Coseismic deformation from buried slip M_w 9.05 Cascadia earthquake (Chapter 3). (B) Cross section of vertical deformation from line A-A' in (A). Position of Lynch Cove shown with pink dot. (C) Three different proposed downdip limits of rupture used in U.S. Seismic Hazard Maps (Petersen et al., 2014). (D) Cross sections of A-A' in (C) for each of the down dip limits of rupture. Cross sections after Witter et al. (2013).

rise in the south part of Puget Sound, with a mean sea level rise of 2.1 ± 0.1 mm/yr for the Seattle tide gauge during the 20th Century (Verdonck, 2006).

Additional studies using different methodologies in Puget Sound have yielded rates of absolute sea level rise that are lower than tide gauge studies. A compilation of sea level radiocarbon ages and datums from sites around Puget Sound suggest that relative sea level was within 1 meter of present level by about 800 years ago (Engelhart et al., 2014). In another study, ecological classification of diatom assemblages from a sediment core in northern Puget Sound estimated less than 1 meter of sea level rise in the last 1,000 years (Eronen et al., 1987), and radiocarbon dating of peat records from five northern Puget Sound marshes also estimates sea level rise of less than 1 m in the last 1,000 years (Beale, 1991).

Relative sea level rise is apparent in the marsh at Lynch Cove. There is a fringe of dying trees around the back (landward) edge of the marsh, and snags of growth-position mature Western red cedar trees (*Thuja plicata*) are rooted in soils buried by tidal marsh deposits (Figure 4.3E). A comparison of the modern tidal marsh with a georeferenced U.S. Coast Survey map (Gilbert, 1884) shows that the seaward edge of the marsh has eroded back as much as 20 meters in places, and the back edge of the central part of the marsh is correspondingly about 20 meters farther inland than it was in 1884 (Figure 4.3A-D); while in other parts of the marsh, the outermost and back edges of the tidal marsh remain similar to their position in 1884. Forest soils overlain by tidal marsh deposits are also documented at several other southern Puget Sound tidal marshes including North Bay, Catfish Lake, Burley, and Gorst (Bucknam et al., 1992; Sherrod et al., 2004; Arcos, 2012). At these sites, more than a meter of submergence has been noted since the "millennial earthquake series" of crustal earthquakes in Puget Sound around ~1000 yr B.P. (Nelson et al., 2014).

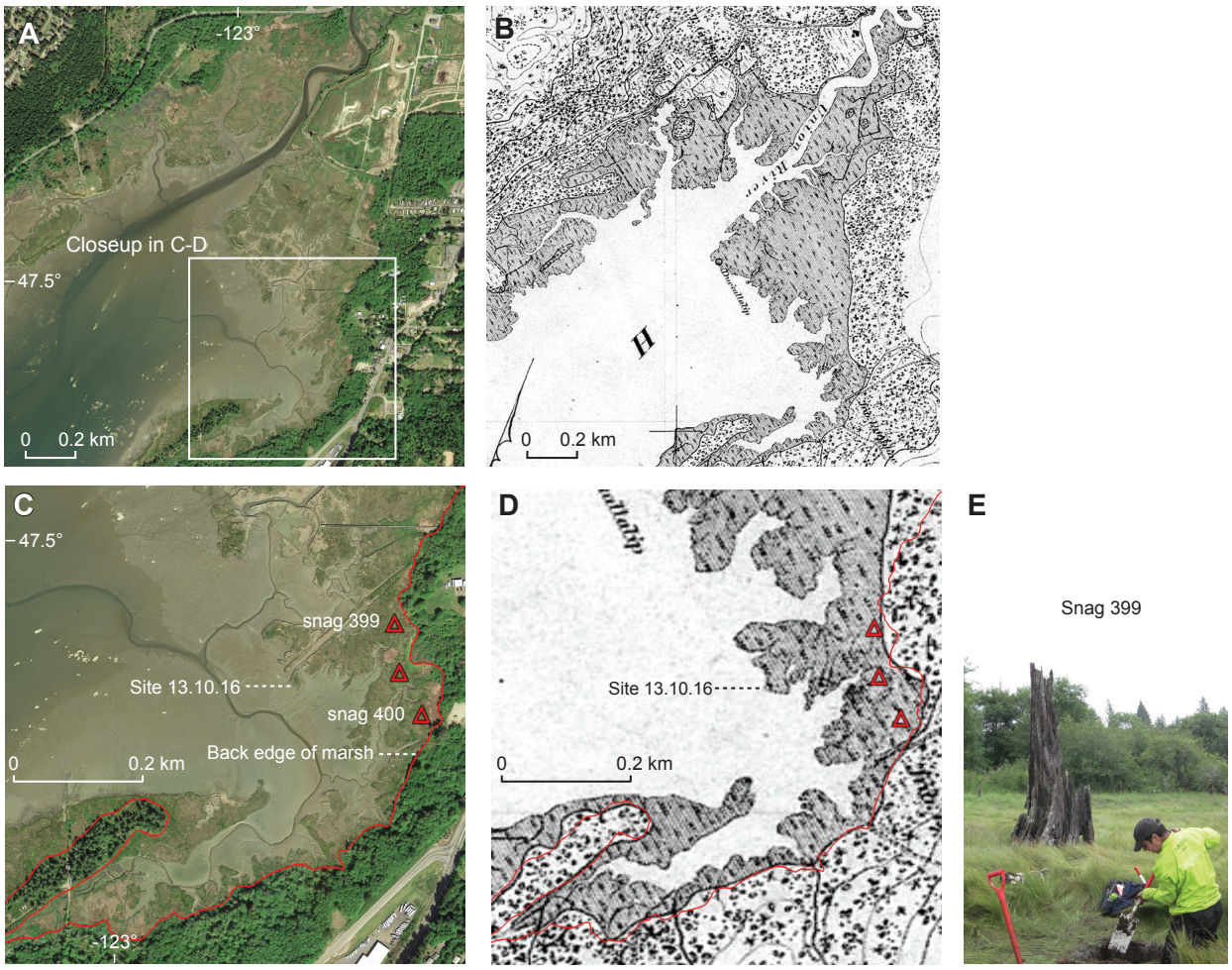

Figure 4.3. A comparison of recent and historical marsh extent at Lynch Cove. (A) 2013 Google Earth image and (B) U.S. Coast Survey map (Gilbert, 1884), (C) Locations of snags (red triangles) and back edge of tidal marsh (red line), (D) location of snags and back edge of 2013 marsh plotted in red on georeferenced 1884 map, (E) snag of Western red cedar (*Thuja plicata*) near back edge of tidal marsh.

Fossil diatoms are used to study the sea level history at Lynch Cove. Distinctive diatom assemblages occupy different intertidal elevation zones, similar to the vertical zonation of tidal marsh plants (Figure 2.10). Tidal marsh diatom distributions are cosmopolitan, with similar assemblages found in intertidal marshes in temperate climates worldwide (Hemphill-Haley, 1995; Hemphill-Haley, 1996; Dura et al., 2016; Sawai et al., 2016; Sawai et al., 2017). Fossil diatoms from tidal marsh sediment records can be used to characterize paleoenvironment by

employing statistical transfer function methods that compare the distribution of living diatoms from the same region with fossil diatoms in the sediment record. To quantify the amount of relative sea level rise at Lynch Cove, a diatom-based transfer function is developed for the last ~1,000 years of sedimentary deposition. The transfer function statistically compares the distribution of modern diatoms in the intertidal zone to fossil diatoms found in the sediments of Lynch Cove. From the transfer function, a paleomarsh surface elevation history is calculated, and then sea level history constructed for Lynch Cove. Similar studies have been used to construct relative sea level histories and subduction zone deformation for sites on the outer coast of Cascadia (Hawkes et al., 2011; Engelhart et al., 2013); in Japan (Sawai et al., 2004a; Sawai et al., 2004b); and in Alaska (Shennan and Hamilton, 2006; Watcham et al., 2013; Shennan et al., 2016); and in Chile (Dura et al., 2015).

4.2 SETTING

Lynch Cove is a salt marsh located at the head of Hood Canal, an arm of Puget Sound in the Puget Lowland. Hood Canal is a narrow (~2 km wide) deep glacially-carved fjord, with an abundant sediment supply from unconsolidated and unstable glacial deposits. The tidal marsh at Lynch Cove is about one square kilometer in area (Figure 4.1D). Historical channeling has modified some of the natural channels in the marsh, but otherwise the marsh is largely unchanged since the time the area was first mapped in 1884 by the U.S. Coast Survey (Gilbert, 1884), Figure 4.3

The marsh at Lynch Cove has been previously studied for evidence of coseismic deformation from crustal earthquakes. The marsh at Lynch Cove is located within the Seattle Uplift, an area bounded by the Seattle fault to the north, the Tacoma fault to the south, and the Saddle Mountain fault to the west (Figure 4.1B, C). Lynch Cove experienced at least 2 meters of

coseismic uplift (Bucknam et al., 1992; Sherrod et al., 2004), during an earthquake or earthquakes on these bounding faults, about 1000 ± 200 years ago (Bucknam et al., 1992; Sherrod, 2001; Sherrod et al., 2004; Nelson et al., 2014). This uplift raised a tidal flat out of the intertidal zone, and later it was colonized by supratidal forest and fresh water marsh.

Within 300 years after the uplift, sea-level rise had begun to encroach the forested landscape, and as the rise continued, began to convert previously forested areas to salt marsh. Evidence of this is seen in rooted Western red cedar (*Thuja plicata*) snags that are overlain by tidal marsh sediments (Figure 4.3E). Based on the modern vertical zonation of vegetation at Lynch Cove (Sherrod, 1999), and the lowest expected elevation that salt intolerant *Thuja plicata* can grow, a minimum of 1 m of submergence had occurred at Lynch Cove between 545-745 years after the Seattle Uplift.

4.3 METHODS

4.3.1 *Sample Collection, Preparation, and Diatom Identification*

Diatoms were sampled, prepared, and identified following standard methods. Fossil diatoms were sampled from two sediment monoliths collected from the top 181 cm of sediment at Lynch Cove field location 13.10.16 (Figure 4.4). Samples were collected at >10 cm intervals over the length of the 1.8 m section, with additional samples collected at closer intervals adjacent to two tsunami deposits. Diatom samples were prepared by reacting 1 cc of sediment with 100 ml of 35% H_2O_2 and gently heating to remove organics. Samples were rinsed with filtered water and centrifuged several times. Slides were made by allowing an aliquot of sediment and water to settle through a water column onto cover slips at the bottom of a 250-ml beaker for 8 hours (Warnock and Scherer, 2015). The coverslips were air dried, and then glued to slides with Meltmount

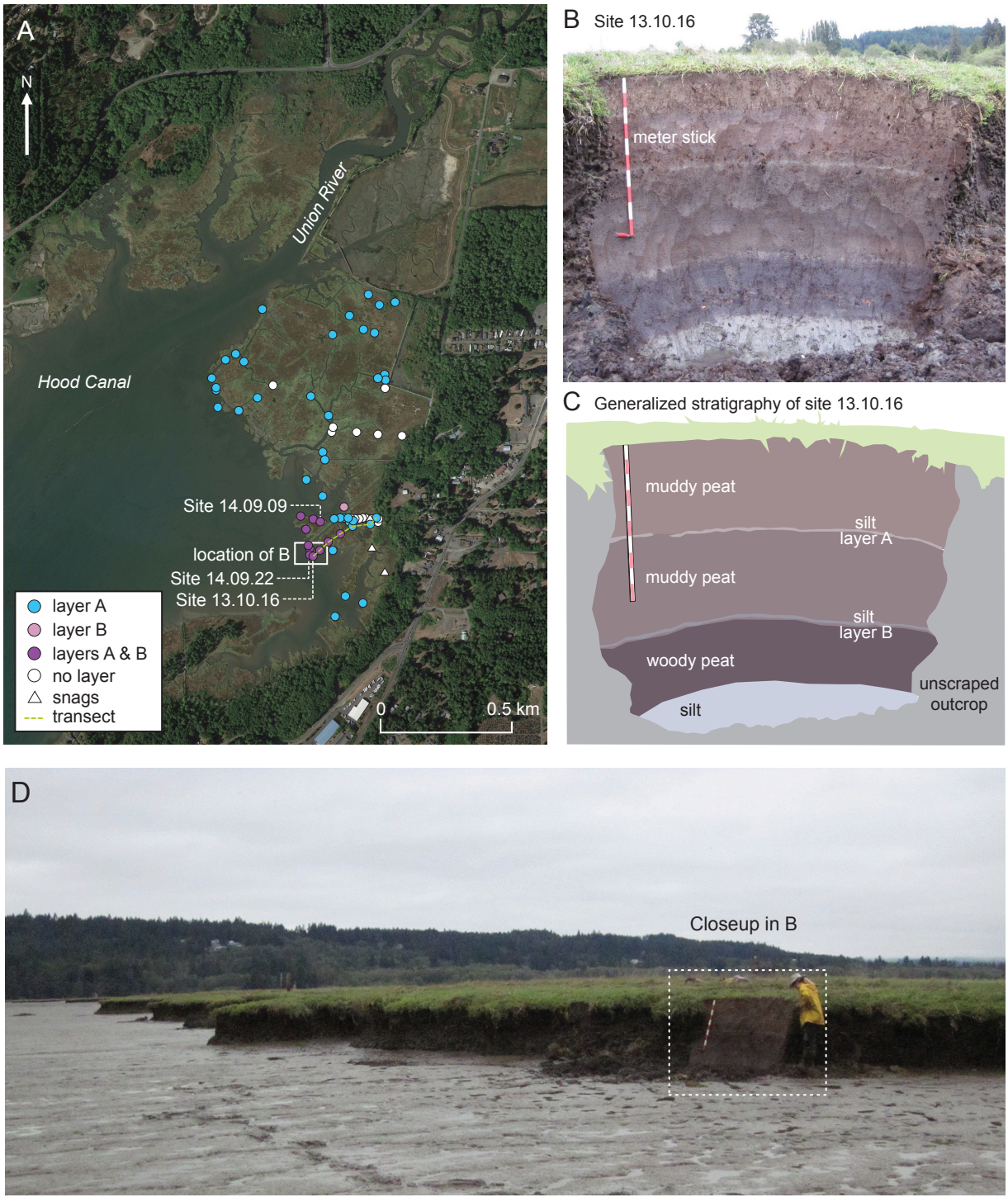

Figure 4.4. (A) Lynch Cove marsh study site showing locations of layers A and B, (B and C) outcrop and Generalized stratigraphy of site 13.10.16, with layers A (upper) and B (lower). There are between 3-5 cm of muddy peat below layer B. Layer B does not exactly coincide with the contact between the woody peat and the overlying muddy peat. (D) Eroding edge of marsh at location of (B) showing adjacent tidal flat.

mounting medium. Diatoms were counted to a minimum of 400 valves per slide at magnifications of 1000x, and 1500x as necessary for identification. Identifications were made using several widely-used diatom references (Hemphill-Haley, 1993; Hemphill-Haley and Lewis, 1996; Horn, 1987; Horn, 1992; John, 1983; Krammer and Lange-Bertalot, 1985; Krammer and Lange-Bertalot, 1986; Kramer and Lange-Bertalot, 1993; Krammer and Lange-Bertalot, 2001; Laws, 1988; Witkowski, 2000), and grouped into ecological assemblages following classification used in Oregon and Washington tidal environments (Sawai and Nagumo, 2003; Sawai et al., 2016; Sherrod, 1999), and from other studies of intertidal diatoms (Dura et al., 2015; Dura et al., 2016; Sawai et al., 2017; Vos and de Wolf, 1993; Zong and Horton, 1998). A total of 109 diatom species were identified in 36 samples. Complete fossil diatom counts are in Appendix 4.

4.3.2 *Development of a Diatom-Based Transfer Function*

Diatom-based transfer functions have been widely-used to generate sea level histories from the sedimentary record (Kemp and Telford, 2015). This method statistically compares the distribution of living diatoms in the intertidal zone, known as the "training set" with fossil specimens preserved in tidal marsh sediments. This method identifies co-occurrences among species in modern assemblages that are characteristic of a particular elevation in the intertidal zone. These are then statistically compared to species from fossil assemblages to estimate paleo-elevation at time of deposition.

A modern diatom sampling transect across the intertidal zone was completed by Sherrod (1999) for Lynch Cove. This training set of modern diatoms was combined with additional samples (Sawai and Sherrod, unpublished data), and has since been used by Kelsey et al. (2012). This set, with an additional three samples collected at Lynch Cove, was used in this study to generate a sea level history of the last ~1,000 years at Lynch Cove. The training set was updated

to reflect taxonomic changes to diatoms since 1999, to make sure that fossil names aligned with training set names. This study follows methodology outlined by Kemp and Telford (2015), and used in many similar studies (Dura et al., 2015; Dura et al., 2016; Nelson et al., 2008b; Sawai et al., 2004b; Watcham et al., 2013; Zong and Horton, 1999).

A transfer function was developed to reconstruct the amount of relative sea level change over the last ~1,000 years at Lynch Cove. The transfer function was developed using C2 software (Juggins, 2007). C2 software allows statistical comparisons between the training set for a specific environmental variable, in this case elevation in the intertidal zone, between fossil and modern diatom assemblages. The analysis characterizes assemblages of known environmental distribution.

Because the samples in the training set were collected at different locations in Puget Sound with varying tidal ranges, the samples were standardized with respect to mean higher high water (MHHW) by using a standardized water level index (SWLI):

$$SWLIx = [\frac{100(ELEVx - MTL)}{MHHW - MTL}] + 100 \quad (4.1)$$

This transformation yields an indexed level for each sample at a collection location (SWLIx) between mean tidal level (MTL) and mean higher high water level (MHHW) based on sample elevation x (ELEVx). A constant of 100 is added to ensure that all samples have a positive SWLI value. In the SWLI index, MTL = 100, and MHHW = 200 (Kemp and Telford, 2015; Zong and Horton, 1999). At Lynch Cove, MTL= 2.16m, and MHHW = 3.69m. All statistics were run on SWLI values and then converted back to MHHW elevations for Lynch Cove for the resulting sea level curve.

The transfer function models developed here use the widely-used unimodal statistical technique of weighted averaging partial least squares (WA-PLS). In this method, species abundance in the training set is the predictor of an environmental variable, in this case elevation, which is the response variable. This method assumes that the more abundant a species is, the more favorable the environmental conditions are at the sample location for that particular species. Where species are at their maximum abundance are the optima, whereas the tolerance is the range in which the species is found. Elevation is calculated where the optima, or highest abundance, of each species occurs, and sample with high species abundance is weighted more in calculating elevation than in samples where it has lower abundance. The range of elevations, or species tolerance, is the weighted standard deviation of the species abundance (Juggins and Birks, 2012).

The reconstruction is made by calculating the weighted average of the species optima in the fossil samples. In addition to the weighted averaging, the WA-PLS also includes the calculation of the partial least squares (PLS) to the residuals, thereby improving the fit of the fossil taxa elevation to the training set. The WA-PLS calculations generate a designated number of different components, which are linear combinations of the training set data, where the first is weighted averaging without the PLS, and the subsequent components includes the PLS inverse deshrinking. It is best practice to use only the minimum number of components to avoid a model that over-fits the data. Typically, 2-3 components are sufficient, and each additional component should only be used if it improves the performance of the model by reducing the root mean square error of prediction (RSMEP) by at least 5% (Kemp and Telford, 2015). RMSEP, reported in SWLI units, is a measure of the differences between measured and predicted differences, and the square root of the standard error plus the mean bias squared. Lower RMSEP values indicate better transfer

function performance. The coefficient of determination, r^2 is a measure of the observed vs predicted values for 1000 bootstrap trials, with perfect predictive value $r^2 = 1$.

Outlier samples in the training set are those that the transfer function does not accurately predict. In the development of the transfer function, samples may be screened from models if they have known or suspected inaccuracies, low total specimens counts, or if the transfer function model has large residuals for those samples when cross-validated (Kemp and Telford, 2015). Juggins and Birks (2012) recommend removing samples that have residuals outside the 95% confidence interval. Such removals have the effect of improving transfer function performance, though the results may be artificially improved (Kemp and Telford, 2015). In addition, excluding individual species with less than 2% abundance from the statistical calculations, improves the transfer function performance (Juggins and Birks, 2012).

The transfer function models were validated by using bootstrapping cross-validation (ter Braak and Juggins, 1993; Juggins and Birks, 2012). The bootstrapping calculation generates a new training set from the original training set to test the transfer function. The bootstrapping was repeated 1000 times to improve uncertainty (Kemp and Telford, 2015).

4.4 RESULTS

4.4.1 *Diatom Paleoecology*

Figure 4.5 shows the stratigraphy, diatom sample locations, and tsunami deposit ages for outcrop 13.10.16 (Figure 4.4 B-D). Select diatom species are plotted grouped by ecological affinity. The base of the outcrop is dominated by tidal flat species, followed by a period of time in which soil conditions were too dry to support diatoms (“X” in preservation column). This soil formed after the tidal flat was coseismically uplifted out of the intertidal zone about 1,000 cal yr

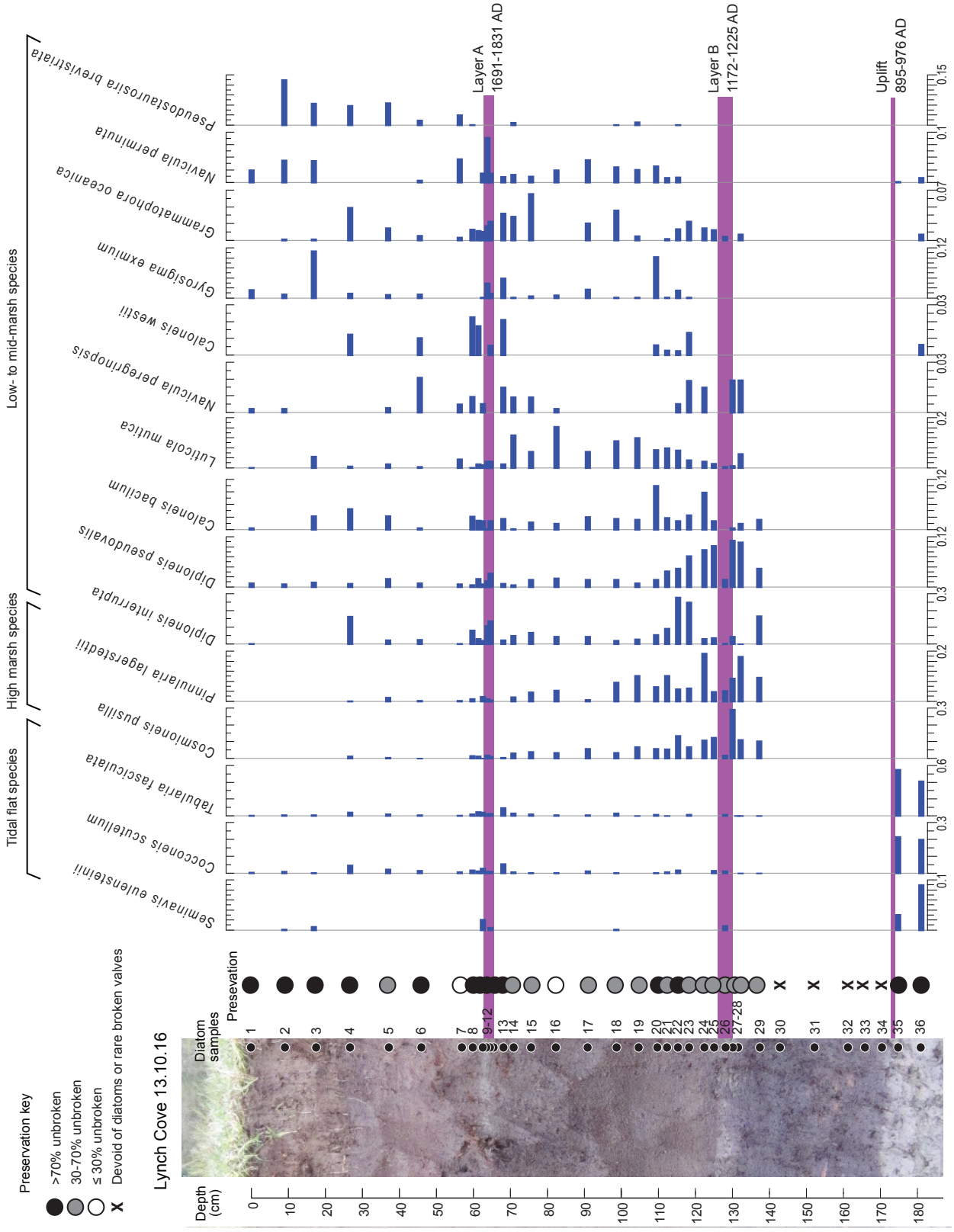
Lynch Cove 13.10.16
Depth (cm)
Diatom samples
Presevation
Preservation key
>70% unbroken
30-70% unbroken
≤ 30% unbroken
Devoid of diatoms or rare broken valves
Tidal flat species
High marsh species
Low- to mid-marsh species
Seminavis eulenstenii
Cocconeis scutellum
Tabularia fasciculata
Cosmioneis pusilla
Pinnularia lagerstedtii
Diploneis interrupta
Diploneis pseudovalis
Caloneis bacillum
Luticola mutica
Navicula peregrinopsis
Caloneis westii
Gyrosigma exmium
Grammatophora oceanica
Navicula perminuta
Pseudostaurosira brevistriata
Layer A
1691-1831 AD
Layer B
1172-1225 AD
Uplift
895-976 AD

(Previous page) Figure 4.5. Diatom data for Lynch Cove section 13.10.16. Select diatom species are plotted in groups by ecological affinity. Horizontal purple bars show the times of deposition of layers A and B, and coseismic uplift. An overall rise in sea level is seen over time as the shift from high marsh species dominant to low to mid-marsh species dominant. The base of the section is dominated by tidal flat species, and the brown sediments above are devoid of diatoms and represent the soil that formed on the tidal flat after coseismic uplift ~1,000 cal yr BP, when the surface was higher than the highest tides.

BP. Sample 29 marks the initial return to intertidal conditions, with high marsh species dominant. Samples 17–1 show a shift to mid to low marsh species dominating the samples. For both layers A and B, the percentage of low to high marsh species is lower than in the samples below and above the layers. A plot of the same stratigraphic section with all combined species grouped by ecological affinity is shown in Figure 2.11. In that figure, a relative percentage increase in tidal flat diatoms coincides with layers A and B, suggesting that the sediment was derived from the adjacent tidal flat area.

4.4.2 *Transfer Function Models*

From the combined modern and fossil diatom data, four slightly different transfer function models were developed. All four models were restricted to the second component, as subsequent components did not improve RMSEP by at least 5%. Figure 4.6 shows a comparison of the four models. Model 1 was run with no excluded samples or species from the modern diatom training set. Model 2 was run with the four highest residual samples excluded from the WA-PLS. Model 3 was run with species that had maximum percentages less than 2% excluded from the WA-PLS (Kemp and Telford, 2015). Model 4 is a combination of Models 2 and three, with the four highest residual samples, and the species less than 2% excluded from the WA-PLS. All four models have good predictive power, but Model 4 has the highest coefficient of determination ($r^2 = 0.95$), and the lowest root mean square error of prediction (RSMEP = 12.92). Figure 4.7 shows the results of Model 4 (preferred model) compared with the results of a modern analog technique (MAT)

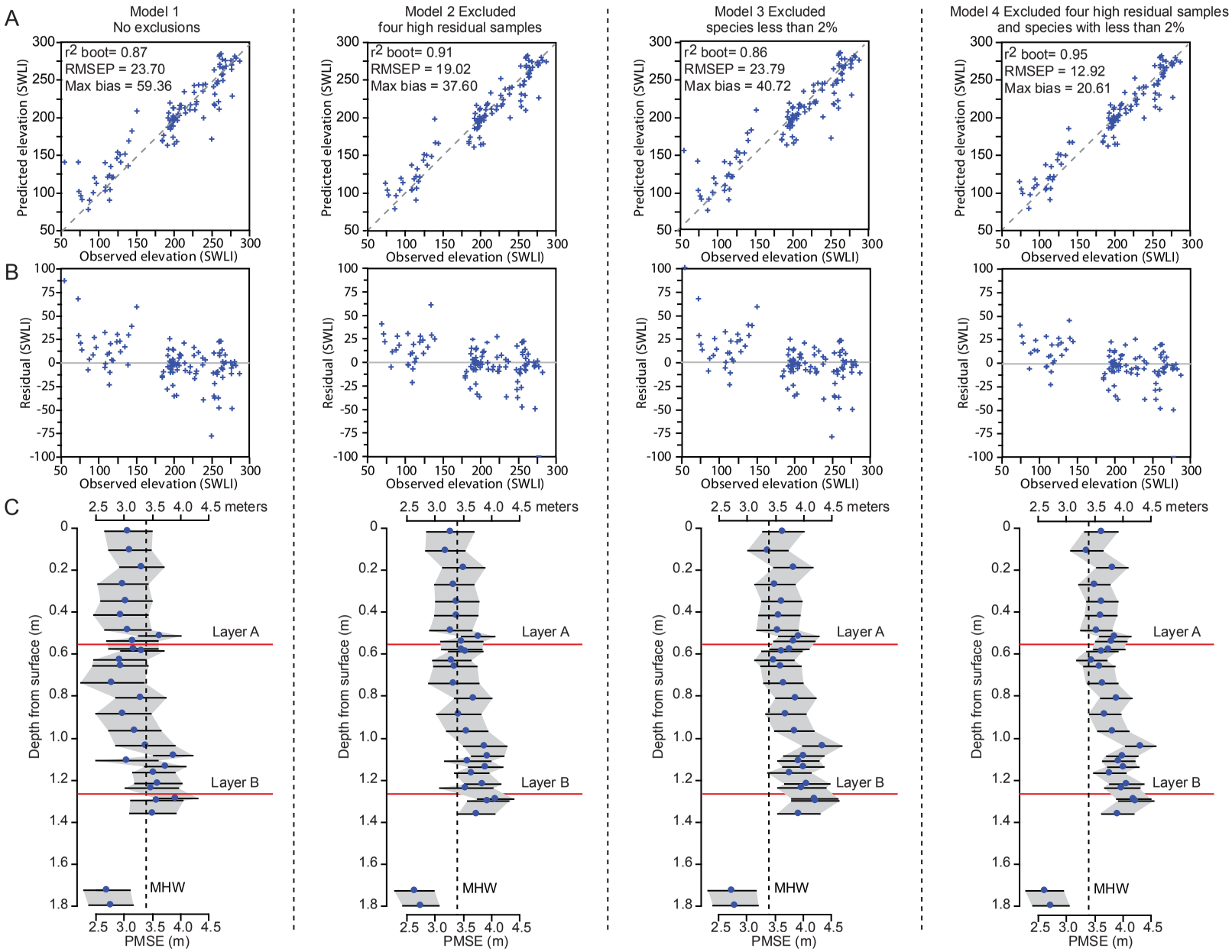
A
Model 1
No exclusions
r2 boot= 0.87
RMSEP = 23.70
Max bias = 59.36
Model 2 Excluded
four high residual samples
r2 boot= 0.91
RMSEP = 19.02
Max bias = 37.60
Model 3 Excluded
species less than 2%
r2 boot= 0.86
RMSEP = 23.79
Max bias = 40.72
Model 4 Excluded four high residual samples
and species with less than 2%
r2 boot= 0.95
RMSEP = 12.92
Max bias = 20.61
Predicted elevation (SWLI)
Observed elevation (SWLI)
B
Residual (SWLI)
C
2.5 3.0 3.5 4.0 4.5 meters
Depth from surface (m)
Layer A
Layer B
MHW
PMSE (m)

(Previous page) Figure 4.6. Transfer function model comparison. Row (A) Coefficient of determination for 1000 bootstrapped trials predicted elevations vs observed from the training set. The root mean square error of prediction (RMSEP) and maximum bias are given in SWLI units. Dashed line is 1:1. Row (B) observed elevation residual values. Values closest to zero indicate better fit. Row (C) Reconstructions converted from SWLI to PMSE (paleomarsh surface elevations). Mean high water (MHW) plotted as vertical dashed line. Model 1 (left) was run with no excluded samples or species from the modern diatom training set. Model 2 was run with the four highest residual samples excluded from the WA-PLS. Model 3 had species with maximum percentages less than 2% excluded. Model 4 is a combination of Models 2 and three, with the four highest residual samples, and the species less than 2% excluded from the WA-PLS, and is the preferred model.

comparison of modern and fossil assemblages. All dissimilarity values for the samples are well below the 5th percentile of dissimilarities, which indicates that the fossil diatoms are well represented by the modern diatom set.

4.4.3 *Sea Level Reconstruction*

Figure 4.8 shows the sea level reconstruction for Lynch Cove (site 13.10.16) based on the paleomarsh elevation reconstructions and depth below the modern surface. The overall sea level curve shows a rise of approximately 2.8 mm/yr for the last 300 years, with a total of at least 2 meters since coseismic uplift ~1,000 years ago. Each age-controlled point (boxes) in the curve has an elevation point with an error of approximately 0.5 m, as calculated by the paleomarsh elevation values.

4.5 DISCUSSION

4.5.1 *Late Holocene Sea Level at Lynch Cove*

Sea level estimates from peat records in northern Puget Sound predict about 1 m of sea level rise in the last 1,000 years (Eronen et al., 1987; Beale, 1990). Sea level rise estimates based on long term tidal gauge records for southern Puget Sound yield rates of 2.2 ± 0.01 mm/yr (Mazzotti et al., 2008), and 2.1 ± 0.1 mm/yr for the Seattle tide gauge during the 20th Century

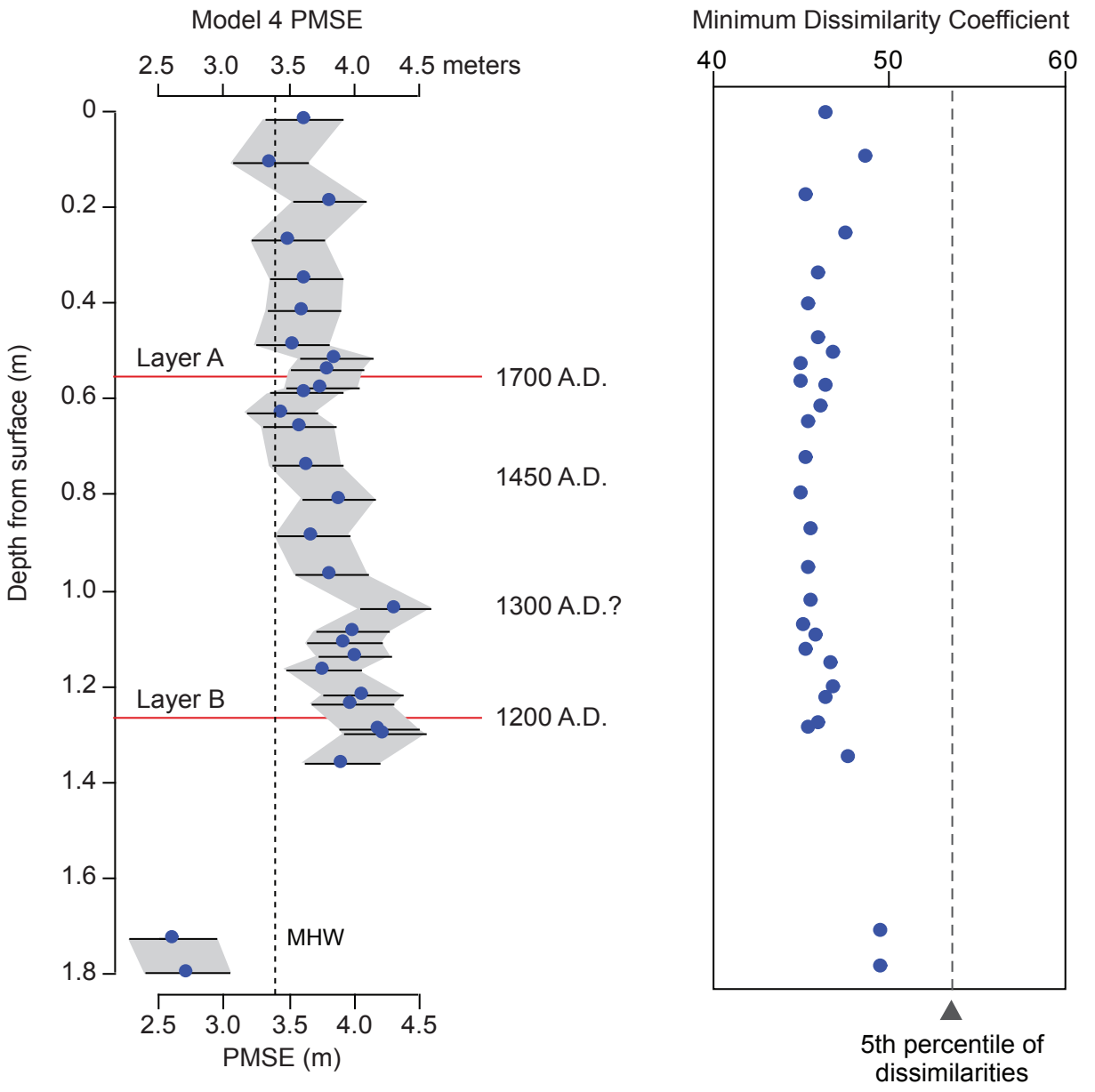

Figure 4.7. Comparison of WA-PLS Model 4 results with modern analog technique (MAT) results. (Left) Model 4 (Preferred model from Figure 4.6). Mean high water (MHW) is modern marsh datum. Radiocarbon age of layer A inferred to be 1700 A.D., and 1300 A.D. (age of Bed 2 at Discovery Bay) as the potential age of the higher adjacent PMSE point, based on observed pattern of PMSE rise before layers A and B. There is no deposit of Bed 2 age at Lynch Cove. (Right) plot of results of Modern analog technique (MAT) test of similarity. The MAT produces a dissimilarity coefficient for each fossil sample and the modern diatom dataset. A perfect match between fossil and modern gives a dissimilarity coefficient of zero. The 5th percentile of dissimilarities (vertical line) is the threshold for "good" modern analogs for the fossil samples in the modern dataset. All samples were well below the 5th percentile, which indicates that there were good modern analogs in the modern diatom set for the fossil samples.

(Verdonck, 2006). The overall rate of sea level rise in Figure 4.8 is 2.6 mm/yr, a rate higher than the rates based on tidal gauges. Faster rates of sea level rise in the southern part of Puget Sound have been attributed to tectonic subsidence in addition to sea level rise (Mazzotti et al., 2008).

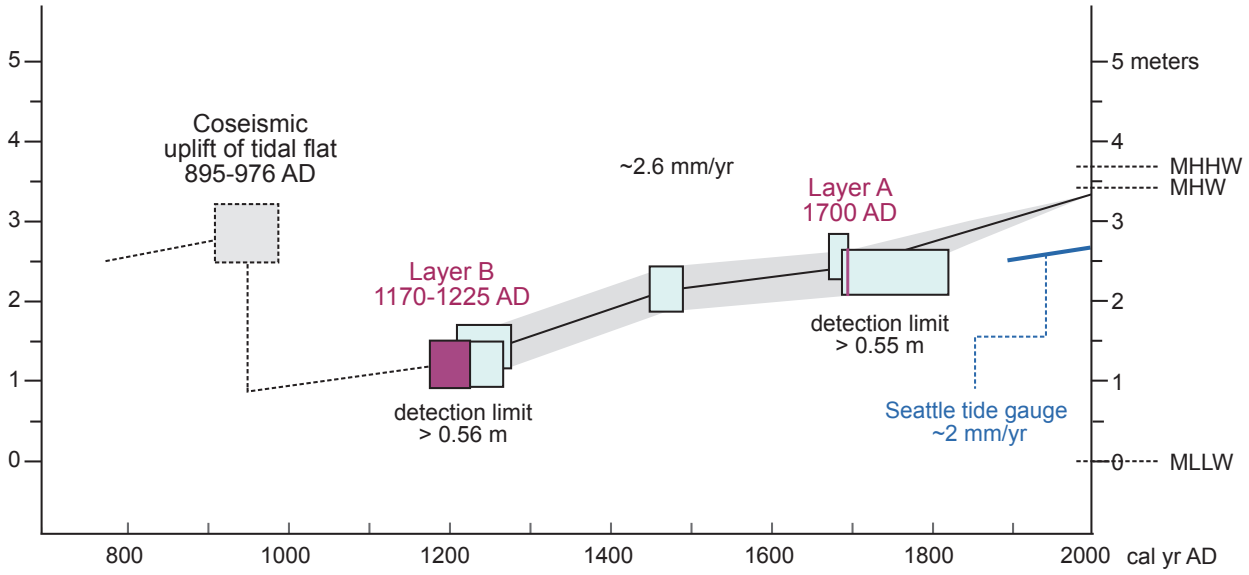

Figure 4.8. Sea level reconstruction from paleomarsh surface elevation values in Model 4 and radiocarbon ages in Chapter 2. Overall sea level has risen by at least 2 m since layer B was deposited, a rise of about 2.6 mm/yr if rise has been linear. The ~100-year record for the Seattle tide gauge (right lower) is about 2 mm/yr. The Seattle tide gauge plot is for reference, and its intersection with the y-axis is arbitrary.

4.5.2 *Does Lynch Cove Record Cascadia Subduction Zone Deformation?*

All four of the transfer function models show an overall trend of a lowering of the paleomarsh surface elevation (PMSE) and rise in relative sea level over the last ~750 years. All the models also show a slight increase in PMSE prior to the deposition of both layers A and B. These increases of about 0.25 m are within the error of each of the calculated PMSE values of about ± 0.25 m, so are inconclusive. If these PMSE increases are actual, they may represent

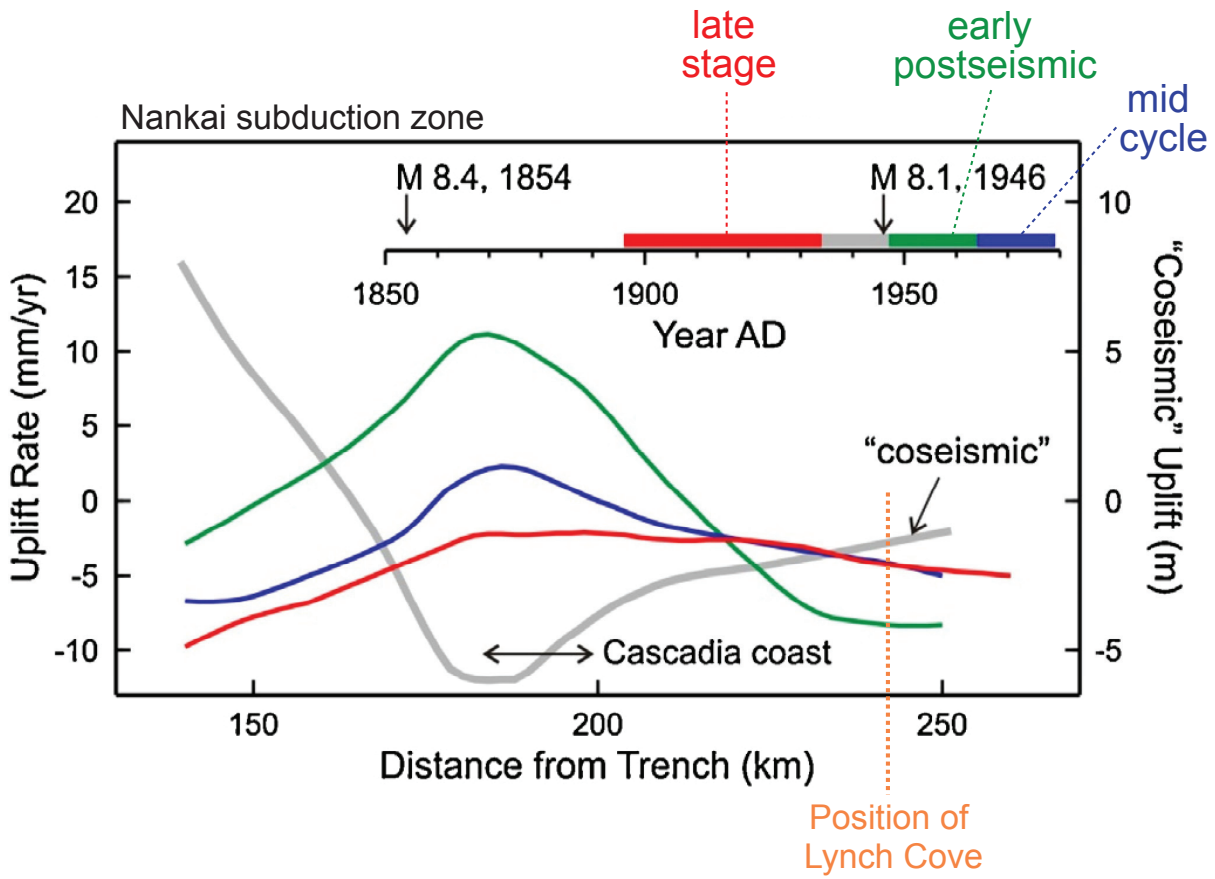

Figure 4.9. Changes in uplift rate over the earthquake cycle for the Nankai subduction zone, adapted from Wang and Tréhu (2016). The location of Cascadia coast and position of Lynch Cove at 240 km from the deformation front plotted. As observed for the Nankai subduction zone, the overall uplift rate at the comparable position of Lynch Cove may decrease prior to great earthquakes (gray line) before resuming higher rate of uplift (negative uplift = subsidence) post earthquake (green line).

vertical deformation due to viscoelastic relaxation of the mantle preceding and following Cascadia subduction zone earthquakes (Wang et al., 2012). Wang and Tréhu (2016) plot ~100 years of leveling data from the Nankai subduction zone (Thatcher, 1984) to examine variations of vertical deformation during the earthquake cycle, and found that vertical interseismic deformation varies in over the earthquake cycle, and is dependent upon distance from the deformation front (Figure 4.9). Figure 4.9 shows that sites greater than 125-175 km away from the trench showed postseismic subsidence following the 1946 Mw = 8.2 earthquake (Thatcher, 1984; Wang and

Tréhu, 2016). Referencing the Nankai leveling data to the Cascadia subduction zone shoreline (Figure 4.9), a point as far inland as Lynch Cove (240 km from the deformation front) may record very subtle variations in vertical interseismic deformation over an earthquake cycle. If layers A and B are markers of Cascadia subduction zone earthquakes, rises in PMSE at Lynch Cove prior to their deposition (Figure 4.7) may represent slowing of the rate of overall net negative uplift before these great earthquakes.

On the left side of Figure 4.7, radiocarbon ages are plotted for layer A, inferred to be 1700 A.D.; layer B, about 1200 A.D.; and a radiocarbon age from 20 cm below layer A (Chapter 2.4.2 and Sample 7, Table 2.1). The age 1300 A.D. is plotted next to the PMSE data point that also exhibits a similar increase like that seen below layers A and B. There is no silt deposit of that age at Lynch Cove, nor any other indication of earthquake or tsunami, but if rises in PMSE occur prior to subduction zone earthquakes at Lynch Cove, the point labeled 1300 A.D. may represent deformation associated with the Cascadia earthquake that deposited Bed 2 at Discovery Bay.

Diatom transfer function studies from other subduction zones have shown the opposite pattern of interseismic deformation than what may be recorded by these slight PMSE variations at Lynch Cove, instead showing preseismic subsidence and postseismic uplift. Sawai et al. (2004) observed both pre-seismic subsidence and postseismic uplift at Hokkaido associated with a large 17^{th} century earthquake on the Kuril subduction zone. The marsh recorded nearly a meter of subsidence prior to the earthquake, and then about a meter of uplift in the decades following the earthquake. In Alaska, preseismic and coseismic subsidence were seen at Girdwood, near the area of maximum coseismic subsidence in 1964. There, 0.24 ± 0.13 m of pre-seismic subsidence was estimated to have occurred before the 1964 earthquake. In addition, 0.14 ± 0.14 m of pre-seismic subsidence was estimated to have occurred before the penultimate earthquake of ~900 cal yr BP

(Shennan and Hamilton, 2006). These sites were closer to their respective deformation fronts, and therefore closer to the areas of maximum subsidence, where the preseismic signal (gray line in Figure 4.9) and early postseismic signal (green line in Figure 4.9) are both the steepest, and the greatest difference in values from each other. Variations in subduction angle for different subduction zones would create different spatial patterns, but because Nankai is a good analog for Cascadia because the subduction angle is similar (Wang and Tréhu, 2016), vertical data from more trench-normal sites will help to determine whether similar patterns can be determined for Cascadia in the future. Despite the possibility that the PMSEs may be showing variations between 0.25–0.5 m over the subduction zone cycle, the error bars associated with the PMSEs of ± 0.25 m mean that changes below about 0.5 m cannot be detected by this transfer function. Therefore, Lynch Cove is interpreted as a site that records no Cascadia earthquake cycle deformation over the last 1,000 years at Lynch Cove, and that vertical deformation would need to exceed about 0.5 meters to be identified by this method.

4.5.3 *Sea Level Rise from Sedimentation Rates*

Relative sea level rise estimates based on the transfer function PSME reconstructions yield a rate of about 2.6 mm/yr. The thickness of sediment between layer B (about 750 years old) and the marsh surface is about 1.25 meters, so the sediment accumulation rate, if continuous and uniform, would be roughly 1.5 mm/yr. While there are multiple uncertainties with this sedimentation rate estimate, it allows a comparison with the transfer function reconstruction, and with sea level rise rates based on 20th Century tide gauge records of about 2 mm/yr (Verdonck, 2006; Mazzotti et al., 2008; Burgette et al., 2009; Alba et al., 2011; Burgette et al., 2012). The discrepancies between the sediment accumulation rate and those based on shorter-term tide gauge records may be because short-term records capture additional rise of eustatic sea level due to

climate change. The faster transfer function sea level rise rate is based on relatively few data points, and would benefit from additional age control points and smaller errors on PMSE values to obtain the best estimate of the rate of sea level rise at Lynch Cove.

4.5.4 *Transfer Function Limitations*

Sea level curves derived from transfer functions can contain several sources of error. One source of error is a training set of modern diatoms has an unequal distribution of samples along the environmental gradient that is being tested (elevation in this case). Uneven sampling of the environmental gradient can cause errors in the reconstruction (Kemp and Telford, 2015). Most samples in the study training set had SWLI values closer to the higher part of the intertidal range, which is a common problem in training sets because samples at these elevations are the easiest to collect. The unevenness of the distribution in sample elevations can be seen in the both the r^2 and residual plots of SWLI values (Figure 4.6).

Another source of error is a lack of good analogs in the training set for the fossil samples. One way to counter this problem is to have a large number of samples in the training set, and to use samples from a wide geographical region (Kemp and Telford, 2015; Watcham et al., 2013). Transfer function analysis assumes that the fossil sample can be represented by modern samples. Because of this, post-depositional and taphonomic changes are unaccounted for, as are potential sediment reworking or diatom valve sorting and breaking which may modify the modern sample assemblage. However, there is always a component of allochthonous valves in any modern sample, and some studies have suggested that intertidal distribution and preservation of modern intertidal assemblages need not have major differences in taphonomy than their fossil counterparts (Hassan et al., 2008). The MAT analysis shows that the modern diatom data set used was a good representation of the fossil samples at Lynch Cove (Figure 4.7).

Because the WA-PLS transfer function is referenced to the single environmental variable of elevation, the reconstructions based on this single variable may not account for the influence of other environmental variables such as salinity (Horton et al., 2006). Additional error may occur because elevation is not a true environmental variable, but rather it is a proxy for exposure, tidal inundation, and salinity, which are the true controls of species distribution (Kelsey et al., 2012; Kemp and Telford, 2015).

In a study of diatom distribution in Washington and Oregon coast tidal marshes, Sawai et al. (2016) found that the presence of mud was a secondary control of diatom distribution in addition to elevation or tidal exposure. Because the tidal marsh at Lynch Cove is adjacent to a large muddy tidal flat, clay and silt sized grains are the dominant grain size in the sedimentary record of the last ~750 years, grain size may influence diatom distributions in addition to elevation in the intertidal zone. Salinity has also been confirmed as another secondary influence of diatom distribution (Sherrod, 1999). Without developing transfer functions that use these environmental gradients, it is unclear what other factors influence diatom distribution and therefore how much additional error the elevation reconstructions have.

4.6 CONCLUSIONS

A diatom-based transfer function for Lynch Cove produces paleomarsh surface elevations and a reconstructed sea level that shows an overall sea level rise over the last 1,000 years. This is consistent the stratigraphic evidence of forest soil overlain by tidal marsh deposits, and also with studies of sea level in Puget Sound history that employ different methodologies (Beale, 1991; Eronen et al., 1987; Mazzotti et al., 2008; Verdonck, 2006). The overall rate of sea level rise at Lynch Cove is estimated to be 2.6 mm/yr, which is in closer agreement with, though still higher

than, rates determined by shorter-term studies that utilize the 100+ year record of the Seattle tide gauge (e.g. Burgette et al., 2009), than with longer-term rates derived from peat records (e.g. Eronen et al., 1987). An apparent rise in PMSE values preceding the deposition of tsunami deposits layers A and B, may represent preseismic uplift associated with Cascadia interseismic deformation, but these small changes are within the error range of adjacent points, and may not represent actual elevational differences. Because of this, I conclude that Lynch Cove is a location that probably does not record Cascadia earthquake cycle deformation. Potential factors that may influence the PMSEs are a lower representation of low tidal elevation samples in the modern training set, and the presence of large amounts of silt and clay grain sizes common throughout Lynch Cove as they may influence the distribution of intertidal diatoms in addition to tidal elevation.

Chapter 5. **Conclusions**

5.1 REVIEW

This study focused on the record of marsh sediments at Lynch Cove marsh in Hood Canal, Puget Sound, and used different tools to study the history of tsunamis and relative sea level change at the site. I used stratigraphy and sedimentology to characterize two sandy silt layers and concluded that they are tsunami deposits. I determined the ecological affinity of fossil diatoms within the tsunami deposits to conclude that the source area of the deposits was the tidal flat adjacent to the marsh. I used radiocarbon dating to determine ages for the deposits at Lynch Cove, and compared these ages to the ages of earthquakes and tsunamis on the coasts of Washington, Oregon, and British Columbia; and from Puget Sound. I concluded that the ages of the tsunami deposits best aligned with the ages of two Cascadia earthquakes preserved on the coast of Washington. I compared the ages of Lynch Cove tsunami deposits with those from Discovery Bay after improving the radiocarbon dating of Beds 1-6, but especially Bed 2 at Discovery Bay. Bed 2, along with other tsunami deposits of similar age between Vancouver Island and northern Oregon, are strong evidence for a Cascadia earthquake around 600 cal yr BP. I tested different earthquake source tsunamis in simulations and found that simulated Cascadia tsunamis inundate the marshes at Lynch Cove and Discovery Bay, and are the most likely sources of the tsunami deposits at Lynch Cove, and many of the tsunami deposits at Discovery Bay. Finally, using the tsunami deposits as time markers of great Cascadia earthquakes, I developed a diatom-based transfer function to reconstruct the sea level history at Lynch Cove. The reconstruction shows an overall sea level rise over the last 1,000 years at Lynch Cove. The paleomarsh surface elevations show a slight pre-tsunami emergence, followed by a slight post-tsunami submergence that fits with expected vertical deformation of a distal site in the position of Lynch Cove, 240 km inland of the

Cascadia deformation front. These changes in elevation are close to the error for each point, so overall Lynch Cove is interpreted as a site with no vertical Cascadia earthquake cycle deformation.

In Chapter 2, I described two sandy silt layers, layers A and B at Lynch Cove, and concluded that they are tsunami deposits. I examined the stratigraphy of tidal marsh sediments and the sedimentary characteristics of layers A and B that support deposition by tsunami. I determined the diatom paleoecology of the marsh sediments, and found that the diatoms are different within layers A and B than in the sediments above and below. Layers A and B contain higher concentrations of tidal flat diatoms than in the sediments below and above each layer. This suggests that the adjacent tidal flat is the likely source area of layer A and B's sediment.

In Chapter 2 I also established a chronology of the last ~1,000 years at Lynch Cove, and ages of the two inferred tsunami deposits. Layer A's age is modeled between A.D. 1690-1830, but the actual age is almost certainly in the older part of the range, based on the depth of layer A of ~55-60 cm from the marsh surface, and the fact that the tidal marsh had nearly the same extent when it was mapped in 1884. In addition, using a radiocarbon age from 20 cm below layer A, an age can be estimated for layer A using an approximate sediment accumulation rate for the top 80 cm of sediment since 1450-1620 A.D. suggests that layer A was deposited prior to about 1740 A.D. Layer B's age is modeled at A.D. 1170-1230 (720-780 cal yr BP).

These ages were compared with ages of known earthquakes and tsunamis in the Puget Sound region, including a refined chronology of the last ~2,500 years at Discovery Bay and with the ages of Cascadia earthquakes from the coast of Washington. The ages of layers A and B suggest that they could be Cascadia-generated tsunami deposits. Bed 2 at Discovery Bay has a new age of 560-630 cal yr BP, and was probably deposited by a Cascadia earthquake that is still not well characterized.

In Chapter 3 I compared five different tsunami simulations from different earthquake sources. Each of these predicted flow depths and speeds for tsunamis at both Lynch Cove and Discovery Bay. The tsunamis generated by three different rupture styles of Cascadia earthquake, the A.D. 900-930 Seattle fault earthquake, and an earthquake within the rupture area of the 1964 Alaska earthquake are compared at Lynch Cove and Discovery Bay, and were evaluated as potential sources of tsunami deposits at both sites. Based on these simulations, Cascadia earthquakes are the most likely source of the tsunami deposits at Lynch Cove and Discovery Bay. The Alaska simulated tsunami overestimated flow depths at Lynch Cove, though did agree with historical observations of tsunami flooding at Discovery Bay. The Alaska tsunami left only a trace of sediment at Discovery Bay, and no known sediment deposit at Lynch Cove, so transoceanic tsunamis are a less likely source of the thicker tsunami deposits at both sites.

In Chapter 4 I developed a diatom-based transfer function. The transfer function statistically compared fossil diatoms from the sediments of Lynch Cove to the distribution of a training set of modern diatoms collected in the Puget Sound area. From this, ecological setting and elevation within the tidal zone was determined over time. A sea level history of the last ~750 years was reconstructed, and using the tsunami deposits as time-markers, I concluded that Lynch Cove may preserve subtle Cascadia interseismic vertical deformation, but evidence is inconclusive because it is within the error of the method.

5.2 IMPLICATIONS

This study clarifies several aspects of earthquake and tsunami hazards in Puget Sound and vicinity. The geologic evidence of past tsunamis, and the numerical simulations of Cascadia tsunamis inundating Lynch Cove demonstrate that there is a greater tsunami hazard in Puget Sound

than previously recognized. In addition, there are some areas of Puget Sound that experience greater flow depths and speeds than others, suggesting that tsunami hazards vary by site location, channel morphology, and site topography/bathymetry.

This study also generated a paleogeodetic data point for Cascadia at 240 km east of the deformation front, and about 40 km above the descending Juan de Fuca slab. The inferred pre- and postseismic vertical deformation, interpreted as zero or nearly zero change, places a limit on the inland extent of subduction zone deformation. This finding has implications for future models of subduction zone dynamics and seismic hazards, as it is the only site, to my knowledge, that has a transfer function sea level history in Puget Sound with age control for context within the Cascadia subduction zone earthquake cycle.

This study also provides a secure age for Bed 2 at Discovery Bay, which, along with widespread evidence from coastal areas in the northern part of the Cascadia subduction zone, probably represents a Cascadia earthquake about 600 years ago. This earthquake is of uncertain size and rupture length, and it is unknown why it did not cause coastal subsidence in south Washington. This earthquake has implications for recurrence intervals of earthquakes in northern Cascadia.

5.3 Future Work

To continue this work, more sites in Puget Sound should be modeled for tsunami inundation from a variety of earthquake sources. Further simulations with high resolution grids should be done for Puget Sound areas that show high flow depths in the simulation animations in Appendix 5. Studies should be prioritized to include terminal waterways, and areas of high population and critical infrastructure. Additional tidal marshes in Puget Sound contain potential

tsunami deposits. These deposits should be described and radiocarbon dated, so that tsunami sources and recurrence can be determined.

Because of the high likelihood that past tsunamigenic landslides have occurred in Puget Sound, geomorphic studies of hillsides and high-resolution bathymetric surveys should be used to identify such slides. Tsunami modeling would help to determine the tsunami propagation from slides where volume of sediment and water depth are known.

Additional modern diatoms should be collected in Puget Sound to add to the modern diatom training set, particularly in the lower tidal elevations. Future transfer functions could, in addition to elevation, consider additional environmental gradients, such as substrate, as it appears that the abundance of silt and clay sized particles likely influence diatom distributions at Lynch Cove.

Further radiocarbon dating could further refine the timing of Discovery Bay tsunamis as was done for Bed 2. To help to characterize the Cascadia earthquake or earthquakes that formed Bed 2, and the multiple other tsunami deposits of the same age, Washington coast marshes could be revisited with a goal of detecting coseismic subsidence from about 600 cal yr BP, that may not have preserved buried soils, but may preserve relative sea level changes that could be detected by microfossil analysis.

References

Abramson, H., 1998, Evidence for tsunamis and earthquakes during the last 3500 years from Lagoon Creek, a coastal freshwater marsh, northern California: Humboldt State University, 76 p.

Alba, S.K., Weldon, R.J., Livelybrooks, D., Schmidt, D.A., and Krogstad, R., 2011, ETS related uplift and strain accumulation in northern Cascadia from tidal records: American Geophysical Union Fall Meeting.

Arcos, M.E.M., 2012, The A.D. 900-930 Seattle-fault-zone earthquake with a wider coseismic rupture patch and postseismic submergence; inferences from new sedimentary evidence: Bulletin of the Seismological Society of America, v. 102, no. 3, p. 1079-1098.

Atwater, B.F., and Griggs, G.B., 2012, Deep-sea turbidites as guides to Holocene earthquake history at the Cascadia Subduction Zone—Alternative views for a seismic-hazard workshop: U.S. Geological Survey Open-File Report, v. 2012–1043, 58 p.

Atwater, B.F., and Moore, A.L., 1992, A tsunami about 1000 years ago in Puget Sound, Washington: Science, v. 258, no. 5088, p. 1614-7.

Atwater, B.F., 1999, Radiocarbon dating of a Seattle earthquake to A.D. 900-930: Seismological Research Letters, v. 70, no. 2, p. 232.

Atwater, B.F., 1987, Evidence for Great Holocene Earthquakes along the Outer Coast of Washington State: Science, v. 236, no. 4804, p. 942-944.

Atwater, B.F., and Hemphill-Haley, E., 1997, Recurrence intervals for great earthquakes of the past 3,500 years at northeastern Willapa Bay, Washington: Washington: Denver, CO, US Nuclear Regulatory Commission, Washington: U.S. G.P.O.; For sale by U.S. Geological Survey, Information Services.

Atwater, B.F., Musumi-Rokkaku, S., Satake, K., Tsuji, Y., Ueda, K., and Yamaguchi, D.K., 2005, The orphan tsunami of 1700; Japanese clues to a parent earthquake in North America: United States, University of Washington Press: Seattle, WA, United States.

Atwater, B.F., Tuttle, M.P., Schweig, E.S., Rubin, C.M., Yamaguchi, D.K., and Hemphill-Haley, E., 2004, Earthquake recurrence inferred from paleoseismology: Developments in Quaternary Science, v. 1, p. 331-350.

Baranes, H.E., Woodruff, J.D., Wallace, D.J., Kanamaru, K., and Cook, T.L., 2014, Sedimentological signatures of large scale inundation events; records of the 1707 AD Hoei tsunami from the Bungo Channel, Japan: Boulder, CO, Boulder, CO, United States: Geological Society of America (GSA) 46, 452 p.

Barnett, E.A., Sherrod, B.L., Hughes, J.F., et al., 2015, Paleoseismic evidence for late Holocene tectonic deformation along the Saddle Mountain fault zone, southeastern Olympic Peninsula, Washington: Bulletin of the Seismological Society of America, v. 105, no. 1, p. 38-71.

Beale, H., 1991, Relative rise in sea-level during the past 5000 years at six salt marshes in northern Puget Sound, Washington: Shorelands & Coastal Zone Management Program, Washington (State), Department of Ecology.

Berger, M.J., George, D.L., Leveque, R.J., and Mandli, K.T., 2011, The GeoClaw software for depth- averaged flows with adaptive refinement: Advances in Water Resources, v. 34, no. 9, p. 1195-1206.

Blais-Stevens, A., Rogers, G.C., and Clague, J.J., 2011, A revised earthquake chronology for the last 4,000 years inferred from varve- bounded debris- flow deposits beneath an inlet near Victoria, British Columbia: Bulletin of the Seismological Society of America, v. 101, no. 1, p. 1-12.

Blakely, R.J., Sherrod, B.L., Hughes, J.F., Anderson, M.L., Wells, R.E., and Weaver, C.S., 2009, Saddle Mountain Fault deformation zone, Olympic Peninsula, Washington; western boundary of the Seattle Uplift: Geosphere, v. 5, no. 2, p. 105-125.

Blakely, R.J., Wells, R.E., Weaver, C.S., and Johnson, S.Y., 2002, Location, structure, and seismicity of the Seattle fault zone, Washington: Evidence from aeromagnetic anomalies, geologic mapping, and seismic refection data: Geological Society of America Bulletin, v. 114, no. 2.

Bourgeois, J., 2009, Geologic effects and records of tsunamis. *in* Bernard, E.N. and Robinson, A.R., eds., Tsunamis: Cambridge, MA, Harvard University Press.

Bourgeois, J., and Johnson, S.Y., 2001, Geologic evidence of earthquakes at the Snohomish Delta, Washington, in the past 1200 yr: Geological Society of America Bulletin, v. 113, no. 4, p. 482-494.

Brocher, T.M., Parsons, T., Blakely, R.J., et al., 2001, Upper crustal structure in Puget Lowland, Washington: results from the 1998 Seismic Hazards Investigation in Puget Sound, Journal of Geophysical Research vol. 106, no. B7, ; p. 13,541-13,564.

Bronk Ramsey, C., 1995, Radiocarbon Calibration and Analysis of Stratigraphy: The OxCal Program: Radiocarbon, v. 37, no. 2, p. 425.

Bronk Ramsey, C., 2009, Bayesian Analysis of Radiocarbon Dates: Radiocarbon, v. 51, no. 1, p. 337-360.

Bronk Ramsey, C., 2017, OxCal software version 4.3.2 https://c14.arch.ox.ac.uk/oxcal/OxCal.html

Brothers, D.S., Haeussler, P.J., Liberty, L., Finlayson, D., Geist, E., Labay, K., and Byerly, M., 2016, A submarine landslide source for the devastating 1964 Chenega tsunami, southern Alaska: Earth and Planetary Science Letters, v. 438, p. 112-121.

Bucknam, R.C., Hemphill-Haley, E., and Leopold, E.B., 1992, Abrupt uplift within the past 1700 years at southern Puget Sound, Washington: Science, v. 258, no. 5088, p. 1611-1614.

Bucknam, R., Leopold, E., Hemphill-Haley, E., Ekblaw, D., Atwater, B., Benson, B., and Phipps, J., 1994, Hobcene Tectonics in Western Washington. *in* Swanson, D.A. and Haugerud, R.A., eds., Geologic field trips in the Pacific Northwest: 1994 Geological Society of America Annual Meeting, Geological Society of America, p. 2C15.

Burgette, R.J., Weldon, R.J., and Schmidt, D.A., 2009, Interseismic uplift rates for western Oregon and along-strike variation in locking on the Cascadia subduction zone: J.Geophys.Res.Journal of Geophysical Research, v. 114, no. B1.

Burgette, R.J., Weldon, R.J., Schmidt, D.A., and Williams, T.B., 2012, Constraints on interseismic locking along the southern Cascadia subduction zone from historic and recent leveling and sea level observations: American Geophysical Union Fall Meeting, v. 2012, p. 2719.

Carnigan, K.S., McLean, S.J., Eakins, B.W., Love, M.R., and Sutherland, M., 2014, Digital elevation model of Puget Sound, Washington: Procedures, data sources, and analysis, Prepared for the National Tsunami Hazard Mitigation Program (NTHMP) by the NOAA National Geophysical Data Center (NGDC), https://www.ngdc.noaa.gov/dem/squareCellGrid/download/5164.

Chamberlin, C.D., Arcas, D.R., and Pacific Marine Environmental Laboratory, 2015, Modeling tsunami inundation for hazard mapping at Everett, Washington, from the Seattle Fault, NOAA Technical Memorandum OAR PMEL-147, doi:10.7289/V59Z92V0.

Cherniawsky, J.Y., Titov, V.V., Wang, K., and Li, J., 2007, Numerical Simulations of Tsunami Waves and Currents for Southern Vancouver Island from a Cascadia Megathrust Earthquake: Pure and Applied Geophysics, v. 164, no. 2, p. 465-492.

Chleborad, A.F., 1994, Modeling and Analysis of the 1949 Narrows Landslide, Tacoma, Washington: Environmental & Engineering Geoscience Environmental & Engineering Geoscience, v. xxxi, no. 3, p. 305-327.

Clague, J.J., and Bobrowsky, P.T., 1994a, Evidence for a Large Earthquake and Tsunami 100-400 Years Ago on Western Vancouver Island, British Columbia: Quaternary Research, v. 41, no. 2, p. 176-184.

Clague, J.J., and Bobrowsky, P.T., 1994b, Tsunami deposits beneath tidal marshes on Vancouver Island, British Columbia: GSA Bulletin, v. 106, no. 10, p. 1293-1303.

Clague, J.J., Bobrowsky, P.T., and Hamilton, T.S., 1994, A Sand Sheet Deposited by the 1964 Alaska Tsunami at Port Alberni, British Columbia: Estuarine, Coastal and Shelf Science, v. 38, no. 4, p. 413-421.

Clague, J.J., Bobrowsky, P.T., and Hutchinson, I., 2000, A review of geological records of large tsunamis at Vancouver Island, British Columbia, and implications for hazard: Quaternary Science Reviews, v. 19, no. 9, p. 849-863.

Clawpack Development Team, 2015, Clawpack Software, http://depts.washington.edu/clawpack/geoclaw/.

Costa, P.J.M., Gelfenbaum, G., Dawson, S., et al., 2017, The application of microtextural and heavy mineral analysis to discriminate between storm and tsunami deposits: Special Publication - Geological Society of London, v. 456.

Darienzo, M., 1991, Late Holocene paleoseismicity along the northern Oregon coast [Diss], Portland State University, 183 p.

Darienzo, M.E., Peterson, C.D., and Clough, C., 1994, Stratigraphic evidence for great subduction-zone earthquakes at four estuaries in northern Oregon, U.S.A: Journal of Coastal Research, v. 10, no. 4, p. 850-876.

Dawson, A.G., and Shi, S., 2000, Tsunami Deposits: Pure and Applied Geophysics, v. 157, no. 6-8, p. 875-897.

Dura, T., Hemphill-Haley, E., Sawai, Y., and Horton, B., 2016, The application of diatoms to reconstruct the history of subduction zone earthquakes and tsunamis 152, Earth-Science Reviews, v.152, p. 181-197.

Dura, T., Cisternas, M., Horton, B.P., Ely, L.L., Nelson, A.R., Wesson, R.L., and Pilarczyk, J.E., 2015, Coastal evidence for Holocene subduction- zone earthquakes and tsunamis in central Chile: Quaternary Science Reviews, v. 113, p. 93-111.

Engel, M., and Brueckner, H., 2011, The identification of palaeo-tsunami deposits; a major challenge in coastal sedimentary research: Coastline Reports, v. 17, p. 65-80.

Engelhart, S.E., Horton, B.P., Vane, C.H., Nelson, A.R., Witter, R.C., Brody, S.R., and Hawkes, A.D., 2013, Modern Foraminifera, delta (super 13) C, and bulk geochemistry of central Oregon tidal marshes and their application in paleoseismology: Palaeogeography, Palaeoclimatology, Palaeoecology, v. 377, p. 13-27.

Engelhart, S.E., Vacchi, M., Horton, B.P., Nelson, A.R., and Kopp, R.E., 2014, A sea- level database for the Pacific coast of central North America: Quaternary Science Reviews, v. 113, p. 78-92.

Enkin, R. J., Dallimore, A., Baker, J. R., Southon, J., and Ivanochko, T., 2013, A new high-resolution radiocarbon Bayesian age model of the Holocene and Late Pleistocene from core MD02-2494 and others, Effingham Inlet, British Columbia, Canada; with an application to the paleoseismic event chronology of the Cascadia Subduction Zone: Canadian Journal of Earth Sciences, v. 50, no. 7, p. 746-760.

Eronen, M., Kankainen, T., and Tsukada, M., 1987, Late Holocene sea-level record in a core from the Puget Lowland, Washington: Quaternary Research, v. 27, no. 2, p. 147-159.

Fine, I., Cherniawsky, J., Rabinovich, A., and Stephenson, F., 2008, Numerical Modeling and Observations of Tsunami Waves in Alberni Inlet and Barkley Sound, British Columbia: Pure and Applied Geophysics, v. 165, no. 11, p. 2019-2044.

Finlayson, D., 2005, Combined bathymetry and topography of the Puget Lowland, Washington State, University of Washington, http://www.ocean.washington.edu/data/pugetsound/.

Gao, D., 2016, Defining megathrust tsunami sources at northernmost Cascadia using thermal and structural information [M.S. thesis]: University of Victoria.

Gardner, J.V., van, d.A., and Dartnell, P., 2001, Multibeam mapping of the major deltas of southern Puget Sound, Washington: United States: U. S. Geological Survey Open File Report 2001-266.

Garrison-Laney, C.E., 1998, Diatom Evidence for Tsunami Inundation from Lagoon Creek, a Coastal Freshwater Pond, Del Norte County, California [M.S. thesis]: Humboldt State University, 106 p.

Gilbert, J.J., 1884, Hood's Canal Washington Territory Sheet No. 11, United States Coast & Geodetic Survey Topographic Sheets (T-sheets).

Goff, J., McFadgen, B.G., and Chague-Goff, C., 2004, Sedimentary differences between the 2002 Easter storm and the 15th- century Okoropunga tsunami, southeastern North Island, New Zealand: Marine Geology, v. 204, no. 1, p. 235-250.

Goldfinger, C., Nelson, C.H., Morey, A.E., et al., 2012, Turbidite event history; methods and implications for Holocene paleoseismicity of the Cascadia subduction zone: U. S. Geological Survey Professional Paper 1661-F, 170 p., https://pubs.usgs.gov/pp/pp1661f/.

Goldfinger, C., Wong, I., Kulkarni, R., and Beeson, J.W., 2016, Reply to Comment on Statistical Analyses of Great Earthquake Recurrence along the Cascadia Subduction Zone by Ram Kulkarni, Ivan Wong, Judith Zachariasen, Chris Goldfinger, and Martin Lawrence by Allan Goddard Lindh: Bulletin of the Seismological Society of America, v. 106, no. 6, p. 2935-2944.

Goldfinger, C., Galer, S., Beeson, J., et al., 2017, The importance of site selection, sediment supply, and hydrodynamics: A case study of submarine paleoseismology on the northern Cascadia margin, Washington USA: Marine Geology, v. 384, p. 4–46.

González, F.I., Geist, E.L., Jaffe, B., et al., 2009, Probabilistic tsunami hazard assessment at Seaside, Oregon, for near- and far- field seismic sources: Journal of Geophysical Research: Oceans, v. 114, p. 1-19.

González, F., Geist, E., Synolakis, C., et al., 2006: Seaside, Oregon Tsunami Pilot Study - modernization of FEMA flood hazard maps, Tsunami Pilot Study Working Group, US Geological Survey Open-File Report 2006-1234, http://pubs.er.usgs.gov/publication/ofr20061234.

González, F., LeVeque, R., Adams, L., Goldfinger, C., Priest, G., and Wang, K., 2014, Probabilistic Tsunami Hazard Assessment (PTHA) for Crescent City, CA, University of Washington Department of Applied Mathematics, Final Report, http://hdl.handle.net/1773/22366.

Graehl, N., Kelsey, H., Witter, R., Hemphill-Haley, E., & Engelhart, S., 2015, Stratigraphic and microfossil evidence for a 4500-year history of Cascadia subduction zone earthquakes and tsunamis at Yaquina River estuary, Oregon, USA. Geological Society of America Bulletin, 127(1-2), 211-226.

Guilbault, J., Clague, J.J., and Lapointe, M., 1996, Foraminiferal evidence for the amount of coseismic subsidence during a late Holocene earthquake on Vancouver Island, West Coast of Canada: Quaternary Science Reviews, v. 15, no. 8, p. 913-937.

Hatori, T., Aida, I., and Sakashita, S., 1983, Field survey of the Nankaido tsunamis inundating Yuasa and Miro, Wakayama Prefecture; the 1946 Nankaido, 1707 Hoei and 1854 Ansei tsunamis: Tokyo Daigaku Jishin Kenkyusho Iho, v. 58, no. 1, p. 187-206.

Hatori, T., 1988, Tsunami behaviors in the Seto Inland Sea and Bungo Channel caused by the Nankaido earthquakes in 1707, 1854 and 1946: Jishin, v. 41, no. 2, p. 215-221.

Hawkes, A.D., Horton, B.P., Nelson, A.R., Vane, C.H., and Sawai, Y., 2011, Coastal subsidence in Oregon, USA, during the giant Cascadia earthquake of AD 1700: Quaternary Science Reviews, v. 30, no. 3, p. 364-376.

Hemphill-Haley, E., 1996, Diatoms as an aid in identifying late-Holocene tsunami deposits: The Holocene, v. 6, no. 4, p. 439-448.

Hemphill-Haley, E., 1995, Diatom evidence for earthquake-induced subsidence and tsunami 300 yr ago in southern coastal Washington: Geological Society of America Bulletin, v. 107, no. 3.

Hemphill-Haley, E., 1993, Taxonomy of recent and fossil (Holocene) diatoms (Bacillariophyta) from northern Willapa Bay, Washington: U.S. Geological Survey Open File Report 93-289, 151 p.

Hemphill-Haley, E., and Lewis, R.C., 1996, Distribution and taxonomy of diatoms (Bacillariophyta) in surface samples and a two-meter core from Winslow Marsh, Bainbridge Island, Washington: U.S. Geological Survey, Open-File Reports 95-833, 105 p.

Horn, H., 1992, Süßwasserflora von Mitteleuropa. Band 2/2: Bacillariophyceae-Bacillariaceae, Epithemiaceae, Surirellaceae. Von K. Krammer u. H. Lange-Bertalot. 1. Aufl.-596 S., 184 Tafeln mit 1914 Figuren. Stuttgart - New York: Gustav Fischer Verlag, ISBN 3-437-30508-5. DM 168,—: Berlin 77, 170 p.10.1002/iroh.19920770119.

Horn, H., 1987, Süßwasserflora von Mitteleuropa. Hrsg. J. Ettl, J. Gerloff, H. Heynig, D. Mollen-Hauer. –Band 2/1. Bacillariophyceae, 1. Teil: Naviculaceae. Von Kurt Krammer und Horst Lange-Bertalot. – 876 S., 206 Fig. Jena: VEB Gustav-Fischer Verlag Jena 1986. ISSN 0232–3850. M 220,–: Berlin 72, 374 p.10.1002/iroh.19870720320.

Horton, B.P., Sawai, Y., Hawkes, A.D., and Witter, R.C., 2011, Sedimentology and paleontology of a tsunami deposit accompanying the great Chilean earthquake of February 2010: Marine Micropaleontology, v. 79, no. 3-4; 3-4, p. 132-138.

Houwing, E.J., 1999, Determination of the Critical Erosion Threshold of Cohesive Sediments on Intertidal Mudflats Along the Dutch Wadden Sea Coast: Estuarine, Coastal and Shelf Science, v. 49, no. 4, p. 545-555.

Hughes, J.F., Mathewes, R.W., and Clague, J.J., 2002, Use of pollen and vascular plants to estimate coseismic subsidence at a tidal marsh near Tofino, British Columbia: Palaeogeography, Palaeoclimatology, Palaeoecology, v. 185, no. 1, p. 145-161.

Hutchinson, I., Peterson, C.D., and Sterling, S.L., 2013, Late Holocene tsunami deposits at Salt Creek, Washington, USA: Science of Tsunami Hazards, v. 32, no. 4, p. 221-235.

Hutchinson, I., and Clague, J., 2017, Were they all giants? Perspectives on late Holocene plate-boundary earthquakes at the northern end of the Cascadia subduction zone: Quaternary Science Reviews, v. 169, p. 29-49.

Ichinose, G., Thio, H., and Somerville, P.G., 2006, Moment tensor and rupture model for the 1949 Olympia, Washington, Earthquake and scaling relations for Cascadia and Global Intraslab Earthquakes: Bulletin of the Seismological Society of America, v. 96, no. 3, p. 1029-1037.

Jackson, G.W., 2008, Site and Reach Assessment Union River at SR 300: Washington State Department of Transportation, Environmental Services, Watershed Management Program, Work Order MT0100, 59 p.

Jacoby, G.C., Bunker, D.E., and Benson, B.E., 1997, Tree-ring evidence for an A.D. 1700 Cascadia earthquake in Washington and northern Oregon, Geology, v. 25, no. 11, p. 999-1002.

John, J., 1983, The diatom flora of the Swan River Estuary, Western Australia: Bibliotheca Phycologica ; Bd. 64. Vaduz: J. Cramer, 358 p.

Johnson, S.Y., Blakely, R.J., Stephenson, W.J., Dadisman, S.V., and Fisher, M.A., 2004a, Active shortening of the Cascadia forearc and implications for seismic hazards of the Puget Lowland: Tectonics, v. 23, no. 1, p. TC1011, doi:10.1029/2003TC001507.

Johnson, S.Y., Dadisman, S.V., Childs, J.R., and Stanley, W.D., 1999, Active tectonics of the Seattle Fault and central Puget Sound, Washington; implications for earthquake hazards: Geological Society of America Bulletin, v. 111, no. 7, p. 1042-1053.

Johnson, S.Y., Nelson, A.R., Personius, S.F., et al., 2004b, Evidence for late Holocene earthquakes on the Utsalady Point Fault, northern Puget Lowland, Washington: Bulletin of the Seismological Society of America, v. 94, no. 6, p. 2299-2316.

Jovanelly, T.J., and Moore, A.L., 2009, Sedimentological Analysis of an Ancient Sand Sheet of Multiple Origins at Lynch Cove, Puget Sound, Washington: Journal of Coastal Research, v. 25, no. 2, p. 294-304.

Juggins, S., 2007, C2 Version 1.7.7: Software for ecological and palaeoecological data analysis and visualisation, https://www.staff.ncl.ac.uk/stephen.juggins/software/C2Home.htm.

Juggins, S., and Birks, H.J.B., 2012, Quantitative environmental reconstructions from biological data: Developments in Paleoenvironmental Research, p. 431-494.

Karlin, R.E., Holmes, M., Abella, S.E.B., and Sylwester, R., 2004, Holocene landslides and a 3500-year record of Pacific Northwest earthquakes from sediments in Lake Washington: Geological Society of America Bulletin, v. 116, no. 1-2, p. 94-108.

Kelsey, H.M., Nelson, A.R., Hemphill-Haley, E., and Witter, R.C., 2005, Tsunami history of an Oregon coastal lake reveals a 4600 yr record of great earthquakes on the Cascadia subduction zone, The Geological Society of America Bulletin, v. 117, no. 7, p. 1009.

Kelsey, H.M., Sherrod, B.L., Blakely, R.J., and Haugerud, R.A., 2012, Holocene faulting in the Bellingham forearc basin: Upper-plate deformation at the northern end of the Cascadia subduction zone: Journal of Geophysical Research-Solid Earth, v. 117, p. B03409, doi:10.1029/2011JB008816.

Kelsey, H.M., Witter, R.C., and Hemphill-Haley, E., 2002, Plate- boundary earthquakes and tsunamis of the past 5500 yr, Sixes River estuary, southern Oregon: Bulletin of the Geological Society of America, v. 114, no. 3, p. 298-314.

Kemp, A.C., and Telford, R.J., 2015, Transfer functions. *in* Handbook of Sea-Level Research, John Wiley & Sons, Ltd, p. 470-499.

Kortekaas, S., and Dawson, A.G., 2007, Distinguishing tsunami and storm deposits: An example from Martinhal, SW Portugal: Sedimentary Geology, v. 200, no. 3, p. 208-221.

Kramer, K., and Lange-Bertalot, H., 1993, Süsswasserflora von mitteleuropa 2. Bacillariophyceae 3. Teil. Centrales, fragilariaceae, eunotiaceae: K. Kramer and H. Lange-Bertalot, G. Fischer, Stuttgart, Germany, 1991, XIII + 567 pp., DM 198, ISBN 3-437-30541-7.

Krammer, K., and Lange-Bertalot, H., 1986, Bacillariophyceae: Jena ; New York, Jena ; New York : G. Fischer.

Krammer, K., and Lange-Bertalot, H., 1985, Naviculaceae: neue und wenig bekannte Taxa, neue Kombinationen und Synonyme sowie Bemerkungen zu einigen Gattungen: Berlin, Berlin : J. Cramer.

Krammer, K., and Lange-Bertalot, H., 2001, Diatoms of Europe, Volume 2: Navicula sensu stricto, 10 genera separated from Navicula sensu lato, Frustulia, Gantner Verlag, 526 p.

Kresch, D.L., Kasnick, K.D., Washington (State) Department of Transportation, Washington (State) Department of Ecology, U. S. Geological Survey, and Sumioka, S.S., 1998, Magnitude and frequency of floods in Washington: Water-Resources Investigations Report 97-4277, 95 p., https://pubs.usgs.gov/wri/1997/4277/report.pdf

Kubo, T., Murakami, H., and Kozuki, Y., 2007, Characteristic period of Tsunami in Seto Inland Sea: Proceedings of Coastal Engineering, JSCE, v. 54, p. 191-195.

LaHusen, S.R., Duvall, A.R., Booth, A.M., and Montgomery, D.R., 2015, Surface roughness dating of long-runout landslides near Oso, Washington (USA), reveals persistent postglacial hillslope instability: Geology, v. 44 (2), p. 111-114.

Lamb, A.P., Liberty, L.M., van Wijk, R.J., Blakely, T.L., Pratt, B.L., and Sherrod, K., 2012, Western limits of the Seattle fault zone and its interaction with the Olympic Peninsula, Washington: Geosphere, v. 8, no. 4, p. 915-930.

Lander, J.F., Lockridge, P.A., Kozuch, M.J., and National Geophysical, D.C., 1993, Tsunamis affecting the West Coast of the United States, 1806-1992: Boulder, Colorado, U.S. Dept. of Commerce, National Oceanic and Atmospheric Administration, National Environmental Satellite, Data, and Information Service, National Geophysical Data Center.

Laws, R.A., 1988, Diatoms (Bacillariophyceae) from surface sediments in the San Francisco Bay estuary: Proceedings of the California Academy of Sciences (USA), v. 45, Series 4, p 133-254.

Lee, H.S., Shimoyama, T., and Popinet, S., 2015, Impacts of tides on tsunami propagation due to potential Nankai Trough earthquakes in the Seto Inland Sea, Japan: Journal of Geophysical Research: Oceans, v. 120, no. 10, p. 6865-6883.

LeVeque, R.J., George, D.L., and Berger, M.J., 2011, Tsunami modelling with adaptively refined finite volume methods *: Acta Numerica, v. 20, p. 211-289.

Lienkaemper, J.J., and Bronk Ramsey, C., 2009, OxCal; versatile tool for developing paleoearthquake chronologies--a primer: Seismological Research Letters, v. 80, no. 3, p. 431-434.

Ludwin, R.S., Slemmons, D.B., Engdahl, E.R., Zoback, M.D., Blackwell, D.D., Weaver, C.S., and Crosson, R.S., 1991, Seismicity of Washington and Oregon: Boulder, CO, Boulder, CO, United States: Geol. Soc. Am, 77 p.

Martin, M.E., and Bourgeois, J., 2012, Vented sediments and tsunami deposits in the Puget Lowland, Washington - differentiating sedimentary processes: Sedimentology, v. 59, no. 2.

Masson, D.G., Harbitz, C.B., Wynn, R.B., Pedersen, G., and Løvholt, F., 2006, Submarine Landslides: Processes, Triggers and Hazard Prediction: Philosophical Transactions: Mathematical, Physical and Engineering Sciences, v. 364, no. 1845, p. 2009-2039.

Mazzotti, S., Jones, C., and Thomson, R.E., 2008, Relative and absolute sea level rise in western Canada and northwestern United States from a combined tide gauge- GPS analysis: Journal of Geophysical Research: Oceans, v. 113, p. n/a.

McCrory, P.A., Blair, J.L., Waldhauser, F., and Oppenheimer, D.H., 2012, Juan de Fuca slab geometry and its relation to Wadati-Benioff zone seismicity: Journal of Geophysical Research: Solid Earth, v. 117, p. n/a.

McGarr, A., and Vorhis, R.C., 1968, Seismic seiches from the March 1964 Alaska earthquake, Alaska Earthquake, March 27, 1964: Effects on the Hydrologic Regimen: U.S. Geological Survey Professional Paper 544–E, 43 p., 1 sheet, scale 1:5,000,000, https://pubs.usgs.gov/pp/0544e/.

McHugh, C.M., Seeber, L., Braudy, N., et al., 2011, Offshore sedimentary effects of the 12 January 2010 Haiti earthquake: Geology, v. 39, no. 8, p. 723-726.

Mofjeld, H.O., Foreman, M.G.G., and Ruffman, A., 1997, West Coast tides during Cascadia subduction zone tsunamis: Geophysical Research Letters, v. 24, no. 17, p. 2215-2218.

Morton, R.A., Gelfenbaum, G., and Jaffe, B.E., 2007, Physical criteria for distinguishing sandy tsunami and storm deposits using modern examples: Sedimentary Geology, v. 200, no. 3-4, p. 184-207.

Nelson, A.R., Personius, S.F., Buck, J., et al., 2008a: Field and laboratory data from an earthquake history study of scarps in the hanging wall of the Tacoma fault, Mason and Pierce Counties, Washington.

Nelson, A.R., Johnson, S.Y., Kelsey, H.M., et al., 2003, Late Holocene earthquakes on the Toe Jam Hill Fault, Seattle fault zone, Bainbridge Island, Washington: Geological Society of America Bulletin, v. 115, no. 11, p. 1388-1403.

Nelson, A.R., Kelsey, H.M., and Witter, R.C., 2006, Great earthquakes of variable magnitude at the Cascadia subduction zone: Quaternary Research, v. 65, no. 3, p. 354.

Nelson, A.R., Personius, S.F., Sherrod, B.L., Kelsey, H.M., Johnson, S.Y., Bradley, L., and Wells, R.E., 2014, Diverse rupture modes for surface-deforming upper plate earthquakes in the southern Puget Lowland of Washington State: Geosphere, v 10(4), 769-796.

Nelson, A.R., Sawai, Y., Jennings, A.E., et al., 2008b, Great-earthquake paleogeodesy and tsunamis of the past 2000 years at Alsea Bay, central Oregon coast, USA: Quaternary Science Reviews, v. 27, no. 7-8, p. 747-768.

NOAA, 2015, Extreme Water Levels for Seattle, WA, National Oceanic and Atmospheric Administration (NOAA), https://tidesandcurrents.noaa.gov/est/est_station.shtml?stnid=9447130.

Okada, R., 1985, Surface deformation due to shear and tensile faults in a half-space: Bulletin of the Seismological Society of America, v. 75, p. 1135-1154.

Parsons, T., Geist, E.L., Ryan, H.F., et al., 2014, Source and progression of a submarine landslide and tsunami: The 1964 Great Alaska earthquake at Valdez: Journal of Geophysical Research: Solid Earth, v. 119, no. 11, p. 8502-8516.

Paulson, Anthony J., U.S. Geological Survey, and Hood Canal Dissolved Oxygen Program, 2006, Freshwater and Saline Loads of Dissolved Inorganic Nitrogen to Hood Canal and Lynch Cove, Western Washington. Scientific Investigations Report, 2006-5106. Reston, Virginia: U.S. Dept. of the Interior, U.S. Geological Survey, https://pubs.usgs.gov/sir/2006/5106/.

Petersen, M., & U.S. Geological Survey, 2014, Documentation for the 2014 update of the United States National Seismic Hazard Maps, U.S. Geological Survey open-file report 2014–1091, U.S. Geological Survey, 255 p., https://pubs.usgs.gov/of/2014/1091/pdf/ofr2014-1091.pdf.

Peterson, C.D., Cruikshank, K.M., Darienzo, M.E., Wessen, G.C., Butler, V.L., and Sterlings, S.L., 2013, Coseismic subsidence and paleotsunami run-up records from latest Holocene deposits in the Waatch Valley, Neah Bay, Northwest Washington, U.S.A.: Links to Great Earthquakes in the Northern Cascadia Margin: Journal of Coastal Research, v. 29, no. 1, p. 157-172.

Plafker, George, and Kachadoorian, Reuben, 1966, Geologic Effects of the March 1964 Earthquake and Associated Seismic Sea Waves on Kodiak and Nearby Islands, Alaska. Geological Survey Professional Paper, 543-D.

Pollen, A., 2016, The Sedimentary Record of Past Earthquakes Identified in Holocene Sediments of Lake Crescent, Washington [M.S. thesis]: North Carolina State University.

Port Townsend Leader, April 2, 1964, Tidal Wave Alerts Received by Various Agencies Here.

Ramírez-Herrera, M., Lagos, M., Hutchinson, I., et al., 2011, Extreme wave deposits on the Pacific coast of Mexico: Tsunamis or storms? — A multi-proxy approach: Geomorphology, v. 139-140, p. 360-371.

Reimer, P.J., Bard, E., Bayliss, A., et al., 2013, IntCal13 and Marine13 radiocarbon age calibration curves 0- 50,000 years cal BP: Radiocarbon, v. 55, no. 4, p. 1869-1887.

Richmond, B.M., Watt, S., Buckley, M., Jaffe, B.E., Gelfenbaum, G., and Morton, R.A., 2011, Recent storm and tsunami coarse-clast deposit characteristics, southeast Hawai‘i: Marine Geology, v. 283, no. 1, p. 79-89.

Sarikhan, I.Y., Walsh, T.J., and Cakir, R., 2007, Morphology of the Alderwood landslide; a probable origin for tsunami in Lynch Cove, Puget Sound, Washington: Abstracts with Programs - Geological Society of America, v. 39, no. 4; 4, p. 31.

Sawai, Y., 2009, Relative sea-level change during the last few hundreds years at Discovery Bay, Washington State: Abstracts with Programs - Geological Society of America, v. 41, no. 7, p. 407.

Sawai, Y., Horton, B.P., Kemp, A.C., Hawkes, A.D., Nagumo, T., and Nelson, A.R., 2016, Relationships between diatoms and tidal environments in Oregon and Washington, USA: Diatom Research, v. 31, no. 1, p. 17-38.

Sawai, Y., Horton, B.P., and Nagumo, T., 2004a, The development of a diatom-based transfer function along the Pacific coast of eastern Hokkaido, northern Japan; an aid in paleoseismic studies of the Kuril subduction zone: Quaternary Science Reviews, v. 23, no. 23-24, p. 2467-2483.

Sawai, Y., and Nagumo, T., 2003, Diatoms from Alsea Bay, Oregon, USA: Diatom, v. 19, p. 33-46.

Sawai, Y., Nagumo, T., Namegaya, Y., Cisternas, M.V., Lagos, M., and Shishikura, M., 2017, Diatom (Bacillariophyceae) assemblages in salt marshes of south- central Chile: Relations with tidal inundation time and salinity: Phycological Research, v. 65, no. 1, p. 29-37.

Sawai, Y., Satake, K., Kamataki, T., et al., 2004b, Transient uplift after a 17th-century earthquake along the Kuril subduction zone: Science, v. 306, no. 5703, p. 1918-1920.

Schulz, W.H., 2007, Landslide susceptibility revealed by LIDAR imagery and historical records, Seattle, Washington: Engineering Geology, v. 89, no. 1, p. 67-87.

Seattle Daily Times, March 28, 1964, Seattle Tides Fluctuate After Alaska Earthquake, p. 1.

Shennan, I., Long, A.J., Rutherford, M.M., Innes, J.B., Green, F.M., and Walker, K.J., 1998, Tidal marsh stratigraphy, sea-level change and large earthquakes--ll: submergence events during the last 3,500 years at Netarts Bay, Oregon, USA: Quaternary Science Reviews, v. 17, no. 4-5, p. 365-393.

Shennan, I., Garrett, E., and Barlow, N., 2016, Detection limits of tidal-wetland sequences to identify variable rupture modes of megathrust earthquakes: Quaternary Science Reviews, v. 150, p. 1-30.

Shennan, I., and Hamilton, S., 2006, Coseismic and pre-seismic subsidence associated with great earthquakes in Alaska: Quaternary Science Reviews, v. 25, no. 1-2; 1-2, p. 1-8.

Sherrod, B.L., 1999, Gradient analysis of diatom assemblages in a Puget Sound salt marsh; can such assemblages be used for quantitative paleoecological reconstructions?, Palaeogeography, Palaeoclimatology, Palaeoecology, v. 149, no. 1-4, p. 213-226.

Sherrod, B.L., Brocher, T.M., Weaver, C.S., et al., 2004, Holocene fault scarps near Tacoma, Washington, USA.: Geology, v. 32, no. 1, p. 9-12.

Sherrod, B.L., 2001, Evidence for earthquake-induced subsidence about 1100 yr ago in coastal marshes of southern Puget Sound, Washington: Geological Society of America Bulletin, v. 113, no. 10, p. 1299-1311.

Sherrod, B.L., Blakely, R.J., Weaver, C.S., et al., 2008, Finding concealed active faults: Extending the southern Whidbey Island fault across the Puget Lowland, Washington: J. Geophys. Res., 113, B05313, doi:10.1029/2007JB005060.

Sherrod, B.L., Brocher, T.M., Weaver, C.S., et al., 2003, Evidence for a late Holocene earthquake on the Tacoma Fault, Puget Sound, Washington: Abstracts with Programs - Geological Society of America, v. 35, no. 6, p. 98.

Sherrod, B.L., Bucknam, R.C., and Leopold, E.B., 2000, Holocene Relative Sea Level Changes along the Seattle Fault at Restoration Point, Washington: Quaternary Research, v. 54, no. 3, p. 384-393.

Shipman, H., 2004, Coastal Bluffs and Sea Cliffs on Puget Sound, Washington, in Hampton, M.A. and Griggs, G.B., eds., Formation, evolution, and stability of coastal cliffs : status and trends, U.S. Geological Survey Professional Paper 1693, https://pubs.usgs.gov/pp/pp1693/pp1693.pdf.

Sievers, C., Hellmuth, A., Villegas, G., and Barros, G., 1963, The seismic sea wave of 22 May 1960 along the Chilean coast: Bulletin of the Seismological Society of America, v. 53, no. 6, p. 1125-1190.

Smith, S., 2012, Controls on Large and Very Large Submarine Landslides in Puget Sound, WA, USA: ProQuest Dissertations Publishing.

Tappin, D.R., 2010, Submarine mass failures as tsunami sources: their climate control: Philosophical Transactions of the Royal Society A, v. 368, no. 1919, p. 2417-2434.

ter Braak, C., and Juggins, S., 1993, Weighted averaging partial least squares regression (WA-PLS); an improved method for reconstructing environmental variables from species assemblages: Hydrobiologia, v. 269-270, p. 485-502.

Thatcher, W., 1984, The earthquake deformation cycle at the Nankai Trough, Southwest Japan: Journal of Geophysical Research, v. 89, no. 5, p. 3087-3101.

Tuttle, M.P., Ruffman, A., Anderson, T., and Jeter, H., 2004, Distinguishing tsunami from storm deposits in eastern North America: The 1929 Grand Banks tsunami versus the 1991 Halloween storm: Seismological Research Letters, v. 75, no. 1, p. 117-131.

University of California Berkeley Seismological Laboratory, United States, G.S., Calpine and Unocal Corporations, et al., 2014, Northern California Earthquake Data Center, Northern California Earthquake Data Center10.7932/NCEDC.

Verdonck, D., 2006, Contemporary vertical crustal deformation in Cascadia: Tectonophysics, v. 417, no. 3-4; 3-4, p. 221-230.

Vos, P.C., and de Wolf, H., 1993, Diatoms as a tool for reconstructing sedimentary environments in coastal wetlands; methodological aspects 269-270.

Wallace, D.J., Martini, I.P., Anderson, J.B., and Donnelly, J.P., 2014, Palaeohurricane reconstructions from sedimentary archives along the Gulf of Mexico, Caribbean Sea and western North Atlantic Ocean margins: Special Publication - Geological Society of London, v. 388, no. 1, p. 481-501.

Walsh, T.J., Cakir, R., Logan, R.L., and Johnson, C.N., 2009, Remotely operated vehicle (ROV) video investigation of two large seafloor mounds in southern Hood Canal, Washington: Abstracts with Programs - Geological Society of America, vol. 41, no. 7, 2009, p. 520.

Walsh, T.J., Myers, E.P., Baptista, A.M., and Washington (State) Division of Geology and, Earth Resources, 2002a: Tsunami inundation map of the Port Angeles, Washington, area, Dept. of Natural Resources, Division of Geology and Earth Resources, 1:24,000, http://file.dnr.wa.gov/publications/ger_ofr2002-1_tsunami_hazard_portangeles.pdf

Walsh, T.J., Myers, E.P., Baptista, A.M., and Washington (State) Division of Geology and, Earth Resources, 2002b: Tsunami inundation map of the Port Townsend, Washington, area, Dept. of Natural Resources, Division of Geology and Earth Resources, 1:24,000, http://file.dnr.wa.gov/publications/ger_ofr2002-2_tsunami_hazard_porttownsend.pdf.

Walsh, T.J., Washington (State) Division of Geology and, Earth Resources, Walsh, T.J., and Washington (State) Division of Geology and, Earth Resources, 2005: Tsunami hazard map of the Anacortes-Whidbey Island area, Washington: modeled tsunami inundation from a Cascadia Subduction Zone earthquake, Dept. of Natural Resources, Division of Geology and Earth Resources, 1:62,500, http://file.dnr.wa.gov/publications/ger_ofr2005-1_tsunami_hazard_anacortes_whidbey.pdf.

Walsh, T.J., Washington (State) Division of Geology and, Earth Resources, Walsh, T.J., and Washington (State) Division of Geology and, Earth Resources, 2004: Tsunami hazard map of the Bellingham area, Washington: modeled tsunami inundation from a Cascadia subduction zone earthquake, Dept. of Natural Resources, Division of Geology and Earth Resources, 1:50,000, https://www.pmel.noaa.gov/pubs/PDF/wals2795/wals2795.pdf.

Wang, K., Hu, Y., and He, J., 2012, Deformation cycles of subduction earthquakes in a viscoelastic Earth: Nature, v. 484, no. 7394, p. 327.

Wang, K., and Tréhu, A.M., 2016, Invited review paper: Some outstanding issues in the study of great megathrust earthquakes—The Cascadia example: Journal of Geodynamics, v. 98, p. 1-18.

Wang, P., Engelhart, S.E., Wang, K., Hawkes, A.D., Horton, B.P., Nelson, A.R., and Witter, R.C., 2013, Heterogeneous rupture in the great Cascadia earthquake of 1700 inferred from coastal subsidence estimates: JGRB Journal of Geophysical Research: Solid Earth, v. 118, no. 5, p. 2460-2473.

Warnock, J., and Scherer, R., 2015, A revised method for determining the absolute abundance of diatoms: Journal of Paleolimnology, v. 53, no. 1, p. 157-163.

Wartman, J., Montgomery, D.R., Anderson, S.A., Keaton, J.R., Benoît, J., dela Chapelle, J., and Gilbert, R., 2016, The 22 March 2014 Oso landslide, Washington, USA: Geomorphology, v. 253, p. 275-288.

Watcham, E.P., Shennan, I., and Barlow, N.L.M., 2013, Scale considerations in using diatoms as indicators of sea-level change: lessons from Alaska: JQS Journal of Quaternary Science, v. 28, no. 2, p. 165-179.

Wells, R.E., Weaver, C.S., and Blakely, R.J., 1998, Fore- arc migration in Cascadia and its neotectonic significance: Geology, v. 26, no. 8, p. 759-762.

Wells, R., and Simpson, R., 2001, Northward migration of the Cascadia forearc in the northwestern U.S. and implications for subduction deformation: Earth, Planets and Space, v. 53, no. 4, p. 275-283.

Williams, H.F.L., Hutchinson, I., and Nelson, A.R., 2005, Multiple sources for late-Holocene tsunamis at Discovery Bay, Washington State, USA: Holocene, v. 15, no. 1, p. 60-73.

Williams, H., and Hutchinson, I., 2000, Stratigraphic and Microfossil Evidence for Late Holocene Tsunamis at Swantown Marsh, Whidbey Island, Washington: Quaternary Research, v. 54, no. 2, p. 218-227.

Witkowski, A., 2000, Iconographia Diatomologica: annotated diatom micrographs Vol. 7, Vol. 7,: Ruggell, A.R.G. Gantner.

Witter, R.C., Givler, R.W., and Carson, R.J., 2008a, Two post-glacial earthquakes on the saddle Mountain West fault, Southeastern Olympic Peninsula, Washington: Bulletin of the Seismological Society of America, v. 98, no. 6, p. 2894-2917.

Witter, R.C., Kelsey, H.M., and Hemphill-Haley, E., 2003, Great Cascadia earthquakes and tsunamis of the past 6700 years, Coquille River estuary, southern coastal Oregon: Geological Society of America Bulletin, v. 115, no. 10, p. 1289-1306.

Witter, R.C., Peterson, C.D., Cruikshank, K.M., Hemphill-Haley, E., Schlichting, R.B., and Allan, J.C., 2008b, Prehistoric Cascadia tsunami inundation and runup at Cannon Beach, Clatsop County, Oregon: O-08-12.

Witter, R. C., Yinglong, J. J., Zhang, Y. J., Wang, K. R., Priest, G. T., Stimely, L. A., English, J., Ferro, P. A., Goldfinger, C. (2013). Simulated tsunami inundation for a range of Cascadia megathrust earthquake scenarios at Bandon, Oregon, USA. Geosphere, 9(6), 1783-1803.

Yamaguchi, D.K., Atwater, B.F., Bunker, D.E., Benson, B.E., and Reid, M.S., 1997, Tree-ring dating the 1700 Cascadia earthquake: Nature London], v. 389, no. 6654, p. 922-923.

Yamanaka, R., Kozuki, Y., Tanabe, S., Iwaka, K., and Murakami, H., 2009, Spatiotemporal analysis of Tsunami wave property and hazardous sea area in Seto Island Sea: Journal of Japan Society of Civil Engineers, Ser.B2 (Coastal Engineering), v. 65, no. 1, p. 341-345.

Zong, Y., and Horton, B., 1998, Diatom zones across intertidal flats and coastal saltmarshes in Britain, v. 13, no. 2, p. 375-394.

Zong, Y., and Horton, B.P., 1999, Diatom-based tidal-level transfer functions as an aid in reconstructing Quaternary history of sea-level movements in the UK: JQS.Journal of Quaternary Science, v. 14, no. 2, p. 153-167.

APPENDIX 1. LYNCH COVE TSUNAMI DEPOSIT CHARACTERISTICS, CHAPTER 2

Location	Type	Layer	Depth (cm)	Thickness (cm)	Location		Comment
					Easting (m E)	Northing (m N)	
01.11.15.01	outcrop	A	47	1	511918	5253605	
02.05.30.01	core	none	N.D.	N.D.	511905	5253622	
02.05.30.02	core	none	N.D.	N.D.	511895	5253622	
02.05.30.03	core	none	N.D.	N.D.	511885	5253621	
02.05.31.00	core	none	N.D.	N.D.	511915	5253621	
02.05.31.01	core	none	N.D.	N.D.	511925	5253621	
02.05.31.02	core	none	N.D.	N.D.	511935	5253621	
02.05.31.03	core	none	N.D.	N.D.	511941	5253621	
02.05.31.04	core	none	N.D.	N.D.	511875	5253621	
02.05.31.05	core	none	N.D.	N.D.	511865	5253622	
02.05.31.06	core	A	50	0.5	511855	5253622	
02.05.31.07	core	A?	55	1	511844	5253623	
02.05.31.08	core	A?	67	0.5	511833	5253622	
02.05.31.09	core	A?	62	0.5	511820	5253621	
02.06.11	outcrop	none	N.D.	N.D.	511811	5253860	Channel near boardwalk
02.06.18.01	outcrop	A	53.5	1	511496	5253928	
02.06.18.02	core	A	53.5	1	511606	5253954	
02.06.18.03	outcrop	A	52	1	511491	5253977	Two layers close together at 52-53 & 57-58 cm, similar to 15.07.14 179S1
02.06.18.04	outcrop	none	N.D.	N.D.	511648	5253989	
02.06.21.01	outcrop	A	45	5	511786	5253804	
02.06.21.02	outcrop	A	70	0.5	511753	5253958	Two intermittent silt layers, similar to 03.08.14
02.06.21.03	outcrop	A?	54	0.5	511802	5253905	Black layer at 54 cm, also white and a brown layer
02.06.21.04	core	none	N.D.	N.D.	511881	5253860	
02.06.21.05	core	none	N.D.	N.D.	511939	5253855	
02.06.21.06	core	none	N.D.	N.D.	512006	5253851	
03.08.14	outcrop	A	67	2.5	511793	5253783	Thin intermittent silt layers
03.09.23	outcrop	A	65	1	511741	5253728	Radiocarbon sample from below
03.09.24	outcrop	A?	63	0	511811	5253860	A washed out and collapsed? Possible trace of B
11.10.10	outcrop	A	30	1	511861	5253611	
13.06.26.03	outcrop	A	30	1	511861	5253611	Monolith collected, photos
13.06.26.03							
12.08.08.01	pit	A?	40	~10	511957	5254019	Monolith collected, photos, gray chunks here
12.08.08.02	pit	A?	N.D.	N.D.	511986	5254219	Photos, gray chunks here
12.08.21.01	pit	A?	30	~5	511943	5254211	Monolith collected, photos, gray chunks here
13.06.13.01	outcrop	A	35	1.5	511784	5253689	Fine sand draped over log or root
13.06.26.01	pit	none	N.D.	N.D.	511915	5253620	
13.06.26.02	pit	none	N.D.	N.D.	511913	5253619	
13.06.26.03	outcrop	A	30	~10	511862	5253611	
13.06.26.04	outcrop	A	59	2	511815	5253533	

Location	Type	Layer	Depth (cm)	Thickness (cm)	Location		Comment
					Easting (m E)	Northing (m N)	
13.06.26.05	outcrop	A	62	3	511760	5253517	Revisited on 13.10.16 and 14.09.08
13.06.26.05	outcrop	B	126	4	511760	5253517	
13.10.16.01	outcrop	A	55	1	511757	5253520	Most expanded section, radiocarbon samples, normal grading
13.10.16.01	outcrop	B	125	1	511757	5253520	
14.09.09	outcrop	A	40	2.5	511780	5253614	Radiocarbon samples from this site, layer draped over stick
14.09.09	outcrop	B	95	1.5	511780	5253614	normal grading
15.04.27.01	outcrop	A	20	7	511960	5254004	Thick sand layer
15.04.27.02	outcrop	A	19	3	511938	5254009	Sandy layer A, gray chunks lower, similar to 15.07.21.04
15.04.27.02	outcrop	B?	34	10	511938	5254009	Zone of gray chunks
15.04.27.03	outcrop	none	N.D.	N.D.	511815	5253873	Triglochin collected here at top of uplifted tidal flat
15.05.08.01	outcrop	A	40	1	511869	5253617	Fine sand draped over log
15.07.15 179-S1	outcrop	A	50	20?	511554	5253919	
15.07.21.01	pit	A?	45	5?	511912	5254240	Gray chunks, radiocarbon samples
15.07.21.02	outcrop	A?	45	5?	511860	5254181	Gray chunks, photos
15.07.21.03	core	none	N.D.	N.D.	511812	5254128	Salt pan
15.07.21.04	core	A	56	8	511814	5254129	Gray chunks with sand, similar to 15.04.27.02
15.07.21.04	core	B?	91	4	511814	5254129	Gray chunks and mottled
15.10.09.01	outcrop	A	53	2	511779	5253534	On grain size transect
15.10.09.01	outcrop	B	123	3	511779	5253534	On grain size transect
15.10.09.02	core	A	42	2	511802	5253557	On grain size transect
15.10.09.02	core	B	82	1.5	511802	5253557	On grain size transect
15.10.09.03	core	A	37	1	511835	5253579	On grain size transect
15.10.09.03	core	B	55	1	511835	5253579	On grain size transect
15.10.09.04	core	A	33	1	511869	5253600	On grain size transect (15.09.25)

APPENDIX 2. OXCAL AGE MODELS

Lynch Cove age model:

```
Plot()
 {
  Sequence("Lynch Cove sequence")
  {
   Boundary("Begin");
   Phase("Before layer B")
   {
    R_Date("Detrital twig in base of B 14.09.09 RC3A", 870, 20);
    R_Date("Detrital twig 1 cm below B 14.09.09 RC2", 840, 30);
    R_Date("Detrital twig in base of B 14.09.09 RC3B", 825, 20);
   };
   Date("layer B");
   Phase("After layer B")
   {
    R_Date("Schoenoplectus sp. rhizome 1 cm above B 14.09.22 RC5", 870, 30);
    R_Date("Schoenoplectus sp. rhizome within B 14.09.22 RC3", 860, 20);
    R_Date("Schoenoplectus sp. rhizome within B 14.09.22 RC4", 800, 20);
   };
   R_Date("Triglochin maritima leaf base 20 cm below A 15.05.08 RC1", 400, 15);
   R_Date("Triglochin maritima leaf base 17.5 cm below A 15.05.08 RC2", 330, 15);
   R_Date("Triglochin maritima leaf base 6.5 cm below A 13.10.16 RC8", 165, 20);
   R_Date("Triglochin maritima leaf base 3.5 cm below A 13.10.16 RC4", 120, 30);
   Date("layer A");
   Phase("After layer A")
   {
    R_Date("Triglochin maritima leaf base within A 13.10.16 RC9", 100, 20);
    R_Date("Triglochin maritima leaf base above A 03.09.23.03", 110, 40);
   };
   C_Date("Historic Settlement", 1850, 5);
   Boundary("End");
  };
 };
```

APPENDIX 2. OXCAL AGE MODELS, CONTINUED

Discovery Bay age model:

```
Plot()
 {
  Sequence()
  {
   Boundary("begin");
   Phase("Max ages Bed 6")
   {
    R_Date("Williams Max Bed 6", 1770, 50);
    R_Date("16.08.19 RC17 Twig 1 cm below Bed 6", 1740, 20);
   };
   Date("Bed 6");
   R_Date("Williams Max Bed 5", 1300, 40);
   Date("Bed 5");
   Phase("Min ages Bed 5")
   {
    R_Date("Williams Bed 5 min", 1240, 40);
    R_Date("16.08.19 RC13 Schoenoplectus rhizome 20 cm below Bed 4", 1300, 15);
   };
   R_Date("16.08.19 RC10 Stick 15 cm below Bed 4", 1260, 20);
   R_Date("16.08.19 RC12 Triglochin 12 cm below Bed 4", 1180, 20);
   R_Date("Williams Max Bed 4", 1180, 60);
   Date("Bed 4");
   Date("Bed 3");
   R_Date("Williams Min Bed 3", 730, 70);
   R_Date("16.08.19 RC6 Root/stem through Bed 3", 670, 20);
   R_Date("16.08.19 RC9 Triglochin 11 cm below Bed 2", 610, 25);
   R_Date("Triglochin 6 cm below Bed 2", 590, 20);
   R_Date("16.08.19 RC8A Triglochin 2 cm below Bed 2", 685, 20);
   R_Date("16.06.17 RC5 Triglochin 0.5 cm below Bed 2", 595, 15);
   Date("Bed 2");
   Phase("After Bed 2")
   {
    R_Date("16.06.17 RC3 Triglochin after Bed 2 a", 600, 15);
    R_Date("16.06.17 RC4 Triglochin after Bed 2 b", 610, 20);
    R_Date("16.06.17 RC1 after Bed 2 c", 635, 20);
   };
   R_Date("Before Bed 1 Williams", 223, 30);
   Date("Bed 1");
   Phase("After Bed 1")
   {
    R_Date("After Bed 1 Williams1", 130, 40);
    R_Date("After Bed 1 Williams2", 170, 40);
   };
   Boundary("end");
  };
 };
```

APPENDIX 3. DATES USED IN FIGURES 2.19 AND 2.20 AGE COMPARISONS, CHAPTER 2

LOCATION	REFERENCES	NAME USED BY AUTHORS	COMMENTS
Alsea Bay	Nelson et al., 2008b	Sand B	
Cannon Beach (Ecola Creek)	Witter et al., 2008b	Sands 2 & 3	
Cascadia earthquakes (WA coast estuaries)	Atwater, 1987; Atwater and Hemphill-Haley, 1997; Atwater et al., 2004; Atwater and Griggs, 2012; Nelson et al., 2006	Y, W, U	Age for W from Atwater and Griggs, 2012
Cascadia-wide turbidites and Juan de Fuca turbidites	Goldfinger et al., 2012; Goldfinger et al., 2017	T1-T4	Juan de Fuca channel ages from cores M9907-11 & -12; raw ages from forams, and adjusted ages
Coos Bay	Nelson et al., 2006	Buried soil B	
Deserted Lake	Hutchinson and Clague, 2017	TS2	Cores 97-109 & 96-105
Discovery Bay	Williams et al., 2005	Beds 1-4	Ages published previously
Effingham Inlet	Enkin et al., 2013	E1, E2 a-c, E3	E2 a-c probably record the same event
Fort Clatsop	Atwater and Griggs, 2012	W	Site in Oregon near the mouth of the Columbia River
Lake Washington	Karlin et al., 2004	B, C, D, E	
Lynch Cove	Bucknam et al., 1992; Sherrod, 2001; Hemphill-Haley, 1996; Jovanelly and Moore, 2009; Martin and Bourgeois, 2012	referred to by age	Age for earthquake and liquefaction prior to deposition of layers A & B
Netarts Bay	Darienzo, 1991; Darienzo et al., 1994; Shennan et al., 1998	2MT, OF-III	
Port Alberni	Clague et al., 1994; Clague and Bobrowsky, 1994a; Clague and Bobrowsky, 1994b	referred to by age	
Puget Sound	Smith, 2012	referred to by age	
Saanich Inlet	Blais-Stevens et al., 2011	Events 1-5	
Saddle Mountain fault (SMF)	Witter et al., 2008a; Blakely et al., 2009; Barnett et al., 2015	referred to by age	
Salt Creek	Hutchinson et al., 2013	referred to by age	Youngest event inferred to be from AD 1700
Seattle fault zone (SFZ)	Atwater and Moore, 1992 Bucknam et al., 1992; Atwater, 1999; Nelson et al., 2014	Restoration Point earthquake, Events D & E	Ages from multiple studies summarized in Nelson et al., 2014
Snohomish River delta	Bourgeois and Johnson, 2001	Events B, C, D, E	
Tacoma fault zone (TFZ)	Sherrod, 2001; Sherrod et al., 2004; Nelson et al., 2014	referred to by age	
Tofino	Clague and Bobrowsky, 1994a; Clague and Bobrowsky, 1994b	Sands 2 & 3	
Ucluelet	Clague and Bobrowsky, 1994a; Clague and Bobrowsky, 1994b	Sand 2	
Utsalady Point fault (UPF)	Johnson et al., 2004b	referred to by age	
Yaquina Bay	Graehl et al., 2014	Buried soil A	

APPENDIX 4. DIATOM COUNTS

Sample depth (cm)	Sample number	Achnanthes brevipes C.Agardh	Achnanthes punctulata Simonsen	Actinocyclus normanii (W.Gregory ex Greville) Hustedt	Actinoptychus senarius (Ehrenberg) Ehrenberg	Amphora ovalis (Kützing) Kützing	Amphora libyca Ehrenberg	Amphora sp. 1	Aulacoseira granulata (Ehrenberg) Simonsen	Bacillaria paxillifera (O.F.Müller) T.Marsson	Biremis lucens (Hustedt) K.Sabbe, A.Witkowski & W.Vyverman	Caloneis bacillum (Grunow) Cleve	Caloneis westii (W.Smith) Hendey	Catenula adhaerens (Mereschkowsky) Mereschkowsky	Cocconeis californica Grunow	Cocconeis costata Gregory	Cocconeis disculoides Hustedt	Cocconeis neodiminuta Krammer	Cocconeis neothumensis Krammer	Cocconeis pellucida Grunow	Cocconeis placentula Ehrenberg	Cocconeis scutellum Ehrenberg	Cocconeis scutellum var. parva (Grunow) Cleve	Coscinodiscus centralis Ehrenberg	Coscinodiscus marginatus Ehrenberg	Coscinodiscus radiatus Ehrenberg	Cosmioneis delawarensis (Grunow ex Cleve) D.G.Mann	Cosmioneis pusilla Mann and Stickle	Craticula accomoda (Hustedt) D.G. Mann	Cyclotella striata (Kützing) Grunow	Cymbella aspera (Ehrenberg) Cleve	Cymbopleura naviculiformis (Auerswald) Krammer
1-2	1	5	2				2					2		3				25	28			2	1									
10-11	2					3					1			3			2	2	12			4	1						5			
18-19	3	4				2					1	13		14			2	17	12			2							3			
26-27	4								5			16	4	2				38				16						5				
34-35	5	2				2						11		1				34	7			9						3		1		
41-42	6	3				9					1	2	4	7			1	52	3			5	2					1				
48-49	7													9			6	29				2	2									
51-52	8	5					3					10	7					11				4	2					6				
53-54	9						1					8	6	4				44				3	2					5				
55-56	10	1										8		19				69		1		5	7					1				
57-58	11	3					1	1			2	1		10			1	23	16			1	3					7				
58-59	12	9										7	2	4				20		1		3	1					4				
62-63	13	1					1					9	7	5			17	31				10	9				1	3				
65-66	14	5					1					1		13				45				3						11				
73-74	15	7									1	6		9				72				2						13				
80-81	16	4										6		13				37				2						14				1
88-89	17	5					2				1	10		12				50			1	5						19				
96-97	18	6									8	10		12				57				2						13				
103-104	19					2	1				4	7		10			7	40										20				
108-109	20	6				1	1				2	33	2	1				8				2						19				
110-111	21	1					1					9	1	11				67					3					18				
113-114	22	5					1					8	1	5				16				2	5				14	49				
116-117	23	2									1	13	5	5				13			1							26				
121-122	24										4	29		3				20			1							36				
123-124	25						4	2				7		2				87			1		6					41				
125-126	26	2												13				113					5					7				
128-129	27						1					1						8										60				
129-130	28											5		2				42					1					35				1
135-136	29						9					8		0				19					1					33		1	5	
141-142	30																															
150-151	31																															
158-159	32																															
164-165	33																															
169-170	34																															
172-173	35								2									4		1		81	2			1			6	2		
179-180	36			1	4				4	3			2	1	1	1					7	54	8	2	1					7		

APPENDIX 4. DIATOM COUNTS, CONTINUED

Sample depth (cm)	Denticula subtilis Grunow	Dimeregramma minor (Gregory) Ralfs	Diploneis decipiens var. parallela A.Cleve	Diploneis interrupta (Kützing) Cleve	Diploneis pseudovalis Hustedt	Diploneis smithii (Brébisson) Cleve	Diploneis stroemii Hustedt	Epithemia sorex Kützing	Epithemia turgida var. turgida (Ehrenberg) Kützing	Fallacia oculiformis (Hustedt) D.G.Mann	Fallacia pygmaea (Kützing) Stickle & D.G.Mann	Fragilariopsis doliolus (Wallich) Medlin & P.A.Sims	Frustulia vulgaris (Thwaites) De Toni	Gomphonema parvulum (Kützing) Kützing	Grammatophora oceanica Ehrenberg	Gyrosigma acuminatum (Kützing) Rabenhorst	Gyrosigma eximium (Thwaites) Boyer	Halamphora coffeiformis (C.Agardh) Levkov	Halamphora granulata (Gregory) Levkov	Hantzschia amphioxys (Ehrenberg) Grunow	Hippodonta pseudacceptata Kobayasi	Hyalodiscus scoticus (Kützing) Grunow	Licmophora abbreviata C.Agardh	Luticola mutica (Kützing) D.G.Mann	Mastogloia elliptica (C.Agardh) Cleve	Mastogloia exigua F.W.Lewis	Melosira nummuloides C.Agardh	Navicula cincta (Ehrenberg) Ralfs	Navicula cryptocephala var. veneta (Kützing) Rabenhorst	Navicula cryptotenella Lange-Bertalot	Navicula digitoradiata (W.Gregory)	Navicula erifuga Lange-Bertalot
1-2	2	13		2	4	1					1		2				8				9			1			16		9		
10-11	6	3			3		2			1	1				1		4	2			16						20		4		
18-19	7	9			5					7	1		8		1		43				16			18			6	5		5	5	
26-27		15		52	3					6					15		4		2			1	1	3				2		5	8	
34-35	1	11		9	7	2				7	1				6		3	1						6			15	6		5		
41-42	6	15		11	4	2				13	2				3		4				2			3			22	6		20		
48-49	12	8		2	3					5					2			1			17			14						27	5	
51-52	2		3	26	2	2				3	1				5			2				4	1	1	1	5		1		43		
53-54	6	3		12	7	5				8	1				5			1	1			2		6			2		5	51	1	
55-56	6	18		9	3	1				15	3				5		1				7	1		4		2	16	6			7	
57-58	3	10		36	5	1				10	5				7	2	12	1			28			9		2	6			3		
58-59	10	8		45	11	3				4	3				9	2	4		4		6	3		9	3		11	2			8	
62-63	3	11	2	9	3					2	6				13		16				4			6						10		1
65-66	16	12		17	2					18	1				11		1				5			42			2			1		
73-74	3	13		22	6					8					21		2	1			4			21			4			2		
80-81	18	20		18	8					8	5						3			1	9			61			21					
88-89	9	10		15	6	1				9	2		1	2	8		7	2			14			21			2	1		4		
96-97	4	8		9	7					10				3	16		1	4			11			40				4		5		
103-104	4	3		9	3					15	1		1		2		1				7			34				7		10		
108-109	3	3		18	6					2	1		3	1			31	1			10	1		23				3		3		
110-111	1	21		29	12	1				7					1		1		6		3	1		25			2	1				
113-114		6		100	16	2				4	1				6		7	3			4			26			3	8		1		
116-117		6		91	27	9				4					10		1		31			2		12				1				
121-122		10		11	29	4				10					6				15			1		9								
123-124		19		13	32	10				5					5			3						6							1	
125-126		53		2	6	5				27					2							1		2				2				
128-129		5	1	10	23	11		1	1													7		2								
129-130		12		1	33	8				3					3				13			5		18			8	1				
135-136		9		52	14	36			1													10										
141-142																																
150-151																																
158-159																																
164-165																																
169-170																																
172-173												7		3		7					1											1
179-180		2													3						3						3					

APPENDIX 4. DIATOM COUNTS, CONTINUED

Sample depth (cm)	Navicula gregaria Donkin	Navicula kefvingensis (Ehrenberg) Kützing	Navicula microdigitoradiata Lange-Bertalot	Navicula peregrinopsis Lange-Bertalot & Witkowski	Navicula phyllepta Kützing	Navicula recens (Lange-Bertalot) Lange-Bertalot	Navicula rhynchotella Lange-Bertalot	Navicula salinarum Grunow	Navicula sp. 1	Navicula tripunctata (O.F.Müller) Bory	Navicula sp. 1	Navicymbula pusilla (Grunow) Krammer	Nitzschia angustata (W.Smith) Grunow	Nitzschia bilobata W.Smith	Nitzschia brebissonii W.Smith	Nitzschia compressa (Bailey) C.S.Boyer	Nitzschia compressa var. vexans (Grunow) Lange-Bertalot	Nitzschia constricta (Kützing) Ralfs	Nitzschia dissipata (Kützing) Rabenhorst	Nitzschia frustulum (Kützing) Grunow	Nitzschia hybrida Grunow	Nitzschia palea (Kützing) W.Smith	Nitzschia pararostrata (Lange-Bertalot) Lange-Bertalot	Nitzschia pusilla Grunow	Nitzschia scapelliformis (Grunow) Grunow	Nitzschia sigma (Kützing) W.Smith	Nitzschia terrestris (J.B.Petersen) Hustedt	Nitzschia ventricosa Kitton	Nitzschia vitrea G.Norman	Nitzschia vitrea var. salinarum Grunow	Opephora minuta (Cleve-Euler) A.Witkowski, H.Lange-Bertalot & D.Metzeltin	Opephora pacifica (Grunow) Petit
1-2	14			1				3		1											46	6					7						6
10-11				1	15						11	3	3								27	2					4			2			8
18-19												2	3								2	2					3			1		1	9
26-27								1										1				1								1			9
34-35				1						2		2									3	1			2					3			15
41-42				8			1	1		3		29									2					2	1						24
48-49	5	2		2									2				2				4						8						14
51-52			32	3	4	2	1		3	5		3	1										2				21						3
53-54		10			16	2																					1						4
55-56				2					6			1									1									1	6		26
57-58	3	2			5					2			3								3	1		2			3				2		8
58-59									9			6		2																3	3		6
62-63		2		5	4		5			1							2										3						12
65-66				3	1																10						1			1			34
73-74				3	3							3									15	1					2			2			10
80-81		1		1				1				4																		2	13		24
88-89												7									15						7						24
96-97		1			2																22						3						17
103-104		2			3								1								9									2			
108-109					5							2	1								17						11						3
110-111							3	4																						0	9		14
113-114				2	4														2	1	4						6			1			2
116-117		7		7										0	12													2		3	1		2
121-122		8		5					3																					7	11		6
123-124		2			1	5			15	3																	2			9			
125-126									2																						5		16
128-129				4																					1		8						
129-130				6					2																						2		5
135-136									18					1		1														5	2		
141-142																																	
150-151																																	
158-159																																	
164-165																																	
169-170																																	
172-173																			1							1	2		1				2
179-180										1																							

APPENDIX 4. DIATOM COUNTS, CONTINUED

Sample depth (cm)	Opephora pacifica (Grunow) Petit	Opephora parva (Grunow) Krasske	Paralia sulcata (Ehrenberg) Cleve	Petroneis marina (Ralfs) D.G.Mann in Round, R.M.Crawford & D.G.Mann	Pinnularia appendiculata (C.Agardh) Schaarschmidt	Pinnularia lagerstedtii (Cleve) Cleve-Euler	Pinnularia obscura Krasske	Pinnularia viridis (Nitzsch) Ehrenberg	Plagiogramma staurophorum (W.Gregory) Heiberg	Planothidium delicatulum (Kützing) Round & Bukhtiyarova	Planothidium hauckianum (Grunow) Bukhtiyarova	Planothidium lanceolatum (Brébisson ex Kützing) Lange-Bertalot	Planothidium rostratum (Østrup) Lange-Bertalot	Planothidium sp. 1	Pleurosigma sp. 1	Pseudostaurosira brevistriata (Grunow) D.M.Williams & Round	Pseudostaurosira elliptica (Schumann) Edlund, Morales & Spaulding	Pseudostaurosira subsalina (Hustedt) E.A.Morales	Rhoicosphenia abbreviata (C.Agardh) Lange-Bertalot	Rhopalodia acuminata Krammer	Rhopalodia gibba (Ehrenberg) O. Müller	Rhopalodia gibberula (Ehrenberg) Otto Müller	Rhopalodia musculus (Kützing) Otto Müller	Rhopalodia pacifica Krammer	Scoliopleura tumida (Brébisson ex Kützing) Rabenhorst	Staurosira construens var. venter (Ehrenberg) P.B.Hamilton	Staurosirella pinnata (Ehrenberg) D.M.Williams & Round	Surirella newmani G.D.Hanna & W.M.Grant	Tabularia fasciculata (C.Agardh) D.M.Williams & Round	Thalassiosira eccentrica (Ehrenberg) Cleve	Trachyneis aspera (Ehrenberg) Cleve
1-2	6	28	3				1			39		5											10				43		3		1
10-11	8	18	18							13	29			19		50							15			8	32		5		
18-19	9	26	100						1	8	16	1				25		2				5	7				30		6	1	
26-27	9		117			1			1	37						19						17	3						15		
34-35	15	20	135			6				27						22		30				3	2			4			9		
41-42	24	10	147		1	2			2	23						6		16	1			5	4		1	13	5		7		
48-49	14	39	100		1	2	1			29	31					12	2	4					3			15	41		4		
51-52	3		127			4	1			8					4	1						2	34		3				8		
53-54	4		120	1			2			29									1				29		4		5		17		2
55-56	26		66			8				32	1	8											17		1	1			18		
57-58	8		106			4				24		2							1			3	15				6		9		
58-59	6		117		1	2				15		12											29						11		
62-63	12	3	123						1	24													22		1				15		
65-66	34		130		2	6	1			18						3						1	2						11		
73-74	10		154			12				13												1	5						8		
80-81	24		72		1	17				15													4						5		
88-89	24		125			3				11													8						5		
96-97	17		155			28				18						1							14						13		
103-104			111			29				27						3							4						2		
108-109	3		110			19	2			6													48						7		
110-111	14		181		2	32				7								5					1						1		
113-114	2		100			18				4						1							8								
116-117	2		186			20				2													34						7		
121-122	6		164			62																	25	1							
123-124			165			13	1			6		1											16		1						
125-126	16		409			14							4										8	9					6		
128-129			200			19		1										23				2	6						1		
129-130	5		208			55				6								7					20						2		
135-136			376			30		8											1		1		20				1		2		
141-142																															
150-151																															
158-159																															
164-165																															
169-170																															
172-173	2		105							4												7	7					210	7		
179-180			381						1											1			21					2	128	11	

APPENDIX 4. DIATOM COUNTS, CONTINUED

Sample depth (cm)	Tryblionella acuminata W.Smith	Tryblionella adducta (Hustedt) D.G.Mann	Tryblionella coarctata (Grunow) D.G.Mann	Tryblionella debilis Arnott ex O'Meara	Tryblionella granulata (Grunow) D.G.Mann	Tryblionella lanceola Grunow	Tryblionella levidensis W.Smith	Tryblionella punctata W.Smith	Unknown	Total counted
1-2	10	2		2			3			372
10-11	2	2								384
18-19	1	5		11	1					478
26-27					4		1	1		432
34-35	7	8	1	4	5					462
41-42		2		6						525
48-49		1		3						471
51-52	2				3		3			430
53-54		12		10	3					457
55-56				1		7	6			432
57-58	2	6	1	7	1					430
58-59					3	17	4			438
62-63	7	8	3	9	1		1			432
65-66		7		5	3					446
73-74	2			7	8					466
80-81					11	10	9			439
88-89	1	4		1	10					440
96-97				7	5					517
103-104		2		2	3					388
108-109	2			5					31	422
110-111					3	1	3			488
113-114					8					454
116-117					2					545
121-122					3		3			486
123-124					1					485
125-126					11		2			729
128-129					8					404
129-130					8					512
135-136					20					684
141-142										0
150-151										0
158-159										0
164-165										0
169-170										0
172-173	2	1	3						1	483
179-180	2				5					688

APPENDIX 5. GEOCLAW TSUNAMI SIMULATIONS OUTPUT, CHAPTER 3

URLs to tsunami simulation animations http://staff.washington.edu/cegl/_cegl_Index.html

On each page, "js Movies" lists animations for Pacific, western Strait of Juan de Fuca, eastern Strait Juan de Fuca, Lynch Cove and Discovery Bay. Seattle fault animations are for Puget Sound, Lynch Cove, and Discovery Bay. "Gauges" has individual gauge plots for gauges located at either Lynch Cove or Discovery Bay. "Other plots" contains figures for gauge locations, zeta (flow depth), speed, and arrival time for Lynch Cove and Discovery Bay study grids.

1. Cascadia buried slip tsunami:
   http://staff.washington.edu/cegl/Buried_plots/_PlotIndex.html

2. Cascadia heterogeneous slip tsunami:
   http://staff.washington.edu/cegl/Patchy_plots/_PlotIndex.html

3. Cascadia splay fault slip tsunami:
   http://staff.washington.edu/cegl/Splay_plots/_PlotIndex.html

4. Seattle fault 900-930 Restoration Point earthquake tsunami:
   http://staff.washington.edu/cegl/Seattle_f_plots/_PlotIndex.html

5. Alaska earthquake tsunami:
   http://staff.washington.edu/cegl/Alaska_plots/_PlotIndex.html

APPENDIX 5. GEOCLAW TSUNAMI SIMULATIONS OUTPUT, CHAPTER 3, CONTINUED

Maximum simulated speeds for study area grids

1. Cascadia simulation buried slip earthquake

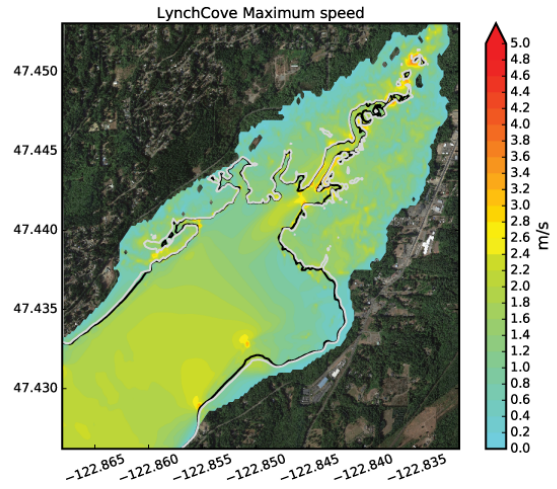

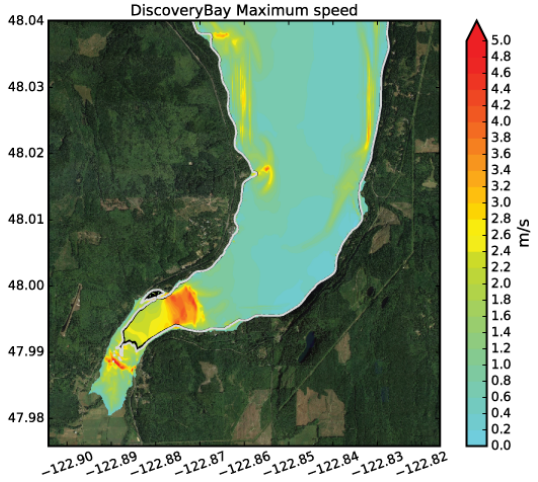

2. Cascadia heterogeneous slip earthquake

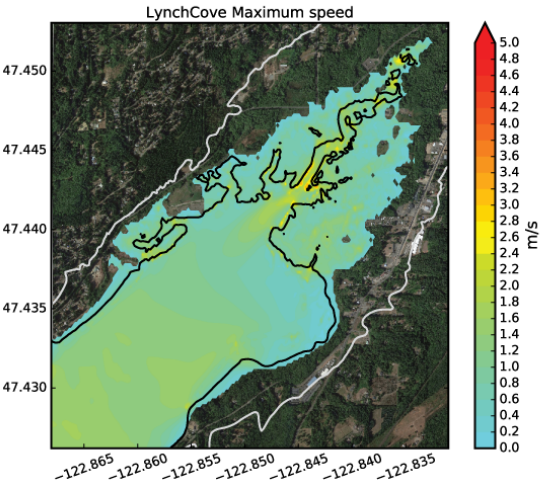

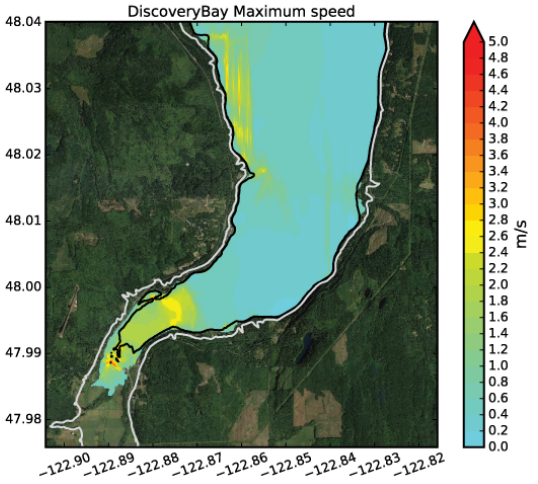

3. Cascadia earthquake with splay fault

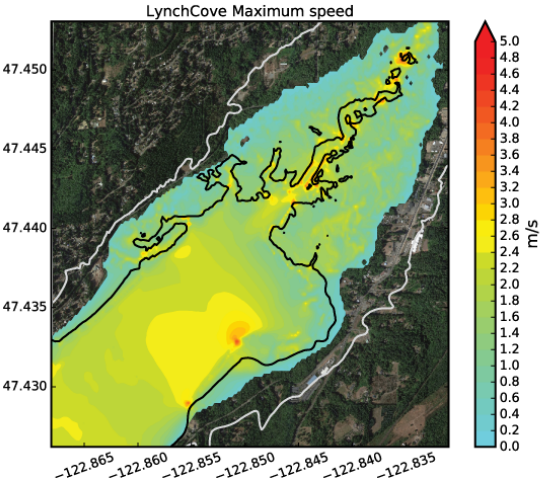

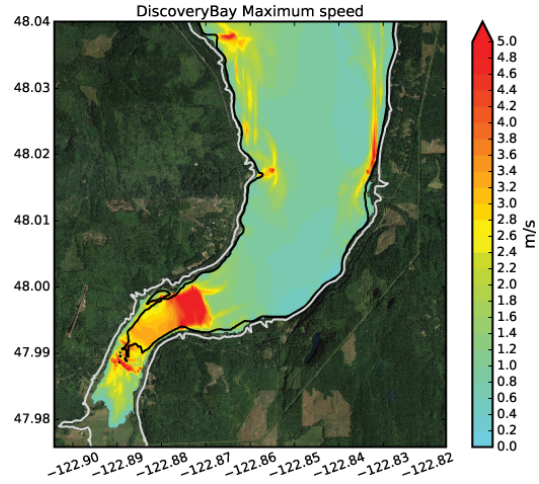

APPENDIX 5. GEOCLAW TSUNAMI SIMULATIONS OUTPUT, CHAPTER 3, CONTINUED

Maximum simulated speeds for study area grids, continued

4. A.D. 900-930 Seattle fault earthquake speeds

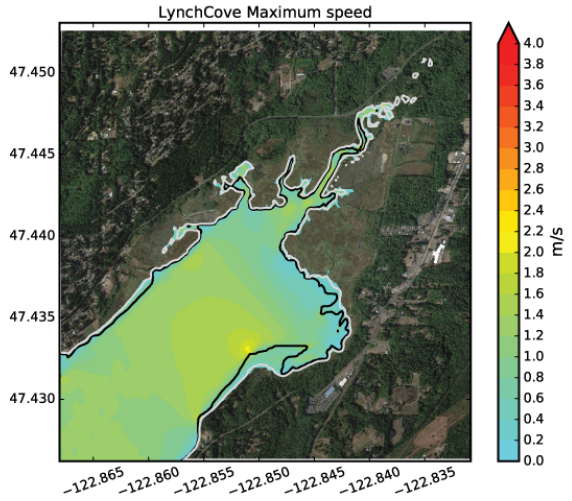

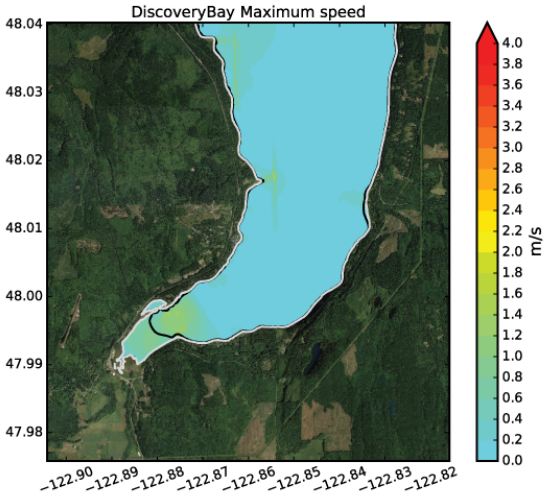

5. Alaska earthquake speeds

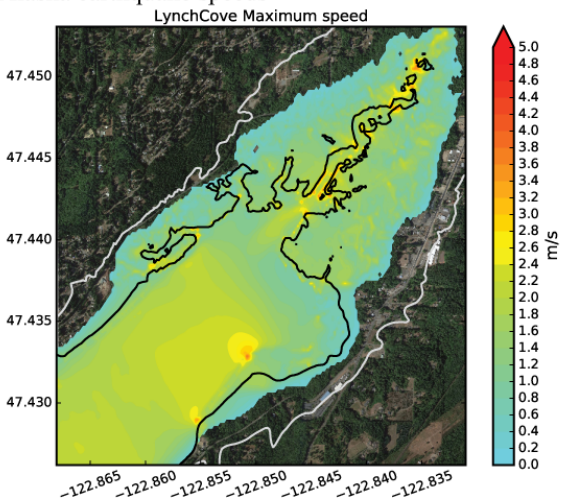

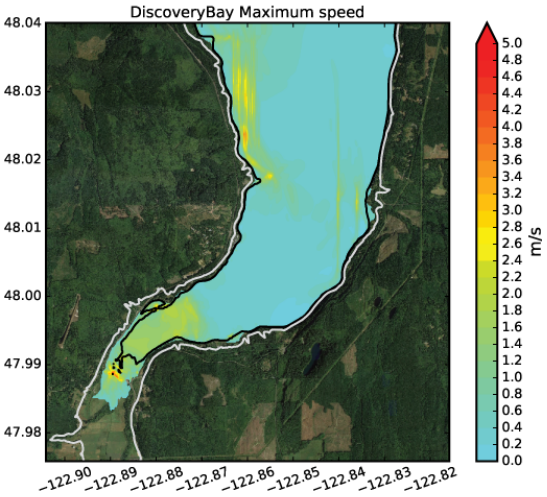

VITA

Carolyn Garrison-Laney was born in Gainesville, Florida. She earned her Bachelor of Science degree in Geosciences from San Francisco State University in 1993. She earned a Master's degree in Environmental Systems from Humboldt State University in 1997. She attended the University of Washington and earned an additional Master's degree in Human Centered Design and Engineering in 2012, and earned her Doctor of Philosophy degree in 2017.